

# FRONTIERS IN LIFE SCIENCES AND RELATED TECHNOLOGIES



SCIENCE  
AND  
TECHNOLOGY

AGRICULTURAL SCIENCES BIOLOGY BIOCHEMISTRY  
BIOPHARMACEUTICALS BIOTECHNOLOGY BIOCONTROL  
BIOMECHANICS BIOCOMPUTERS BIOENGINEERING  
BIOELECTRONICS BIOPHYSICS BIOMATERIALS  
BIOMEDICAL SCIENCES BIOMONITORING BIOPOLYMERS  
CELL BIOLOGY CONSERVATION BIOLOGY CRYOBIOLOGY  
ECOLOGY ENVIRONMENTAL SCIENCES FOOD SCIENCES  
GENETICS GENOMICS IMMUNOTHERAPY MARINE SCIENCES  
MEDICAL SCIENCES MICROBIOLOGY MOLECULAR BIOLOGY  
METABOLOMICS NANOTECHNOLOGY NEUROSCIENCES  
PHYSIOLOGY PHARMACOGENOMICS PHARMACOLOGY  
POPULATION DYNAMICS PROTEOMICS REMEDIATION  
SYNTHETIC BIOLOGY SYSTEMATICS TOXICOLOGY

DECEMBER, 2022, VOLUME 3, ISSUE 3

## Contents

### Research Articles

- **Long-range transport and potential source regions of PM<sub>2.5</sub> during the autumn season in Edirne, Türkiye**

Ilker Oruc

Pages: 95-100

- **Determination of optical constants and band gap variation of Zn<sub>0.98-x</sub>Cu<sub>0.02</sub>Mg<sub>x</sub>O thin films**

Dogan Akcan

Pages: 101-106

- **Effect of different abiotic conditions on biomass and fucoxanthin content of *Amphora capitellata***

Zeliha Demirel, Aysegul Erdogan, Ayca Busra Karatas, Meltem Conk Dalay

Pages: 107-112

- **Self-assembling of surface active drug amitriptyline hydrochloride in association with additives: Role of surface activity in the pharmaceutical applications**

Hasan Tolga Ozcam, Zeynep Berna Tamer, Sinem Gokturk

Pages: 113-120

- **Antiviral peptidlerin SARS COV-2 ana proteaz yapısına bağlanma etkinliklerinin protein-yanıştırma yöntemi ile incelenmesi: *In silico* bir çalışma**
- **Investigation of antiviral peptides in SARS COV-2 major protease structure by protein-e docking method: An *in silico* study**

Ilter Demirhan, Erkan Oner, Ergul Belge Kurutas

Pages: 121-127

- **Üretkenlik karşıtı iş davranışlarının iş kazalarına olan etkisinde güvenlik ikliminin düzenleyici rolü; makine ve ekipman imalatı sektörü örneği**
- **The regulatory role of the safety climate in the effect of counterproductive work behaviors on work accidents; example of machinery and equipment manufacturing industry**

Fahri Oluk, Ahmet Gokcan, Goksel Demir

Pages: 128-133

- **Improving the adventitious rooting ability of hard-to-root olive (*Olea europaea* L.) cultivar cuttings through inhibiting strigolactone biosynthesis**

Aslihan Ozbilen, Fatih Sezer, Kemal Melih Taskin

Pages: 134-137

## Issue Editorial Board

**Prof. Dr. Fahrul Zaman HUYOP**  
Institution: Universiti Teknologi Malaysia

**Prof. Dr. Nusret ERDOGAN**  
Institution: Istinye University

**Editor**

**Prof. Dr. Ibrahim Ilker OZYIGIT**

**Co-Editors**

**Ibrahim Ertugrul YALCIN**

**Assoc. Prof. Dr. Aysegul YILDIZ**

**Prof. Dr. Uğur YAHSI**  
Institution: Marmara University

**Assoc. Prof. Dr. Ilhan DOGAN**  
Institution: Sakarya University of Applied Sciences



## Research article

# Long-range transport and potential source regions of PM<sub>2.5</sub> during the autumn season in Edirne, Türkiye

Ilker Oruc\*<sup>1</sup> 

<sup>1</sup> *Kirklareli University, Vocational College of Technical Sciences, 39010, Kirklareli, Türkiye*

## Abstract

The variation in daily Particulate Matter 2.5 (PM<sub>2.5</sub>) concentrations was studied in Edirne city center from September 1, 2019 to November 30, 2019 (autumn season). The values of daily PM<sub>2.5</sub> concentrations were between 5.65 and 77.59 µg m<sup>-3</sup>. The values of PM<sub>2.5</sub> concentration had the highest average value on Tuesdays compared to other days. The mean value of daily PM<sub>2.5</sub> concentrations on Tuesdays was 23.41 µg m<sup>-3</sup>. The backward trajectories were computed and clustered by applying the Hybrid Single-Particle Lagrangian Integrated Trajectory (HYSPPLIT) model. The backward trajectories clustered in eight major clusters during the autumn. In Cluster 4 (C4), which has more short-range transport according to the other seven clusters, the mean value of PM<sub>2.5</sub> concentrations was 19.52 µg m<sup>-3</sup>. The mean value of PM<sub>2.5</sub> concentrations was 28.11 µg m<sup>-3</sup> in C8 (3.3%), which has more long-range transport than the other seven clusters. Potential source areas of PM<sub>2.5</sub> have been determined by the Potential Source Contribution Function (PSCF) model. The results of PSCF analyses illustrated that the north, northeast, south, and southeast regions of the sampling area as major potential source areas for PM<sub>2.5</sub>. The results obtained in this study can make important contributions to the evaluation of PM<sub>2.5</sub> concentration in the region in terms of health and long-range transport.

**Keywords:** *Backward trajectory; HYSPPLIT; particulate matter; PM<sub>2.5</sub>; PSCF*

## 1. Introduction

Due to their properties and weather conditions, pollutants released into the atmosphere can be transported long distances from emission sources (Lagzi et al., 2013; Ozdemir et al., 2021). It has been described that when aerosols are generated by gas-to-particle conversion, long-distance transport is possible because the duration needed for gas-to-particle conversion and the relatively small particle sizes produced by this process result in long residence times in the atmosphere (Wallace and Hobbs, 2006; Flores et al., 2020). Various air pollutants released into the atmosphere can be cited as the cause of many current and potential environmental problems (Lagzi et al., 2013). Air pollution in cities is very complex due to many emission sources, meteorological processes, and chemical transformations (Ho, 2012). Because of the large number of anthropogenic emission

sources in urban and industrialized locations, the concentrations of various undesirable pollutants can cause deterioration of air quality and visibility and reach levels that threaten human health (Wallace and Hobbs, 2006). In a study carried out by Hao et al. (2019), it was stated that the southerly route represents the main transport route of PM<sub>2.5</sub> for all seasons. It was noted that the northwesterly transport route passes through the natural source areas, while the southerly transport route passes through the anthropogenic source areas. The percentage of pollution trajectories in each cluster (C1, C2, C3, C4, C5, C6) during the autumn season was 71.40%, 9.30%, 32.00%, 24.30%, 60.10%, 10.60%, respectively. The mean values of PM<sub>2.5</sub> concentrations were 142, 144, 119, 144, 129, and 117 µg m<sup>-3</sup> in these clusters. The study by Cheng et al. (2017) noted that the percentage of all trajectories during the autumn season was 12.71% in C1, 3.84% in C2, 11.10% in C3, 18.23% in C4, 31.01% in C5, 13.69% in

\* Corresponding author.

E-mail address: [ilkeroruc@klu.edu.tr](mailto:ilkeroruc@klu.edu.tr) (I. Oruc).

<https://doi.org/10.51753/flsrt.1113251> Author contributions

Received 09 May 2022; Accepted 20 September 2022

Available online 20 October 2022

2718-062X © 2022 This is an open access article published by Dergipark under the [CC BY](https://creativecommons.org/licenses/by/4.0/) license.

C6, 0.84% in C7, 6.84% in C8, and 1.75% in C9. They explained that mean values of PM<sub>2.5</sub> concentrations in these clusters were 73.12, 41.52, 69.93, 37.71, 50.24, 34.41, 44.97, 28.85, 60.64 μg m<sup>-3</sup>, respectively. In the study performed by Zhao et al. (2015), the mean values of PM<sub>2.5</sub> concentration in C1, C2, C3, C4, and C5 during the autumn season were 63.14, 78.47, 119.94, 95.96, and 38.34 μg m<sup>-3</sup>, respectively. Li et al. (2020) stated that the distribution of air masses in the autumn season is similar to that in the spring and winter seasons. In their study, the mean values of PM<sub>2.5</sub> concentrations in C1, C2, C3, C4, C5, and C6 during the autumn season were 8.79, 7.25, 9.88, 7.32, 8.75, and 9.76 μg m<sup>-3</sup>, respectively. They explained that the percentage of all trajectories in these clusters were 14.3%, 29.7%, 16.2%, 7.6%, 25.4%, 6.8%, respectively. Cluster analysis performed by Li et al. (2017) indicated that Beijing in autumn was influenced by trajectories from both the south and southeast. The percentage of all trajectories during the autumn was 16.76% in C1, 36.08% in C2, 13.32% in C3, 12.77% in C4, 5.72% in C5, and 15.34% in C6. The mean values of PM<sub>2.5</sub> concentrations in these clusters during the autumn were 94.19, 41.64, 169.78, 46.56, 91.59, and 165.17 μg m<sup>-3</sup>, respectively. In the study of Lv et al. (2021), the number of trajectories was 2160 in autumn. It was stated that in the autumn, other clusters except for C5 gathered trajectories from the north, and these trajectories represented 91.90% of all trajectories. The percentage of trajectory numbers of each cluster in all trajectories during the autumn season was 41.02% in C1, 24.91% in C2, 14.77% in C3, 11.20% in C4, and 8.10% in C5. The average values of PM<sub>2.5</sub> concentration in these clusters were 38.35, 33.27, 34.06, 25.38, and 63.83 μg m<sup>-3</sup>, respectively.

In many studies, the PSCF approach has been performed to identify potential source areas of PM<sub>2.5</sub> (Wang et al., 2015; Cheng et al., 2017; Mukherjee and Agrawal, 2018; Li et al., 2020). It was stated by Wang et al. (2015) that the regional emission source's probable locations during relatively polluted periods are mainly south and west of Beijing. It was explained that the PM<sub>2.5</sub> sources are primarily areas on the regional scale owing to the long-distance transport tendency. Cheng et al. (2017) stated that the potential source areas of PM<sub>2.5</sub> extend further northward in autumn, but the transport routes are the same as in the spring. External PM<sub>2.5</sub> source areas were reported to be mainly located in the southeast and northwest in autumn. The study by Li et al. (2020) noted that in the northern part of Xinjiang are concentrated severe pollution source areas of PM<sub>2.5</sub> in autumn. According to the PSCF results in the study of Mukherjee and Agrawal (2018), the northwest has been defined as the main source area with a higher possibility of contributing to the higher fine particulate matter load in Varanasi city. Further, they stated that there are other possible sources from the east and north directions. They also stated that the contribution probability of the sources coming from the east direction is the lowest. Li et al. (2017) stated that their study's potential source areas of PM<sub>10</sub> and PM<sub>2.5</sub> are similar according to the concentration weighted trajectory (CWT) and PSCF results. Wu et al. (2018) explained that according to the PSCF analysis performed in their study, the main reason for the high PM<sub>2.5</sub> levels detected in northern Henan could be extraneous polluted air masses.

In this study, daily PM<sub>2.5</sub> concentrations in the Edirne city center during the autumn season (between September 1, 2019, and November 30, 2019) have been studied. The backward trajectories have been run and clustered by applying the

HYSPLIT Model. Transport pathways and potential source areas of PM<sub>2.5</sub> have been determined.

## 2. Materials and methods

### 2.1. Sampling location

Edirne Province is located between 41° 40' North latitude and 26° 30' East longitude (Fig. 1). Edirne Province is a border city neighboring Greece to the west and Bulgaria to the north. In addition, Kırklareli and Tekirdag Provinces are located to the east of Edirne Province, and Canakkale Province to the south. Certain parts of the Meric, Tunca, Arda, and Ergene rivers are located within the borders of Edirne Province. The continental climate is dominant in Edirne Province (ECDR, 2020). Daily PM<sub>2.5</sub> concentrations obtained from the Air Quality Monitoring Station in Edirne city center were used (MEUCC, 2022).

### 2.2. Backward trajectories analysis

In this study, to define the origins and transport pathways of air masses reaching the study point the HYSPLIT model was used. The backward trajectories were computed and clustered at 1-hour intervals for 72 hours and at an arrival height of 1500 meters above the ground. The weekly stored data consisting of 1° resolution outputs of the Global Data Analysis System (GDAS) were used as input (Stein et al., 2015; Rolph et al., 2017). The Euclidean distance used for clustering backward trajectories is presented below (Carslaw and Ropkins, 2012; Carslaw, 2019).

$$d_{1,2} = \left( \sum_{i=1}^n ((X_{1i} - X_{2i})^2 + (Y_{1i} - Y_{2i})^2) \right)^{1/2} \quad (\text{Equation 1})$$

In the equation,  $X_1$ ,  $Y_1$  and  $X_2$ ,  $Y_2$  are coordinates (the latitude and longitude) of the backward trajectories 1 and 2, respectively.  $n$  is the number of backward trajectories points.

### 2.3. PSCF analysis

The PSCF approach is a widely used method to identify possible source areas of pollutants (Begum et al. 2005; Pekney et al., 2006; Carslaw and Ropkins, 2012; Li et al. 2017; Kuzu and Saral, 2017; Carslaw, 2019; Neykova and Hristova, 2020; Oruc, 2022). PSCF solves

$$PSCF_{ij} = \frac{m_{ij}}{n_{ij}} \quad (\text{Equation 2})$$

In the equation, while the number of trajectories passing in the  $ij^{th}$  grid cell is defined as  $n_{ij}$ , the number of times a source concentration is high than a given value of criterion when trajectories pass in the  $ij^{th}$  grid cell was defined as  $m_{ij}$ . The value of the criterion was specified as 75% of all samples (Jain et al., 2017; Bie et al., 2021; Oruc, 2022). PSCF scores were multiplied by weighting values. The weight values ( $W(n_{ij})$ ) given in the equation below are used (Petroselli et al., 2018; Oruc, 2022).

In the equation,  $\bar{n}$  represents the mean number of endpoints per cell, which is calculated on every cell with at least one end-

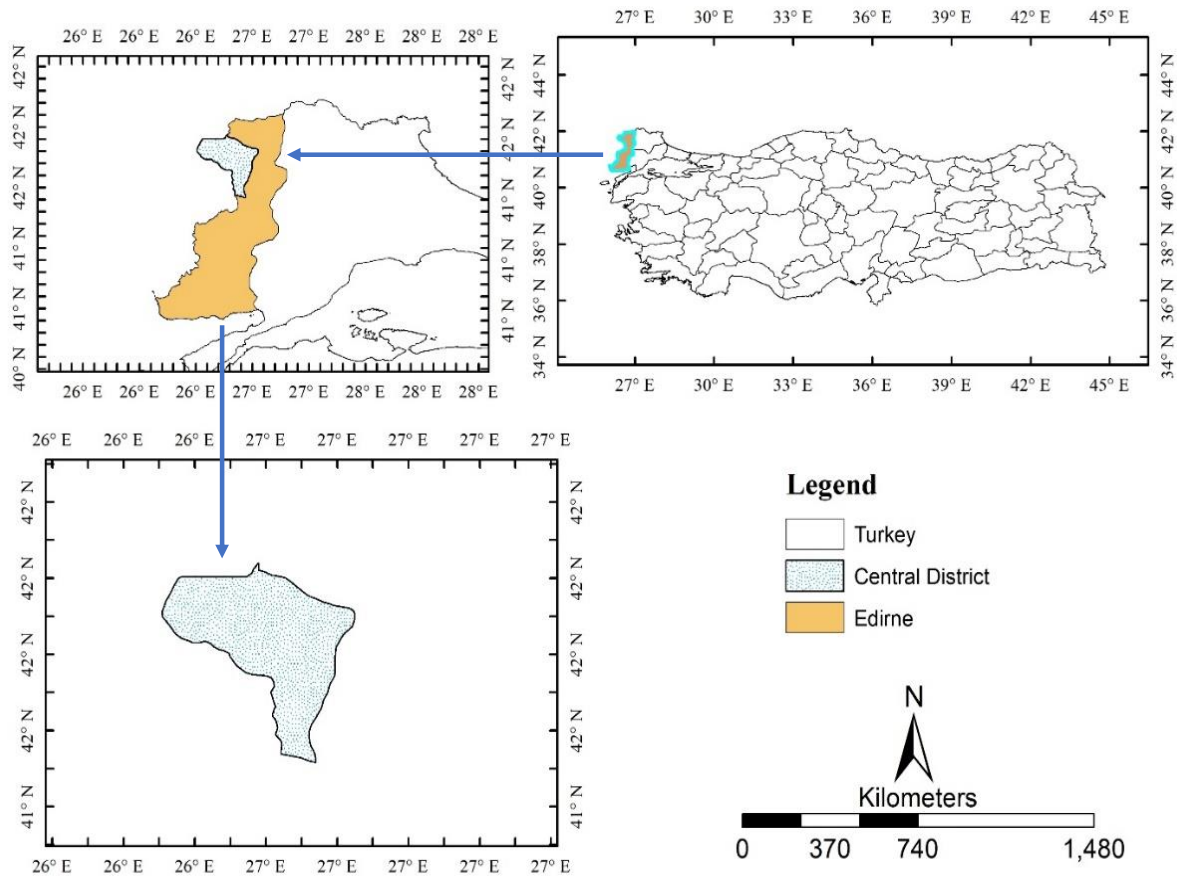


Fig. 1. Sampling location.

point. The figures in this study were created by applying the OpenAir statistical analysis package with the R-Studio program (Carslaw and Ropkins, 2012; Carslaw, 2019).

$$W(n_{ij}) = \begin{cases} 1.00, n_{ij} > 2\bar{n} \\ 0.75, \bar{n} < n_{ij} \leq 2\bar{n} \\ 0.50, \bar{n}/2 < n_{ij} \leq \bar{n} \\ 0.15, n_{ij} \leq \bar{n}/2 \end{cases}$$

(Equation 3)

### 3. Results and discussion

The mean value of daily PM<sub>2.5</sub> concentrations measured during the study period was 20.40 μg m<sup>-3</sup>. The values of PM<sub>2.5</sub> are relatively higher in October compared to September and November (Fig. 2). The PM<sub>2.5</sub> concentrations had the highest daily values on October 29 (77.59 μg m<sup>-3</sup>) and, the lowest (5.65 μg m<sup>-3</sup>) on September 11. The maximum concentration of PM<sub>2.5</sub> was 25.02 μg m<sup>-3</sup> in September. The minimum value for October was 6.08 μg m<sup>-3</sup>. The mean values of PM<sub>2.5</sub> concentrations were 10.61, 27.39, and 22.12 μg m<sup>-3</sup> in September, October, and November, respectively. The PM<sub>2.5</sub> concentrations were between 7.09 and 43.57 μg m<sup>-3</sup> in November.

The results shown on Fig. 3 demonstrate the variations in the mean PM<sub>2.5</sub> concentrations among the weekdays. The shading expresses the 95% confidence intervals of the mean PM<sub>2.5</sub> concentration values. The mean values of PM<sub>2.5</sub> concentrations were 22.81, 20.30, 21.91, 19.04, and 18.10 μg m<sup>-3</sup> on Mondays, Wednesdays, Thursdays, Saturdays, and Sundays, respectively. The minimum values of PM<sub>2.5</sub> concentra-

tions were 5.92, 7.00, 5.65, 6.62, 5.99, 6.08, and 6.64 μg m<sup>-3</sup> on Mondays, Tuesdays, Wednesdays, Thursdays, Fridays, Saturdays, and Sundays, respectively. The maximum values of PM<sub>2.5</sub> concentrations were 50.62, 77.59, 43.57, 51.86, 45.95, 49.00, and 47.19 μg m<sup>-3</sup> on these days, respectively. The values obtained during the study draw the trend of observing the highest values of PM<sub>2.5</sub> on Tuesdays (23.41 μg m<sup>-3</sup>) and the lowest concentrations on Fridays (17.42 μg m<sup>-3</sup>).



Fig. 2. CalendarPlot of PM<sub>2.5</sub> concentrations during the autumn in 2019.

The backward trajectories are clustered in an 8-cluster solution (Fig. 4). Trajectories within C1 accounted for 11% of

all trajectories. The values of  $PM_{2.5}$  concentrations were seen to range between 5.65 and 31.22  $\mu g m^{-3}$  in C1. Among the clusters, the average value of  $PM_{2.5}$  concentrations was the lowest in C1 (13.76  $\mu g m^{-3}$ ). The transport in C1 originated from Russia. It was seen that arrived at the sampling area by passing over the Sea of Azov, Ukraine, the Black Sea, and Bulgaria. Trajectories within both C2 and C7 accounted for 14.3% of all trajectories. In C2, the mean value of  $PM_{2.5}$  concentrations was 20.46  $\mu g m^{-3}$ . It was observed that  $PM_{2.5}$  concentration values in C2 ranged between 5.99 and 47.03  $\mu g m^{-3}$ . The transport in C2 started from Ukraine. It was seen that arrived at the sampling area via the Black Sea and Bulgaria. The values of  $PM_{2.5}$  concentrations in C7 ranged between 10.02 and 42.59  $\mu g m^{-3}$ , with a mean value of 26.78  $\mu g m^{-3}$ .

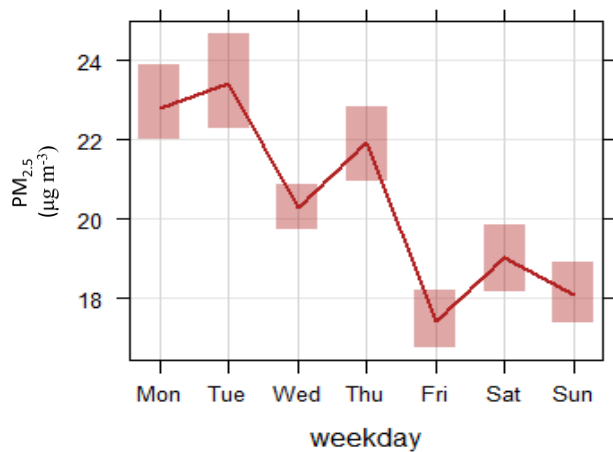


Fig. 3. The mean  $PM_{2.5}$  concentrations on weekday.

The transport in C7 originated from the Mediterranean and reached the sampling area by passing over Turkey's Mediterranean, Aegean, and Marmara Regions. It was observed that C3 (17.6%) originated from the Nederland-German land border region. The values of  $PM_{2.5}$  in C3 were 8.76 and 50.62  $\mu g m^{-3}$ , with a mean value of 20.08  $\mu g m^{-3}$ . The percentage of all trajectories during the study period was higher in C4 (20.9%) compared to the other seven clusters. The mean value of  $PM_{2.5}$  concentrations in C4 was 19.52  $\mu g m^{-3}$ . The values of  $PM_{2.5}$  were between 6.08 and 77.59  $\mu g m^{-3}$  in C4. It was seen that C4, which has short-range trajectories according to other clusters, originated from Bulgaria.

The study by Ecer et al. (2017) stated that backward trajectories were grouped in 6 main clusters during the data collection period. They suggested that the transport in these clusters originates from Syria (C1), France and Southern Europe (C2), Eastern Anatolia (C3), Mediterranean (C4), Middle East (C5), and Central-Western Europe (C6). The percentage of all trajectories in these clusters was 31.1%, 12.2%, 16.9%, 20.1%, 9.3%, and 10.3%, respectively. Zeydan and Wang (2019) stated the backward trajectories during the study period were clustered in 9 main clusters. C1 was noted to originate from the southeast of the United Kingdom and C4 was noted to transport Saharan dust to the sampling area. Tepe and Dogan (2021) pointed out that the backward trajectories in the period of their study were gathered in 5 main clusters. These clusters are named C1 as Northern Europe, C2 as Central Europe, C3 as Anatolia, and the Middle East, C4 as North Africa and Western Mediterranean, and C5 as Levant Region and the Aegean Sea. They stated that the highest percentage of trajectories from C3 with 41%, followed by C5 (23%) and C4 (15%).

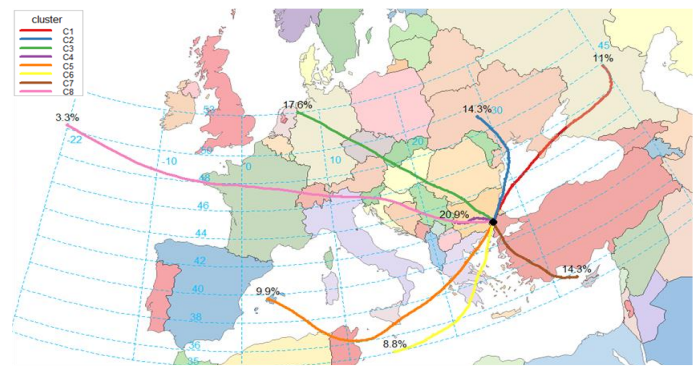


Fig. 4. Backward trajectory clusters.

The values of  $PM_{2.5}$  concentrations in C5 were between 6.88 and 51.86  $\mu g m^{-3}$ , with a mean value of 19.58  $\mu g m^{-3}$ . The transport in C5 originated from the west coasts of Majorca Island. It was seen that reached the sampling area by passing over the Mediterranean, Algeria, Tunisia, Italy, Greece, and Bulgaria. It was observed that trajectories within C5 and C6 accounted for 9.9% and 8.8% of all trajectories, respectively. The values of  $PM_{2.5}$  concentration were between 10.61 and 49.00  $\mu g m^{-3}$  in C6, while the mean value is 20.87  $\mu g m^{-3}$ .

It was observed that C6, which originated from the Mediterranean, arrived at the sampling area via Greece and the Aegean Sea. The percentage of all trajectories during the study period was lower in C8 (3.3%) compared to the other seven clusters. C8 had more long-range transport than the other seven clusters. The values of  $PM_{2.5}$  concentration were observed to range between 20.72 and 43.57  $\mu g m^{-3}$  in C8. Among the clusters, the average value of  $PM_{2.5}$  concentrations was the highest in C8 (28.11  $\mu g m^{-3}$ ). The transport in C8 originated from the North Atlantic Ocean.

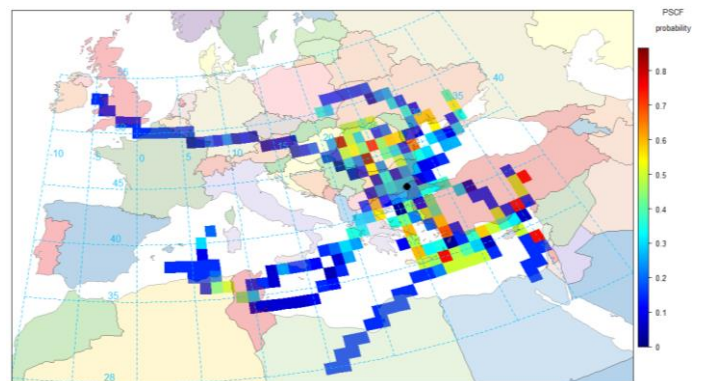


Fig. 5. PSCF distribution of  $PM_{2.5}$ .

PSCF analysis was carried out to enable the determination of possible potential  $PM_{2.5}$  source areas. PSCF distribution illustrated the sampling area's north, northeast, south, and southeast regions as the major potential source areas for  $PM_{2.5}$  (Fig. 5).

The higher PSCF values were seen in Romania, Hungary, Turkey, the Mediterranean, and Lebanon than in other locations. In the study carried out by Kuzu and Saral (2017), they explained that trajectories over the Sea of Marmara had the highest PSCF scores on each of the particle sizes. They stated that this confirmed the contribution of marine aerosols. They also explained that sizes of particles between 7.2-3 and 3-1.5  $\mu m$ , in addition to the marine aerosol contribution, appear to have originated from the crust from the south of Istanbul.

#### 4. Conclusion

The mean value of daily PM<sub>2.5</sub> concentrations was 20.40 µg m<sup>-3</sup> in Edirne city center during the autumn season. The lowest and highest values of daily PM<sub>2.5</sub> concentrations ranged between 5.65 and 77.59 µg m<sup>-3</sup>, respectively.

The values of PM<sub>2.5</sub> concentration had the highest average value on Tuesdays compared to other days, with a mean of 23.41 µg m<sup>-3</sup>. The mean values of daily PM<sub>2.5</sub> concentration had the lowest daily mean value on Fridays (lowest days), Saturdays, and Sundays to other days. The mean values of daily PM<sub>2.5</sub> concentrations these days were 17.42, 19.04, and 18.10 µg m<sup>-3</sup>, respectively. It was determined that the percentage of all backward trajectories of each cluster represented 11% in C1,

#### References

- Begum, B. A., Kim, E., Jeong, C. H., Lee, D. W., & Hopke, P. K. (2005). Evaluation of the potential source contribution function using the 2002 Quebec forest fire episode. *Atmospheric Environment*, 39(20), 3719-3724.
- Bie, S., Yang, L., Zhang, Y., Huang, Q., Li, J., Zhao, T., ... & Wang, W. (2021). Source appointment of PM<sub>2.5</sub> in Qingdao port, east of China. *Science of the Total Environment*, 755, 142456.
- Carslaw, D. C., & Ropkins, K. (2012). Openair-An R package for air quality data analysis. *Environmental Modelling & Software*, 27-28, 52-61.
- Carslaw, D. C. (2019). *The openair manual - open-source tools for analysing air pollution data*. Manual for version 2.6-6, University of York.
- Cheng, F., Zha, Y., Zhang, J., He, J., & Yan, S. (2017). A study on distance transport of PM<sub>2.5</sub> to Xianlin in Nanjing, China and its source areas. *Aerosol and Air Quality Research*, 17(7), 1672-1683.
- Ecer, A., Sarikaya, B., Tepe, A. M., & Dogan, G. (2017). Mardin hava kirliliğinin değerlendirilmesi. *VII. Ulusal Hava Kirliliği ve Kontrolü Sempozyumu*, Antalya, Türkiye. 853-862.
- ECDR, (2020). Edirne İli 2019 Yılı Çevre Durum Raporu, Türkiye Cumhuriyeti Edirne Valiliği Çevre ve Şehircilik İl Müdürlüğü. <https://webdosya.csb.gov.tr/db/edirne/icerikler/2019-yili-ed-rne-il-cevre-durum-raporu-n-ha-20201216122442.pdf>, Last accessed on July 30, 2022.
- Flores, R. M., Mertoglu, E., Ozdemir, H., Akkoyunlu, B. O., Demir, G., Unal, A., & Tayanc, M. (2020). A high-time resolution study of PM<sub>2.5</sub>, organic carbon, and elemental carbon at an urban traffic site in Istanbul. *Atmospheric Environment*, 223, 117241.
- Hao, T., Cai, Z., Chen, S., Han, S., Yao, Q., & Fan, W. (2019). Transport pathways and potential source regions of PM<sub>2.5</sub> on the west coast of Bohai Bay during 2009-2018. *Atmosphere*, 10(6), 345.
- Ho, B. Q. (2012). Urban air pollution. In: Mukesh Khare (ed) *Air Pollution-Monitoring, Modelling and Health* (pp. 1-38). InTech, Rijeka, Croatia.
- Jain, S., Sharma, S. K., Choudhary, N., Masiwal, R., Saxena, M., Sharma, A., ... & Sharma, C. (2017). Chemical characteristics and source apportionment of PM<sub>2.5</sub> using PCA/APCS, UNMIX, and PMF at an urban site of Delhi, India. *Environmental Science and Pollution Research*, 24(17), 14637-14656.
- Kuzu, S. L., & Saral, A. (2017). The effect of meteorological conditions on aerosol size distribution in Istanbul. *Air Quality, Atmosphere & Health*, 10, 1029-1038.
- Lagzi, I., Mészáros, R., Gelybó, G., & Leelőssy, Á. (2013). *Atmospheric chemistry* (pp. 1-201). Eötvös Lorand University.
- Li, D., Liu, J., Zhang, J., Gui, H., Du, P., Yu, T., ... & Cheng, Y. (2017). Identification of long-range transport pathways and potential sources of PM<sub>2.5</sub> and PM<sub>10</sub> in Beijing from 2014 to 2015. *Journal of Environmental Sciences*, 56, 214-229.
- Li, H., He, Q., & Liu, X. (2020). Identification of long-range transport pathways and potential source regions of PM<sub>2.5</sub> and PM<sub>10</sub> at Akedala Station, Central Asia. *Atmosphere*, 11(11), 1183.
- Lv, M., Hu, A., Chen, J., & Wan, B. (2021). Evolution, transport characteristics, and potential source regions of PM<sub>2.5</sub> and O<sub>3</sub> pollution in a Coastal City of China during 2015-2020. *Atmosphere*, 12(10), 1282.
- MEUCC, (2022). Air Quality Monitoring Station of Republic of Turkey Ministry of Environment, Urbanization and Climate Change, [https://sim.csb.gov.tr/STN/STN\\_Report/StationDataDownloadNew](https://sim.csb.gov.tr/STN/STN_Report/StationDataDownloadNew), Last accessed on July 30, 2022.
- Mukherjee, A., & Agrawal, M. (2018). Assessment of local and distant sources of urban PM<sub>2.5</sub> in middle Indo-Gangetic plain of India using statistical modeling. *Atmospheric Research*, 213, 275-287.
- Neykova, R., & Hristova, E. (2020). Backward trajectories and cluster analyses for study of PM<sub>10</sub> concentration variations in Bulgarian urban areas. *Bulgarian Journal of Meteorology and Hydrology*, 24(2), 66-83.
- Oruc, I. (2022). Transport routes and potential source areas of PM<sub>10</sub> in Kırklareli, Turkey. *Environmental Monitoring and Assessment*, 194(2), 104.
- Ozdemir, H., Aktas, M. A., Yalcin, I. E., Alyuz, U., Okten, H. E., Ozcan, H. K., ... & Alper, U. (2021). Noktasal kaynaklar için ulusal hava kirliliği emisyon faktörleri ve envanterinin belirlenmesi: Metal sektörü için örnek bir çalışma. *International Journal of Advances in Engineering and Pure Sciences*, 33(3), 337-346.
- Pekney, N. J., Davidson, C. I., Zhou, L., & Hopke, P. K. (2006). Application of PSCF and CPF to PMF-Modeled sources of PM<sub>2.5</sub> in Pittsburgh. *Aerosol Science and Technology*, 40(10), 952-961.
- Petroselli, C., Crocchianti, S., Moroni, B., Castellini, S., Selvaggi, R., Nava, S., ... & Cappelletti, D. (2018). Disentangling the major source areas for an intense aerosol advection in the Central Mediterranean on the basis of Potential Source Contribution Function modeling of chemical and size distribution measurements. *Atmospheric Research*, 204, 67-77.
- Rolph, G., Stein, A., & Stunder, B. (2017). Real-time environmental applications and display system: READY. *Environmental Modelling & Software*, 95, 210-228.
- Stein, A. F., Draxler, R. R., Rolph, G. D., Stunder, B. J. B., Cohen, M. D., & Ngan, F. (2015). NOAA's HYSPLIT atmospheric transport and dispersion modeling system. *Bulletin of the American Meteorological Society*, 96(12), 2059-2077.
- Tepe, A. M., & Dogan, G. (2021). Chemical characterization of PM<sub>2.5</sub> and PM<sub>2.5-10</sub> samples collected in urban site in Mediterranean coast of Turkey. *Atmospheric Pollution Research*, 12(1), 46-59.
- Wallace, J. M., & Hobbs, P. V. (2006). *Atmospheric science an introductory survey (2nd ed.)*. (pp. 1-483). Elsevier Inc., San Diego.
- Wang, L., Liu, Z., Sun, Y., Ji, D., & Wang, Y. (2015). Long-range transport and regional sources of PM<sub>2.5</sub> in Beijing based on long-term observations from 2005 to 2010. *Atmospheric Research*, 157, 37-48.
- Wu, X., Ding, Y., Zhou, S., & Tan, Y. (2018). Temporal characteristic and source analysis of PM<sub>2.5</sub> in the most polluted city agglomeration of China. *Atmospheric Pollution Research*, 9(6), 1221-1230.
- Zeydan, O., & Wang, Y. (2019). Using MODIS derived aerosol optical depth to estimate ground-level PM<sub>2.5</sub> concentrations over Turkey. *Atmospheric Pollution Research*, 10(5), 1565-1576.
- Zhao, M., Huang, Z., Qiao, T., Zhang, Y., Xiu, G., & Yu, J. (2015). Chemical characterization, the transport pathways and potential sources of PM<sub>2.5</sub> in Shanghai: Seasonal variations. *Atmospheric Research*, 158-159, 66-78.

**Cite as:** Oruc, I. (2022). Long-range transport and potential source regions of PM<sub>2.5</sub> during the autumn season in Edirne, Türkiye. *Front Life Sci RT*, 3(3), 95-100.



Research article

## Determination of optical constants and band gap variation of $Zn_{0.98-x}Cu_{0.02}Mg_xO$ thin films

Dogan Akcan\*<sup>1</sup> <sup>1</sup> Bahcesehir University, Faculty of Engineering and Natural Sciences, Department of Mathematics, 34353, Istanbul, Türkiye

### Abstract

Cu doped ZnO ( $ZnCuO$ ) is a very important candidate for electronic applications, since it has been shown that it possesses p-type conductivity. In order to broaden its applications, it is crucial to tune optical and electronic properties. In this study, by doping  $ZnCuO$  with magnesium, variation of refractive index, extinction coefficient, and band gap of thin films were investigated. Optical constants were evaluated using a transmittance model which is derived from Fresnel equations. Refractive indices of thin films were expressed as a dispersion relation in a polynomial form, while extinction coefficients were modelled as a convolution by Lorentzian curves. It was observed that magnesium doping decreased the refractive index and also caused a blue shift in absorption edge which is a clear indicator of band gap widening.

**Keywords:** Doping; refractive index; sol-gel; thin films; ZnO

### 1. Introduction

Owing to its superior physical properties such as direct wide band gap of 3.37eV, high transparency in wide optical region, radiation hardness, and tunable conductivity ZnO is subjected to many studies (Look, 2001; Kang and Joung, 2007; Sennik et al., 2015). Researchers aim to benefit from ZnO in numerous fields such as gas sensors, lasers, field-effect transistors, and solar cells (Ozgur et al., 2005; Park et al., 2012; Sahin et al., 2014; Tulun et al., 2016; Ning et al., 2018; Zang, 2018).

Physical properties of ZnO can further be improved by various dopant materials. For this reason, implementation of various different elements into ZnO structure is widely studied. For instance, group IIA elements and among them especially magnesium doping to widen the band gap (Cao et al., 2013; Kim et al., 2014), aluminum to increase electrical conductivity (Tonbul et al., 2021), and yttrium to increase hardness (Kaya et al., 2018). Influence of copper doping into ZnO structure is studied by many researchers. Mhamdi et al. (2014) showed that

2 at. copper % doping greatly improves crystallinity of sprayed ZnO thin films. Suja et al. (2015) showed that copper doping introduces p-type conductivity to ZnO films, though this p-type conductivity is not stable and turns to n-type conductivity over time due to extrinsic defects.

ZnO is also a very important material for its catalytic properties. Due to its catalytic nature, ZnO is subjected to many studies in life sciences such as antibacterial activity and breath analysis. In their study, Alev et al. (2021) showed that copper doping increases density of point defects in ZnO structure and thus greatly enhances ethanol sensing properties of ZnO based nanorods. On the other hand, Yalcin et al. (2020) showed that 2% magnesium doping into ZnO structure greatly inhibits hemolytic activity while leading an advanced antibacterial property. Since antibacterial property is mainly driven by interaction between incoming electromagnetic wave and catalytic material, determination of optical constants of catalytic materials is crucial.

If ZnO based materials are to be used in devices with heterostructures that composed of layers of different materials

\* Corresponding author.

E-mail address: [dogan.akcan@eng.bau.edu.tr](mailto:dogan.akcan@eng.bau.edu.tr) (D. Akcan).<https://doi.org/10.51753/flsrt.1120679> Author contributions

Received 24 May 2022; Accepted 21 September 2022

Available online 20 October 2022

2718-062X © 2022 This is an open access article published by Dergipark under the [CC BY](https://creativecommons.org/licenses/by/4.0/) license.

that provides carrier or optical confinement such as LEDs and high electron mobility transistors (HEMTs), the most relevant parameters would be the band gaps of each layer and the valence- and conduction-band offsets between the individual layers (Janotti and Van de Walle, 2009). Hence, success of application of ZnO based materials relies on band-gap engineering. In light of these discussions, it is also crucial to investigate modulation of band-gaps of Cu doped ZnO thin films (ZnCuO) which can be achieved by introduction of magnesium into material. To the best of our knowledge, variation of these properties of ZnCuO films with magnesium doping has not yet been investigated.

In this study effect of magnesium doping on optical constants (refractive index and extinction coefficient) of  $Zn_{0.98-x}Cu_{0.02}Mg_xO$  ( $x=0.0, 0.01, 0.02, 0.05, \text{ and } 0.1$ ) thin films were investigated. Optical constants were determined by application of Fresnel Equations to transmittance data numerically. Determined optical constants were then used to determine the band gap variation of samples.

## 2. Materials and methods

The  $Zn_{0.98-x}Cu_{0.02}Mg_xO$  thin films were deposited by sol-gel dip coating method with a varying magnesium molar ratio of  $x = 0.0$  ( $Zn_{0.98}Cu_{0.02}O$ ), 0.01, 0.02, 0.05, and 0.1. Zinc acetate dihydrate, magnesium acetate tetrahydrate, and copper (II) acetate monohydrate were used as precursors while Methanol was used as solvent and monoethanolamine (MEA) as sol stabilizer.

All chemicals were analytical grade and used as they were received from supplier (Merck). 0.25M precursor solution was prepared in solvent and MEA was added dropwise as precursors dissolved. MEA/total precursor molar ratio in solution was arranged as 1:1. Resultant solution was stirred in ambient conditions overnight to age. Soda-lime glass slides (ISOLAB) were used as substrate.

In order to coat the glass slides, slides were dipped into coating solution and withdrawn directly into vertical furnace. A preheat treatment was applied at 300°C for 2 minutes to remove organic materials, then coated substrate was cooled for 3 minutes. This process was repeated 20 times to achieve an appropriate thickness of thin films.

Film coated slides were finally annealed at 600°C to obtain crystalline structure. Shimadzu UV-mini 1240 spectrophotometer was used to measure optical transmittance of thin films.

## 3. Results and discussion

### 3.1. Transmittance measurements

As shown in Fig. 1 all films exhibit high transmittance in visible and NIR region. Besides slight fluctuation in transmittance due to interference caused by internal reflections, no other significant absorption troughs were observed. Average transmittance slightly decreased with low magnesium doping ratios of 1% and 2%, but further increase of magnesium doping ratio resulted with distinctive increase in blue region of spectrum.

While  $Zn_{0.98}Cu_{0.02}O$  film exhibit a sharp optical cutting edge around 380 nm, cutting edge shifted towards shorter wavelengths with increasing magnesium doping. Detailed representation of this blue shift in cutting edge is shown as an inset in Fig. 1.

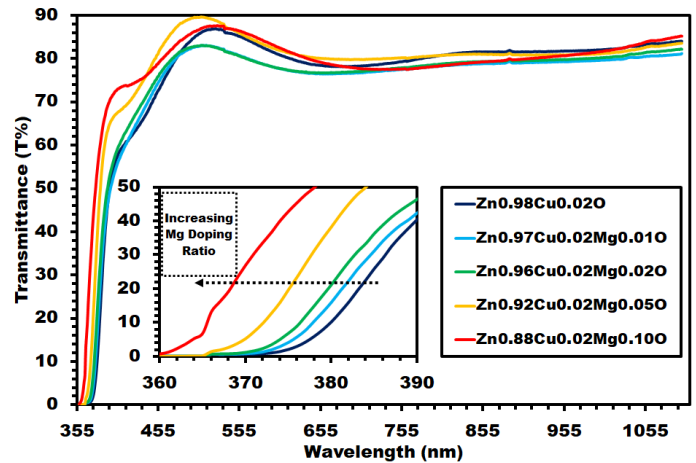


Fig. 1. Optical transmittance of the  $Zn_{0.98-x}Cu_{0.02}Mg_xO$  thin films. Inset figure shows close up view of transmittance in 360-390 nm wavelength interval.

### 3.2. Determination of optical constants and modeling transmittance of films

Details of transmittance model of “Double Facet Coated Substrate” (DFCS) were discussed in an earlier study of our research group (Akcan et al., 2019). This transmittance model can be summarized as follows:

Coefficients of reflection and transmission of the electric field ( $r_{12}$  and  $t_{12}$ , respectively) from one medium to another with complex refractive indices ( $\eta_1$  and  $\eta_2$ , respectively) at a normal incidence is given by:

$$r_{12} = \frac{\eta_1 - \eta_2}{\eta_1 + \eta_2} \dots \dots \dots (1)$$

$$t_{12} = \frac{2\eta_1}{\eta_1 + \eta_2} \dots \dots \dots (2)$$

Here complex refractive index  $\eta$  is defined as  $\eta = n + ik$ , where  $n$  is the refractive index and  $k$  is the extinction coefficient. Resultant transmitted electric field is infinite summation of coherent electric fields which is subjected to reflection from air-film and film-substrate interfaces and experience wavelength dependent phase shift which is given by  $\theta = 4\pi\eta_{film}d_{film}/\lambda$ . The resultant reflection and transmission coefficients of electric field for air-film-substrate system ( $r_{afs}$  and  $t_{afs}$ , respectively) are given by:

$$r_{afs} = \frac{r_{af} + r_{fs} \times \exp(i\theta)}{1 + r_{af} \times r_{fs} \times \exp(i\theta)} \dots \dots \dots (3)$$

$$t_{afs} = \frac{t_{af} \times t_{fs} \times \exp(i\theta/2)}{1 + r_{af} \times r_{fs} \times \exp(i\theta)} \dots \dots \dots (4)$$

Using these coefficients reflectance and transmittance in air-film-substrate direction can be calculated as:

$$R_{afs} = r_{afs} \times r_{afs}^* \dots \dots \dots (5)$$

$$T_{afs} = \frac{n_s}{n_a} \times t_{afs} \times t_{afs}^* \dots \dots \dots (6)$$

where  $r_{afs}^*$  and  $t_{afs}^*$  are complex conjugates of reflection and transmission coefficients, respectively. Considering absorption loss of the substrate, which is given by  $U = \exp(-\alpha_{sub}d_{sub})$

where  $\alpha_{sub}$  is absorption coefficient of substrate and  $d_{sub}$  is the substrate thickness (1.1mm), resultant transmittance DFCS system is given by:

$$T_{system} = \frac{T_{afs} \times T_{sfa} \times U}{1 - R_{sfa}^2 \times U^2} \dots\dots\dots(7)$$

Various models are proposed and widely used to model refractive index of a material. Some of them are rather complex but also works well even in high absorption conditions, such as Adachi-Forouhi-Drude model or Tauc-Lorentz model (Ferlauto et al., 2002; Latzel et al., 2015). On the other hand, simpler models such as Cauchy's model or Sellmeier's model work well in low absorption conditions (Sun and Kwok, 1999; Ozgur et al., 2005; Ozharar et al., 2016). Despite their limitations, all these models work in a large wavelength interval. In this study, inspired from series expansion of functions, refractive indices of thin films were modelled as a 6<sup>th</sup> degree polynomial. This method is advantageous as it is simple, possible to use in high absorption conditions, and more sensitive to subtle variations in refractive index, though it can only be used in narrow wavelength intervals, since interval of convergence is limited.

Extinction coefficients were modelled as summation of Lorentzian curves which is given by:

$$k_{film} = \frac{A}{1 + \left(\frac{E - E_A}{\Delta E_A}\right)^2} + \frac{B}{1 + \left(\frac{E - E_B}{\Delta E_B}\right)^2} + \frac{C}{1 + \left(\frac{E - E_C}{\Delta E_C}\right)^2} \dots\dots\dots(8)$$

where  $A$ ,  $B$ , and  $C$  are peak heights;  $E_A$ ,  $E_B$ , and  $E_C$  are peak centers; and  $\Delta E_A$ ,  $\Delta E_B$ , and  $\Delta E_C$  are peak widths.

Curve fitting was performed in 360-1100 nm wavelength interval, and fitting was performed by using built in functions of MATLAB software. Calculated refractive index of thin films is shown in Fig. 2 and dispersion equations of refractive index model is given in Table 1. The calculated refractive index values are in accordance with the values in the literature (Baig et al., 2020; El Hamidi et al., 2021). As seen in the Fig. 2, refractive indices of films have a broad trend of decrease with increasing magnesium doping ratio. A similar trend was also observed by Yang et al. (2009) in Mg-doped ZnO thin films.

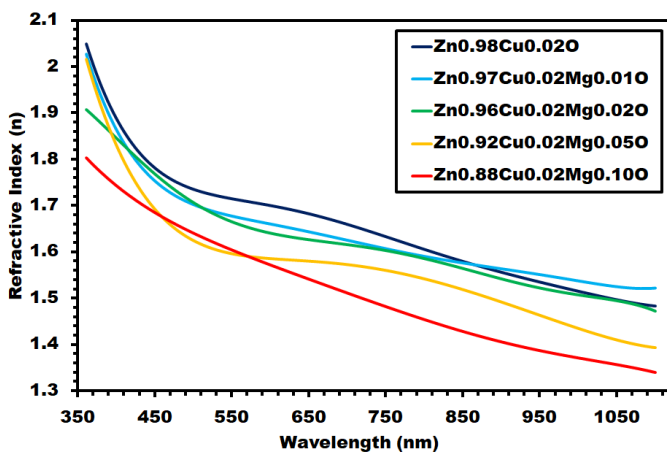


Fig. 2. Variation of refractive index of  $Zn_{0.98-x}Cu_{0.02}Mg_xO$  thin films.

Calculated extinction coefficients of thin films are shown in Fig. 3. Intense absorption due to intrinsic band - gap in UV range can clearly be seen. Absorption edge shifts shorter wavelengths with increasing magnesium doping ratio which also was evident in transmittance graph [inset Fig. (3a)]. All films

exhibit very low absorption in visible and NIR region. While there's no particular trend in variation of absorption in visible region, in NIR region absorbance was greatly increased with 1% doping but steadily decreased with further increase of magnesium doping, as shown in the inset Fig. (3b). Parameters of Lorentzian curves that constitute extinction coefficient are given in Table 2. Negative peak heights in  $Zn_{0.93}Cu_{0.02}Mg_{0.05}O$  and  $Zn_{0.88}Cu_{0.02}Mg_{0.10}O$  thin films do not have a physical significance. Since determination of extinction coefficient by summation of Lorentzian curves is an empirical method, "negative peaks" only act as a correction factor in their respective regions.

Besides refractive index and extinction coefficient, this model also enables determination of thickness of thin films. Evaluated thin film thicknesses are shared in Table 3.

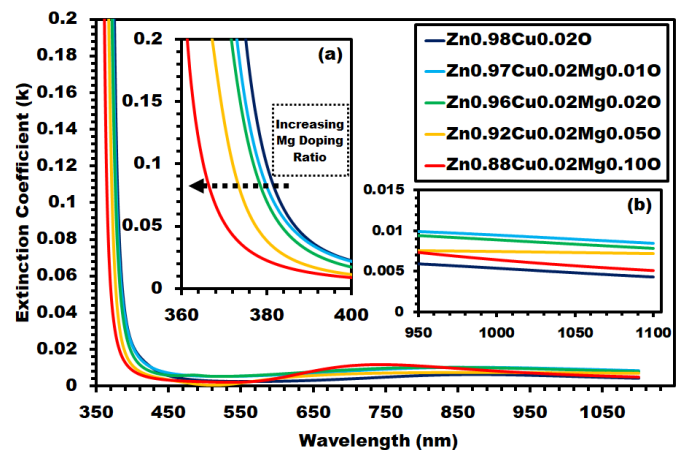


Fig. 3. Extinction coefficients of  $Zn_{0.98-x}Cu_{0.02}Mg_xO$  thin films. Close up view of extinction coefficients in 360-400 nm and 950-1100 nm wavelength intervals were shown in inset figures (a) and (b) respectively.

Transmittance of thin films were modelled from calculated refractive index and extinction coefficient. Accuracy of transmittance model is determined from correlation coefficient  $R^2$ . As seen in the Fig. 4, transmittance model is highly accurate as  $R^2$  values are very close to 1.

### 3.3. Determination of band gap

Energy gap or band gap ( $E_g$ ) of a material is the energy required to excite an electron from the valence band to the conduction band. This energy gap obeys the relation which is given as

$$(ah\nu)^n = A(h\nu - E_g) \dots\dots\dots(9)$$

Here  $\alpha$  is absorption coefficient,  $h$  is Planck constant,  $\nu$  is frequency of incoming light,  $A$  is proportionality constant, and  $E_g$  is band gap of the material. The exponent  $n$  get its value according to nature of electronic transition. Since ZnO is a direct band gap material,  $n$  is equal to 2.  $E_g$  can be estimated from extrapolating linear part of  $h\nu$  vs.  $(ah\nu)^2$  graph which is also known as Tauc plot. Many studies evaluate  $\alpha$  from Beer-Lambert law, which is given by (Scarminio et al., 1999; Za'Abu et al., 2014; Chen and Jaramillo, 2017).

$$I = I_0 e^{-\alpha t} \dots\dots\dots(10)$$

**Table 1**  
Refractive index dispersion relations with varying Mg doping ratio.

Mg Doping Ratio (at.%)	Refractive index dispersion relation (Wavelength – $\lambda$ – is given in $\mu\text{m}$ )
0	$n_{Mg=0\%} = 70.014 \cdot \lambda^6 - 347.99 \cdot \lambda^5 + 710.5 \cdot \lambda^4 - 761.01 \cdot \lambda^3 + 449.96 \cdot \lambda^2 - 139.41 \cdot \lambda + 19.451$
1	$n_{Mg=1\%} = 86.40 \cdot \lambda^6 - 413.39 \cdot \lambda^5 + 813.52 \cdot \lambda^4 - 842.31 \cdot \lambda^3 + 483.87 \cdot \lambda^2 - 146.58 \cdot \lambda + 20.04$
2	$n_{Mg=2\%} = -81.16 \cdot \lambda^6 + 360.17 \cdot \lambda^5 - 644.25 \cdot \lambda^4 + 590.32 \cdot \lambda^3 - 289.08 \cdot \lambda^2 + 70.10 \cdot \lambda - 4.59$
5	$n_{Mg=5\%} = 35.01 \cdot \lambda^6 - 181.50 \cdot \lambda^5 + 393.94 \cdot \lambda^4 - 455.86 \cdot \lambda^3 + 294.56 \cdot \lambda^2 - 100.35 \cdot \lambda + 15.65$
10	$n_{Mg=10\%} = -1.67 \cdot \lambda^6 - 2.32 \cdot \lambda^5 + 24.79 \cdot \lambda^4 - 46.05 \cdot \lambda^3 + 37.91 \cdot \lambda^2 - 15.52 \cdot \lambda + 4.23$

**Table 2**  
Lorentzian curve parameters of extinction coefficient.

Parameter	$\text{Zn}_{0.98}\text{Cu}_{0.02}\text{O}$	$\text{Zn}_{0.97}\text{Cu}_{0.02}\text{Mg}_{0.01}\text{O}$	$\text{Zn}_{0.96}\text{Cu}_{0.02}\text{Mg}_{0.02}\text{O}$	$\text{Zn}_{0.93}\text{Cu}_{0.02}\text{Mg}_{0.05}\text{O}$	$\text{Zn}_{0.88}\text{Cu}_{0.02}\text{Mg}_{0.10}\text{O}$
A	0.5181	2.0138	0.3386	0.2479	0.9114
B	0.0040	0.4137	0.0012	-0.0063	-0.0047
C	0.0059	0.0095	0.0098	0.0083	0.0129
$E_A$ (eV)	3.3739	3.7479	3.3900	3.4073	3.5046
$E_B$ (eV)	3.0115	3.3874	2.5583	2.3980	2.1336
$E_C$ (eV)	1.4102	1.4146	1.4904	1.5790	1.7001
$\Delta E_A$ (eV)	0.0535	0.0322	0.0640	0.0597	0.0379
$\Delta E_B$ (eV)	0.1877	0.0571	0.1046	0.3652	0.2932
$\Delta E_C$ (eV)	0.4073	0.6320	0.6708	1.3946	0.4721

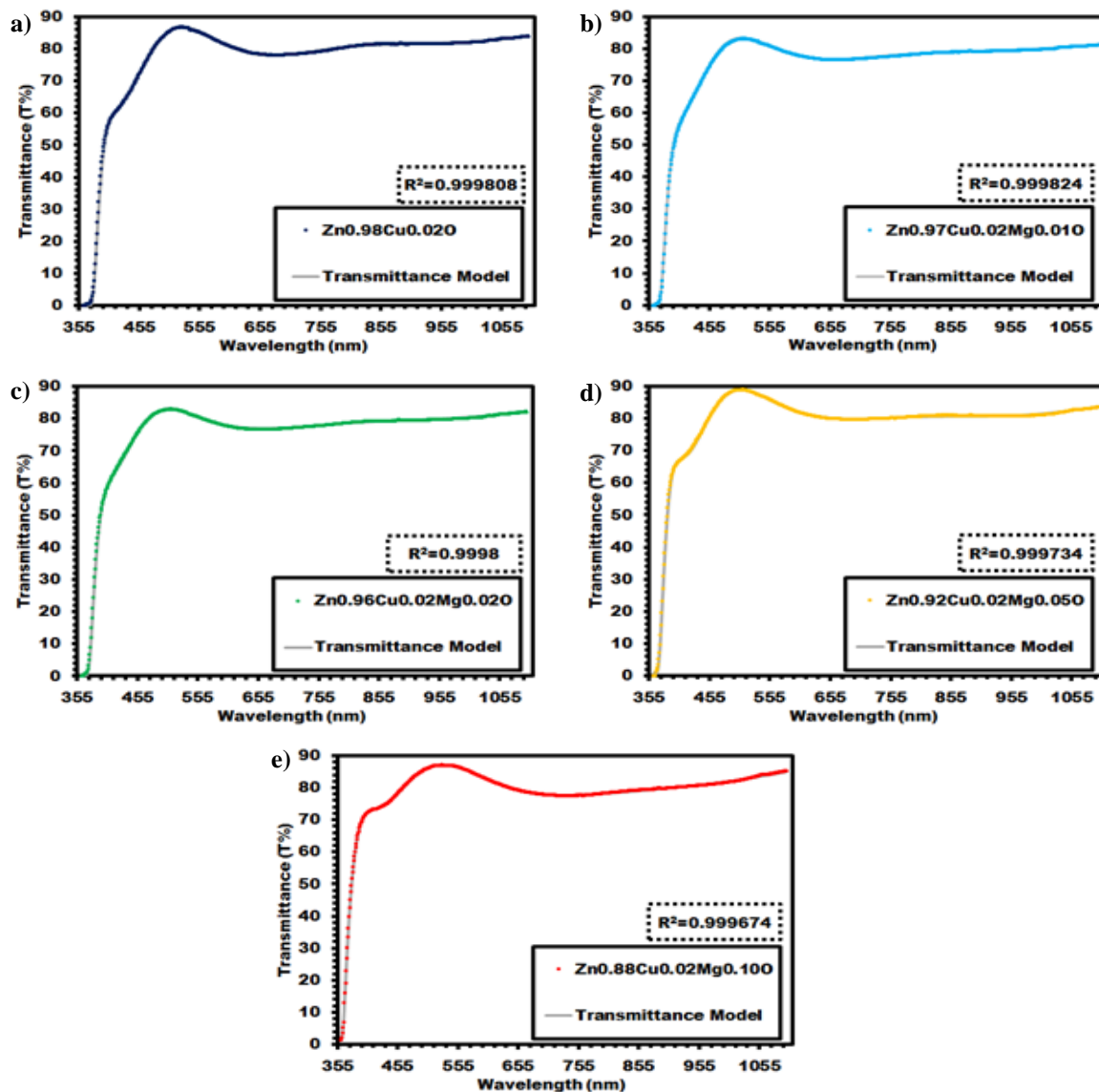


**Fig. 4.** Comparison of transmittance model with measurement results: (a)  $\text{Zn}_{0.98}\text{Cu}_{0.02}\text{O}$ , (b)  $\text{Zn}_{0.97}\text{Cu}_{0.02}\text{Mg}_{0.01}\text{O}$ , (c)  $\text{Zn}_{0.96}\text{Cu}_{0.02}\text{Mg}_{0.02}\text{O}$ , (d)  $\text{Zn}_{0.92}\text{Cu}_{0.02}\text{Mg}_{0.05}\text{O}$ , (e)  $\text{Zn}_{0.88}\text{Cu}_{0.02}\text{Mg}_{0.10}\text{O}$ .

where  $I$  is transmitted light intensity,  $I_0$  is incoming light intensity and  $t$  is film thickness. In order to obtain  $\alpha$ , considering  $I/I_0 = 1/T$ , equation (10) can be re-written as:

$$\alpha = \frac{-1}{t} \ln \left( \frac{1}{T} \right) \dots\dots\dots(11)$$

**Table 3**  
Evaluated thicknesses of  $Zn_{0.98-x}Cu_{0.02}Mg_xO$  thin films with transmittance model.

Mg Doping Ratio (at.%)	Film Thickness (nm)
0	302
1	295
2	290
5	305
10	320

where  $T$  is the transmittance of the sample. To be fair, this approach is very simple and gives a rough idea about value of the band gap of sample and allows to estimate the trends about modifications made in samples. However, considering Beer's Law only to calculate band gap leads to errors, since thin films have a finite thickness and light traveling through the film is subjected to multiple reflections and interferences. For this reason, the evaluated band gap value is slightly erroneous and the error is considerable for applications requiring band gap engineering. Band gap of  $Zn_{0.98}Cu_{0.02}O$  thin film was calculated using this method as an example. Tauc plot of subjected sample can be seen in Fig. 5. Band gap of sample calculated with this method was  $E_g = 3.227\text{eV}$ . Considering theoretical band gap of ZnO, this value is slightly less than expected.

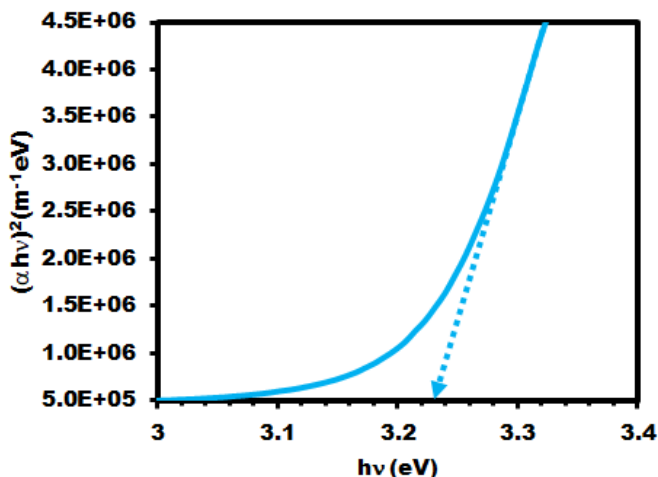


**Fig. 5.** Tauc plot of  $Zn_{0.98}Cu_{0.02}O$  evaluated from Beer-Lambert Law.

Relation between extinction coefficient and absorption coefficient is given as:

$$\alpha = \frac{4\pi k}{\lambda} \dots\dots\dots(12)$$

In order to calculate band gaps of deposited films accurately, absorption coefficients of thin films were calculated from extinction coefficients which are evaluated from transmittance model.

Resultant Tauc plot of thin films is given in Fig. 6. As seen in the figure, magnesium doping led extrapolation to shift higher energies, which is a clear indicator of band gap widening. As shown in the inset figure, evaluated band gap values has

strong correlation with the relation  $E_g = 0.0008x^2 + 0.0014x + 3.3147$ , where  $x$  denotes for magnesium doping ratio. Evaluated band gap values are listed in Table 4. Comparison of band gap values of  $Zn_{0.98}Cu_{0.02}O$  determined by different models shows that using Beer's law results 2.5% difference to the band gap calculated from transmittance model.

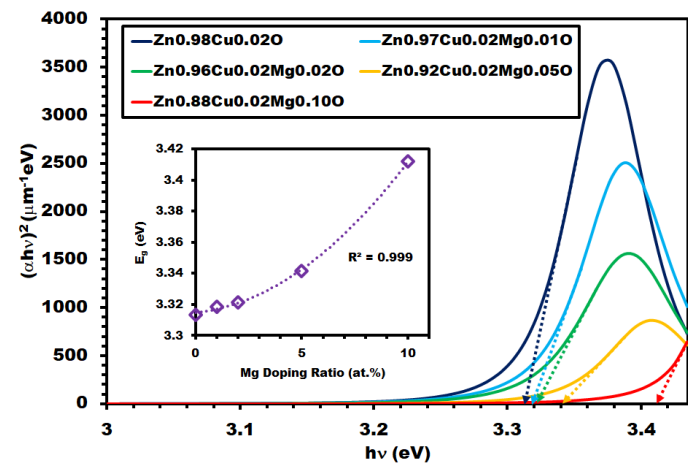


**Fig. 6.** Tauc plot of  $Zn_{0.98-x}Cu_{0.02}Mg_xO$  thin films evaluated from transmittance model. Inset figure shows variation of band gap with increasing magnesium doping ratio.

**Table 4**  
Evaluated band gap values of  $Zn_{0.98-x}Cu_{0.02}Mg_xO$  thin films with transmittance model.

Mg Doping Ratio (at.%)	$E_g$ (eV)
0	3.313
1	3.319
2	3.321
5	3.342
10	3.412

**4. Conclusion**

In conclusion; optical constants, namely refractive index and extinction coefficient of  $Zn_{0.98-x}Cu_{0.02}Mg_xO$  thin films were calculated from experimental transmittance data numerically with a transmittance model relying on Fresnel equations. Refractive index is observed to be decreasing with increasing magnesium doping ratio. Absorption edge of thin films shifted towards higher energies, which is an indicator of band gap widening. Band gap values are calculated from extinction coefficients and a considerable increase is observed from 3.313eV to 3.412eV for 10 at % magnesium doped films.

This study has shown that Mg increases the band gap in exchange for lowering the refractive index. These results have great importance in development of new and improved antibacterial and sensing materials.

**Acknowledgement:** The presented work was supported by the Research Fund of Bahçeşehir University, Istanbul, Turkey (Project No. BAUBAP.2018.02.16).

**Conflict of interest:** The author declares that he has no conflict of interests.

**Informed consent:** The author declares that this manuscript did not involve human or animal participants and informed consent was not collected.

## References

- Akcan, D., Ozharar, S., Ozugurlu, E., & Arda, L. (2019). The effects of Co/Cu Co-doped ZnO thin films: An optical study. *Journal of Alloys and Compounds*, 797, 253-261.
- Alev, O., Ergun, I., Oezdemir, O., Arslan, L. C., Buyukkose, S., & Ozturk, Z. Z. (2021). Enhanced ethanol sensing performance of Cu-doped ZnO nanorods. *Materials Science in Semiconductor Processing*, 136, 106149.
- Baig, F., Ashraf, M. W., Asif, A., & Imran, M. (2020). A comparative analysis for effects of solvents on optical properties of Mg doped ZnO thin films for optoelectronic applications. *Optik*, 208, 164534.
- Cao, L., Zhu, L., & Ye, Z. (2013). Enhancement of p-type conduction in Ag-doped ZnO thin films via Mg alloying: The role of oxygen vacancy. *Journal of Physics and Chemistry of Solids*, 74(5), 668-672.
- Chen, Z., & Jaramillo, T. (2017). The Use of UV-Visible Spectroscopy to Measure the Band Gap of a Semiconductor. [https://mmrc.caltech.edu/CaryUV-Vis\\_Int.Sphere/Literature/SpectroscopyJaramillo.pdf](https://mmrc.caltech.edu/CaryUV-Vis_Int.Sphere/Literature/SpectroscopyJaramillo.pdf), Last accessed on July, 2022.
- El Hamidi, A., El Mahboub, E., Meziane, K., El Hichou, A., & Almagoussi, A. (2021). The effect of electronegativity on optical properties of Mg doped ZnO. *Optik*, 241, 167070.
- Ferlauto, A. S., Ferreira, G. M., Pearce, J. M., Wronski, C. R., Collins, R. W., Deng, X., & Ganguly, G. (2002). Analytical model for the optical functions of amorphous semiconductors from the near-infrared to ultraviolet: Applications in thin film photovoltaics. *Journal of Applied Physics*, 92(5), 2424-2436.
- Janotti, A., & Van de Walle, C. G. (2009). Fundamentals of zinc oxide as a semiconductor. *Reports on Progress in Physics*, 72(12), 126501.
- Kang, S. J., & Joung, Y. H. (2007). Influence of substrate temperature on the optical and piezoelectric properties of ZnO thin films deposited by rf magnetron sputtering. *Applied Surface Science*, 253(17), 7330-7335.
- Kaya, S., Akcan, D., Ozturk, O., & Arda, L. (2018). Enhanced mechanical properties of yttrium doped ZnO nanoparticles as determined by instrumented indentation technique. *Ceramics International*, 44(9), 10306-10314.
- Kim, I. Y., Shin, S. W., Gang, M. G., Lee, S. H., Gurav, K. V., Patil, P. S., ... & Kim, J. H. (2014). Comparative study of quaternary Mg and Group III element co-doped ZnO thin films with transparent conductive characteristics. *Thin Solid Films*, 570, 321-325.
- Latzel, M., Gobelt, M., Bronstrup, G., Venzago, C., Schmitt, S. W., Sarau, G., & Christiansen, S. H. (2015). Modeling the dielectric function of degenerately doped ZnO: Al thin films grown by ALD using physical parameters. *Optical Materials Express*, 5(9), 1979-1990.
- Look, D. C. (2001). Recent advances in ZnO materials and devices. *Materials Science and Engineering: B*, 80(1-3), 383-387.
- Mhamdi, A., Mimouni, R., Amlouk, A., Amlouk, M., & Belgacem, S. (2014). Study of copper doping effects on structural, optical and electrical properties of sprayed ZnO thin films. *Journal of Alloys and Compounds*, 610, 250-257.
- Ning, Y., Zhang, Z., Teng, F., & Fang, X. (2018). Novel transparent and self-powered UV photodetector based on crossed ZnO nanofiber array homojunction. *Small*, 14(13), 1703754.
- Ozgun, U., Alivov, Y. I., Liu, C., Teke, A., Reshchikov, M., Dogan, S., Avrutin, V., Cho, S.-J., Morkoc, A. H. (2005). A comprehensive review of ZnO materials and devices. *Journal of Applied Physics*, 98(4), 11.
- Park, S. Y., Kim, B. J., Kim, K., Kang, M. S., Lim, K. H., Lee, T. I., Myoung, J.M., Hong Koo Baik Kim, Y. S. (2012). Low-temperature, solution-processed and alkali metal doped ZnO for high-performance thin-film transistors. *Advanced Materials*, 24(6), 834-838.
- Ozharar, S., Akcan, D., & Arda, L. (2016). Determination of the refractive index and the thickness of double side coated thin films. *Journal of Optoelectronics and Advanced Materials*, 18(January-February 2016), 65-69.
- Sahin, Y., Ozturk, S., Kilinc, N., Kosemen, A., Erkovan, M., & Ozturk, Z. Z. (2014). Electrical conduction and NO<sub>2</sub> gas sensing properties of ZnO nanorods. *Applied Surface Science*, 303, 90-96.
- Scarmio, J., Urbano, A., & Gardes, B. (1999). The Beer-Lambert law for electrochromic tungsten oxide thin films. *Materials Chemistry and Physics*, 61(2), 143-146.
- Sennik, E., Kerli, S., Alver, U., & Ozturk, Z. Z. (2015). Effect of fluorine doping on the NO<sub>2</sub>-sensing properties of ZnO thin films. *Sensors and Actuators B: Chemical*, 216, 49-56.
- Suja, M., Bashar, S. B., Morshed, M. M., & Liu, J. (2015). Realization of Cu-doped p-type ZnO thin films by molecular beam epitaxy. *ACS Applied Materials & Interfaces*, 7(16), 8894-8899.
- Sun, X. W., & Kwok, H. S. (1999). Optical properties of epitaxially grown zinc oxide films on sapphire by pulsed laser deposition. *Journal of Applied Physics*, 86(1), 408-411.
- Tonbul, B., Can, H. A., Ozturk, T., & Akyildiz, H. (2021). Solution processed aluminum-doped ZnO thin films for transparent heater applications. *Materials Science in Semiconductor Processing*, 127, 105735.
- Tulun, F. R., Ozturk, S., & Ozturk, Z. Z. (2016). The NO<sub>2</sub> sensing properties of the sensors done with nano-tetrapods. *Acta Physica Polonica A*, 129(4), 797-799.
- Yalcin, B., Akcan, D., Yalcin, I. E., Alphan, M. C., Senturk, K., Ozyigit, I. I., & Arda, L. (2020). Effect of Mg doping on morphology, photocatalytic activity and related biological properties of Zn<sub>1-x</sub>Mg<sub>x</sub>O nanoparticles. *Turkish Journal of Chemistry*, 44(4), 1177-1199.
- Yang, S., Liu, Y., Zhang, Y., & Mo, D. (2009). Spectroscopic ellipsometry studies of Mg-doped ZnO thin films prepared by the sol-gel method. *Physica Status Solidi (A)*, 206(7), 1488-1493.
- Za'Aba, N. K., Sarjidan, M. M., Majid, W. A., Kusrini, E., & Saleh, M. I. (2014). Junction properties and conduction mechanism of new terbium complexes with triethylene glycol ligand for potential application in organic electronic device. *Journal of Rare Earths*, 32(7), 633-640.
- Zang, Z. (2018). Efficiency enhancement of ZnO/Cu<sub>2</sub>O solar cells with well oriented and micrometer grain sized Cu<sub>2</sub>O films. *Applied Physics Letters*, 112(4), 042106.

**Cite as:** Akcan, D. (2022). Determination of optical constants and band gap variation of Zn<sub>0.98-x</sub>Cu<sub>0.02</sub>Mg<sub>x</sub>O thin films. *Front Life Sci RT*, 3(3), 101-106.



Research article

## Effect of different abiotic conditions on biomass and fucoxanthin content of *Amphora capitellata*

Zeliha Demirel<sup>\*1</sup> , Aysegul Erdogan<sup>2</sup> , Ayca Busra Karatas<sup>1</sup> , Meltem Conk Dalay<sup>1</sup> 

<sup>1</sup> Ege University, Faculty of Engineering, Department of Bioengineering, 35040, Izmir, Türkiye

<sup>2</sup> Ege University, Ege University Application and Research Center for Testing and Analysis (EGE MATAL), 35040, Izmir, Türkiye

### Abstract

The aim of the study was to investigate the influence of physical conditions such as aeration rate (1, 3, 5 L/min) as well as chemical conditions including sodium nitrite (NaNO<sub>2</sub>), urea (CH<sub>4</sub>N<sub>2</sub>O) and ammonium chloride (NH<sub>4</sub>Cl) on the biomass productivity and fucoxanthin concentration of *A. capitellata*. The optimum cultures were cultivated in f/2 medium using sodium nitrate (NaNO<sub>3</sub>) in 2 L bubbling bottle photobioreactors under the light intensity of 100 μE/m<sup>2</sup>s with aeration rate of 2 L/min. All the bottles were then incubated at 22.0±2°C, under the light intensities of 300 μE/m<sup>2</sup>s with three different airflow rates of 1, 3, 5 L/min for 16 days. And then, culture medium was prepared with three different nitrogen sources to achieve higher biomass productivity. During the production of *A. capitellata*, the maximum specific growth rate of 0.166 day<sup>-1</sup>, which conformed to the doubling time of 4.166 day, was achieved at the light intensity of 300 μE/m<sup>2</sup>s with an aeration rate of 1 L/min when sodium nitrate was used. Chlorophyll-a and fucoxanthin contents were also at the highest level in the same light intensity. Dry biomass amount reached the maximum level of 0.66±0.17 g/L in case of NaNO<sub>2</sub>. In this study, it was defined that the airflow rate of 1 L/min, the light intensity of 300 μE/m<sup>2</sup>s and sodium nitrate (NaNO<sub>3</sub>) were the optimum values not only for the growth of *A. capitellata* cells but also for the production of biomass and a higher fucoxanthin concentration.

**Keywords:** *Amphora capitellata*; biomass; fucoxanthin; growth conditions; growth rate

### 1. Introduction

Microalgae have achieved much attention as an up-and-coming material because of being a source for high feedstock value industrial products such as food additives, biological fertilizers, aquaculture feedstocks, biofuels etc. that are manufactured from their cell mass. Additionally, microalgae are easily produced compared to terrestrial plant-derived products due to both short life cycle and requirement for a lower amount of land area. However, the limitation of microalgae production is its low mass productivity (Bayu et al., 2020; Nigam et al., 2022). Microalgal biomass productivity depends on nitrogen-rich nutrients included in the growth media and their valuable metabolites are important for biofuels, health care and foodstuffs

(Li et al., 2019).

Diatoms (Bacillariophyta) as eukaryotic microalgae are considered a crucially valuable source of chemicals, especially fatty acids, and carotenoids, in the aquaculture feedstock, food, pharmaceutical and nutraceutical industries. In addition, diatom frustules (silica cell walls) are the most interesting material to be used in nanotechnology. Diatoms are generally found widespread in aquatic ecosystems such as rivers, lakes, oceans, and marine areas which makes them frequently investigated sources for diatoms. Diatoms are either unicellular or multicellular microalgae with cell surfaces creating a siliceous skeleton including the frustule composed of amorphous silica [(SiO<sub>2</sub>)<sub>n</sub>(H<sub>2</sub>O)]. They are aquatic organisms that can move on their own in the water column (planktonic) and

\* Corresponding author.

E-mail address: [zelihademirel@gmail.com](mailto:zelihademirel@gmail.com) (Z. Demirel).

<https://doi.org/10.51753/flsrt.1125696> Author contributions

Received 03 June 2022; Accepted 24 September 2022

Available online 20 October 2022

2718-062X © 2022 This is an open access article published by Dergipark under the [CC BY](https://creativecommons.org/licenses/by/4.0/) license.

lie at the bottom of the underwater bed (benthic) (Brinkmann et al., 2011; Jamali et al., 2012; Cointet et al., 2019). The pennate diatom, *Amphora capitellata*, with a bilaterally asymmetrical valve, sized about 12-18  $\mu\text{m}$  in length and nearly 3-6  $\mu\text{m}$  in width is an isolated halophilic diatom at Izmir Bay, Aegean Sea (Demirel, 2016). Amphoroid taxa are acknowledged in the bright field microscope by their robustly dorsiventral shell outline; their linear ventral margin and raphe system are settled nearby place the ventral margin, and their girdle-band is a distinguishing characteristic group on the dorsal margin (Sato et al., 2013).

Environmental and other affecting factors may be curial on the algal biomass productivity, biomass compositions, and algal photosynthetic performance (Markou and Muylaert, 2016). Nitrogen can serve with a significant nutrient supply for the diatom growth and reproduction. It can have an effect on microalgae growth, subject to the amount, suitability, and type of the nitrogen source (Li et al., 2019).

Nitrogen is the second most vital element required for the cultivation of microalgae after carbon and performs a nitrogen cycle in the cellular processes-containing lipid and fucoxanthin production (Wang et al., 2018a). The major resources of nitrogen for the microalgae are inorganic nitrogen as nitrate, nitrite, ammonium, and many forms of organic nitrogen including urea, amino acids, are utilized for the synthesis of amino acids and proteins (Ruckert and Giani, 2004).

A large fraction of total ammonia nitrogen which consists of unionized ammonia ( $\text{NH}_3$ ) and ammonium ion ( $\text{NH}_4^+$ ) is unprotonated at higher pH values whereas ammonia strongly drops pH at high temperatures. The toxicity of  $\text{NH}_3$  in algae has also been reported (Markou and Muylaert, 2016; Ayre et al., 2017; Berg et al., 2017). Therefore, ammonium ( $\text{NH}_4^+$  or  $\text{NH}_3$ ) is the preferential nitrogen supply for different strains of microalgae, but the high level of ammonium nitrogen is toxic, inhibiting microalgae productivity. The reason for  $\text{NH}_3$  toxicity at alkaline pH in microalgae may be that the algae take in carbon dioxide due to the triggering of photosynthesis as a result of the inhibited photosystem due to high pH (Ayre et al., 2017) or it may perform photophosphorylation separately to reach a low pH to enable the conversion of ADP to ATP (Kumar and Bera, 2020). For microalgae cultivation, ammonium-based fertilizers at cheaper prices are preferred to other nitrogen sources fertilizers (Li et al., 2019).

The purpose of this study was to observe the influence of physical conditions such as aeration rate (1, 3, 5 L/min) in  $\text{NaNO}_3$  containing f/2 medium as well as chemical conditions including sodium nitrite ( $\text{NaNO}_2$ ), urea ( $\text{CH}_4\text{N}_2\text{O}$ ) and ammonium chloride ( $\text{NH}_4\text{Cl}$ ) on the biomass productivity and fucoxanthin concentration of *A. capitellata*. The growth rate, doubling time, biomass dry weight and fucoxanthin amount were detected at a continuous light intensity of  $300 \mu\text{E}/\text{m}^2\text{s}$  at the late phase of the batch production process. Variations of the aeration rate and nitrogen sources were used to measure the fucoxanthin content and cell morphology of diatom.

## 2. Materials and methods

### 2.1. Diatom and growth conditions

The strain was supplied from Ege University Microalgae Culture Collection with collection number of EGE MACC2 on agar-solidified f/2 medium for autotrophic cultivation.

The optimum cultures (control cultures) were cultivated in

f/2 medium using sodium nitrate ( $\text{NaNO}_3$ ) at the light intensity of  $100 \mu\text{mol}/\text{m}^2\text{s}$  with aeration rate of 2 L/min. The f/2 medium was prepared by Guillard's recipe and contained (per liter) 20 g of sea salt (Guillard and Ryther, 1962). The inoculum for all experiments was set at 10% volume in 2 L bubbling bottle photobioreactors. Cultures were then incubated at  $22.0 \pm 2^\circ\text{C}$ , continuously under the light intensities of  $300 \mu\text{E}/\text{m}^2\text{s}$  with three different air at rates of 1, 3, 5 L/min for 16 days.



**Fig. 1.** Cultivation of *A. capitellata* in prepared different nitrogen resources in f/2 medium.

After, different nitrogen sources (sodium nitrite ( $\text{NaNO}_2$ ), urea ( $\text{CH}_4\text{N}_2\text{O}$ ) and ammonium chloride ( $\text{NH}_4\text{Cl}$ )) were added to the culture media containing the same amount of nitrogen to evaluate their effects on *A. capitellata*. These were cultivated with airflow at rate of 1 L/min under the light intensities of  $300 \mu\text{E}/\text{m}^2\text{s}$  (Fig. 1). The optimum culture was cultivated in f/2 medium. The growth of diatom was observed by cell counting using an improved Neubauer haemocytometer. Diatom densities were measured every two days for 16 days using UV-Vis spectrophotometry at 600 nm. The observed maximal growth rate ( $\mu$ ) was calculated using Equation 1 (Sener et al., 2022). Based on the data for each experiment which contained three analytical replicates, the mean values with standard deviations were calculated.

$$\mu = (\ln X_b - \ln X_a) / (T_b - T_a) \quad \text{Eq. 1}$$

where  $\mu$ =specific growth rate,  $X_a$ =cell concentration at time  $T_a$ , and  $X_b$ =cell concentration at time  $T_b$ . Doubling time= $\ln 2/\mu$ .

Diatom cultures were precipitated by centrifugation (about 6000 rpm for 10 min) and then, the pellet was dried using lyophilization and dried pellet was placed in the freezer at  $-20^\circ\text{C}$ .

### 2.2. Fucoxanthin extraction and HPLC-DAD determination

For the extraction of fucoxanthin, a modified protocol reported in our previous study was applied. For this purpose, 0.20 g of dry biomass was weighed and 0.20 g of  $\text{CaCO}_3$  was added (Erdogan et al., 2022).

The mixture was treated using an ultrasonic bath for 15 minutes at  $40^\circ\text{C}$  (40 kHz, 300 W), and then the extracted sample was separated by centrifugation for 2 minutes at 5000 rpm. The supernatant was kept, and the precipitated was re-extracted (3 times) with fresh ethanol until decolourization of the biomass. Finally, all extraction solutions were combined and filtered by vacuum filtration using 47 mm of  $0.20 \mu\text{m}$  nylon filter paper. The mixed solution was evaporated using a rotary evaporator. The residue was resolved in chloroform stabilized with ethanol and kept at  $-20^\circ\text{C}$  prior to HPLC analysis. Fucoxanthin determination was performed with HPLC-DAD using YMC Carotenoid C<sub>30</sub> column (5  $\mu\text{m}$  particle size, L $\times$ ID 250 $\times$ 4.6 mm) at 450 nm with a flow rate of 1 mL/min according to the previous work performed by (Erdogan et al., 2016;

Erdogan et al., 2022).

### 3. Results and discussion

#### 3.1. Microalgae growth optimization

*Amphora capitellata* culture was used to explore the proper conditions for aeration, and light intensity, and also for revealing the effect of different nitrogen sources on enhanced biomass concentration, specific growth rate, and fucoxanthin content. In this study, an experimental approach was applied to maximize biomass concentration and fucoxanthin content in a bubbling bioreactor.

Fucoxanthin, a primary marine carotenoid, constitutes, over 10% of the approximate whole production of carotenoids on earth, and is the major carotenoid pigment existing in chloroplasts of microalgae, especially Bacillariophyta and Haptophyta, and macroalgae brown seaweeds. Fucoxanthin can harvest the light and transfer furthest 60% of the energy to chlorophyll-a in diatoms (Li et al., 2018; Roychoudhury et al., 2021). Physiological and biological properties of fucoxanthin are reported in lots of studies, such as having anticancer, antioxidant, antihypertensive, antiinflammatory, radioprotective, antiobesity, hepatoprotective activities (Maeda, 2013; Sun et al., 2018; Wang et al., 2018b; Mohamadnia et al., 2022).

Diatoms of microalgae, with nearly two-fold higher fucoxanthin amount than brown seaweed, are much more encouraging for fucoxanthin production. Bacillariophyta samples including *Phaeodactylum tricornerutum*, *Odontella aurita* and *Cyclotella cryptica* were studied at an industrial scale for utilization of their commercial productions of fucoxanthin (Wang et al., 2018b). The present study aims to survey the influence of various incident light intensities, aeration rates and nitrogen sources on biomass and fucoxanthin productivity in *A. capitellata*.

In the first experimental group, diatom was grown in f/2 medium using sodium nitrate ( $\text{NaNO}_3$ ) at the light intensity of  $100 \mu\text{E}/\text{m}^2\text{s}$  with an aeration rate of 2 L/min. The growth of diatom was not increased fucoxanthin content and then, diatom culture was exposed to increasing light intensity and various aeration rates. The highest irradiance treatment ( $300 \mu\text{E}/\text{m}^2\text{s}$ ) exposed the most fruitful growth rates and increased the fucoxanthin concentration of *A. capitellata*. It was found that four diatom culture treatments resulted in similar cell densities

during the growth (Fig. 2). However, treatments were determined to double increase the fucoxanthin content from  $6.36 \pm 0.12$  to  $19.66 \pm 0.39$  mg/g at  $300 \mu\text{E}/\text{m}^2\text{s}$  with different aeration rates. Considering the light-harvesting antennas of fucoxanthin chlorophyll binding proteins, it can be concluded that the production of this pigment and proteins enhanced the cultivation of the diatoms. Therefore, for the high-quality production of this precious material, optimal cultural conditions may be determined.

Adequate light intensity and nitrogen sources are required for the efficient production of microalgae. Because microalgal production is a process as a result from the transfer of the energy harvested from absorbed light to the photosynthesis complex (Mata et al., 2010), in theory, increased growth rate can be achieved with higher light intensities. However, both the growth and cell mass yield were diminished with the highest light intensity under phototropic conditions which may be explained by the photo-inhibition (Wang et al., 2018a). Increasing light intensity, the biomass and fucoxanthin concentration do not inhibit photosynthetic activity of *A. capitellata*. Meanwhile, the excessive light intensity cause photoinhibition and diminish the growth conditions. For this reason, light intensity could be calibrated to optimum conditions by the cell turbidity. Besides, several studies were reported that low light intensities were better than the relatively high light intensity on fucoxanthin yield and biomass concentration (Guo et al., 2016; Gómez-Loredo et al., 2016).

During the production, the maximum specific growth rate ( $0.166 \text{ day}^{-1}$ ) was reached with doubling time of 4.166 day, at the light level of  $300 \mu\text{E}/\text{m}^2\text{s}$  at an airflow rate of 1 L/min in  $\text{NaNO}_3$  as presented in Table 1. The highest biomass concentration ( $0.78 \text{ g/L}$ ) could be reached at airflow of 1 L/min in  $\text{NaNO}_2$ . On the other hand, the minimum fucoxanthin content ( $6.36 \pm 0.12 \text{ mg/g}$ ) was determined at airflow of 2 L/min and the light intensity of  $100 \mu\text{mol photons}/\text{m}^2\text{s}$  in  $\text{NaNO}_3$ . Chlorophyll-a and fucoxanthin amounts were also at the highest level in the same light intensity  $\text{NaNO}_3$ . In this study, it was identified that the airflow rate of 1 L/min and the light level of  $300 \mu\text{E}/\text{m}^2\text{s}$  were the optimum values for the growth of *A. capitellata* cells and production of biomass.

Nitrogen supply has a vital influence on biomass and fucoxanthin concentration. In the culture with the enhanced light level of  $300 \mu\text{E}/\text{m}^2\text{s}$ ,  $\text{NaNO}_3$  is consumed rapidly in f/2 medium. Light intensity and nitrogen supply affects not only cell mass productivity but also the quality of cells both physiologically

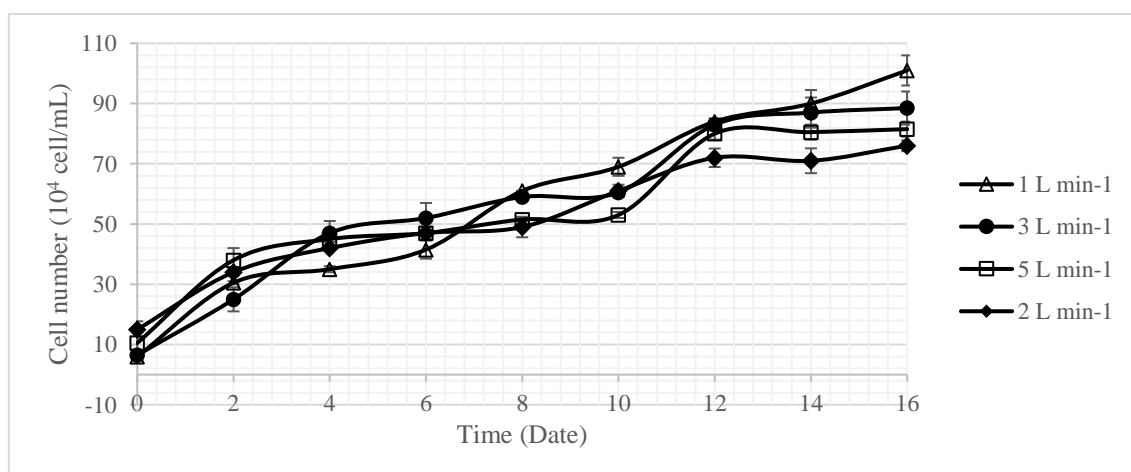


Fig. 2. Growth curves of *A. capitellata* in a photobioreactor under the light intensity of  $300 \mu\text{E}/\text{m}^2\text{s}$  at different aeration rates.

**Table 1**

Specific growth rate, biomass, fucoxanthin concentration and cell number of diatom cultivated with various nitrogen sources and different aeration rates.

	Fucoxanthin (mg/g)	Doubling time (day)	Growth rate (day <sup>-1</sup> )	Biomass (mg/L)	Cell number (10 <sup>6</sup> cell/mL)
NaNO <sub>3</sub> 2 L/min	6.36±0.12	4.864	0.143	0.31±0.05	7.1±0.2
NaNO <sub>3</sub> 1 L/min	19.66±0.39	4.166	0.167	0.36±0.17	10.1±0.9
NaNO <sub>3</sub> 3 L/min	17.97±0.35	4.416	0.157	0.29±0.15	8.9±0.6
NaNO <sub>3</sub> 5 L/min	19.29±0.38	4.659	0.149	0.28±0.18	8.2±0.3
NaNO <sub>2</sub> 1 L/min	9.64±0.19	2.7046	0.256	0.78±0.12	9.3±0.3
CH <sub>4</sub> N <sub>2</sub> O 1 L/min	10.11±0.20	6.7836	0.102	0.29±0.01	7.4±0.2
NH <sub>4</sub> Cl 1 L/min	11.88±0.24	16.1845	0.043	0.17±0.02	3.6±0.6

and morphologically. Alterations in cell morphology were observed with SEM photography analysis of diatom cells in sodium nitrite (NaNO<sub>2</sub>), urea (CH<sub>4</sub>N<sub>2</sub>O), ammonium chloride (NH<sub>4</sub>Cl) and nitrate seem to be in correlation with the observed alterations in chemical compositions (Figure 3-6). For instance, Kaspar et al. (2014) defined that the wide variety in cell size, and the changeable cell surface of *Chaetoceros calcitrans* grown in the culture were attributed to nutrient depletion in growth medium. This experiment proposed that the cell surface alteration could be a result of nutrient starvation. However, the relationship between the cell morphological state and the concentration of the fucoxanthin has not yet been well studied.

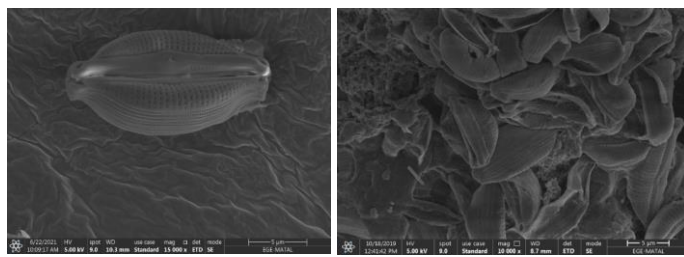


**Fig. 3.** SEM images of *A. capitellata* cultivated in f/2 medium prepared using sodium nitrate.

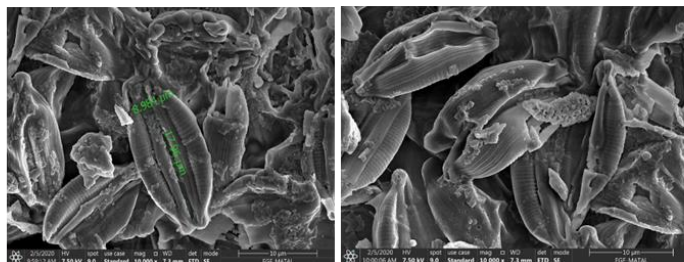


**Fig. 4.** SEM images of *A. capitellata* cultivated in f/2 medium prepared using sodium nitrite.

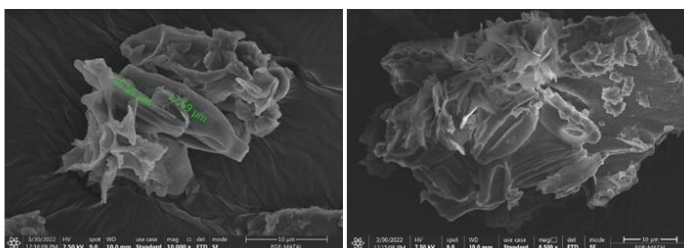


**Fig. 5.** SEM images of *A. capitellata* cultivated in f/2 medium prepared using urea.

Silica skeletons are the diatom walls existing as an envelope of the cell surface, called frustule/shell. The shells of diatoms are characteristic structure with a size and shape indicative of the morphological features of diatoms (Roychoudhury et al., 2016; Legalov and Reshetnikov, 2020).

As seen in Figs. 3-6, *A. capitellata* frustule alteration was observed with different nitrogen sources in f/2 media at an airflow rate of 1 L/min and light intensity of 300 μE/m<sup>2</sup>s. This study aims to measure morphological frustule changes in the monoalgal cultures of *A. capitellata* by cultivation in four different nitrogen sources (Fig. 3, 4, 5, 6). Amphora silica frustules are elliptic in shape with specific adornment and cells possess size pores hierarchically organized in curved bands in the cultivation both with NaNO<sub>3</sub> and NaNO<sub>2</sub>. Nevertheless, cultivated diatoms in urea and ammonium chloride do not clear frustule pores and shapes as seen in the Fig 5, and 6. The presence of macronutrients and micronutrients or pollutants is valuable in inducing frustule morphology changes. In both marine and freshwater diatoms changes in salinity alter the morphological traits of the silica valve (Hervé et al., 2012). In accordance with the results of these studies, our study indicated that the volume of silica frustule decreased in *Amphora* cell cultures grown in urea and ammonium.

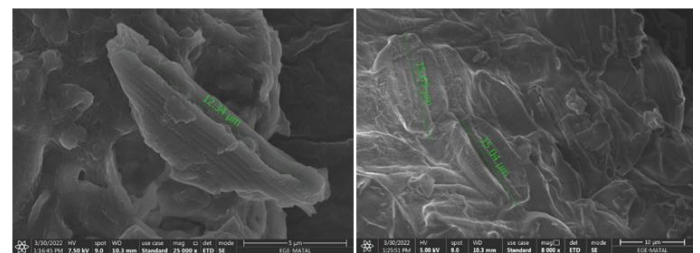


**Fig. 6.** SEM images of *A. capitellata* cultivated in f/2 medium prepared using ammonium chloride.

Diatoms absorb nitrogen from supplies such as nitrate, ammonia, and urea in the growth medium. When ammonium is utilized as the primary nitrogen source at high concentrations for algal cultivation, it causes a decrease in cell viability and may induce cell inhibition by diminishing the pH of the medium (Li et al., 2018, Kumar and Bera, 2020).

Among all treatments, the lowest fucoxanthin content (9.64±0.19 mg/g) was obtained in the same NaNO<sub>2</sub> containing medium where the maximum biomass concentration (0.78±0.12 mg/L) and growth rate (0.256 day<sup>-1</sup>) were achieved in bubbling photobioreactor. Compared to the other nitrogen sources, NaNO<sub>3</sub> significantly enhances the specific growth rate and fucoxanthin content. Diatom cells absorb nitrogen to grow at comparable rates nitrogen from supplies other than ammonium and urea. In a study, cultures of *Phaeodaetylum tricorutum* were cultivated in nitrate (NaNO<sub>3</sub>), nitrite (NaNO<sub>2</sub>), ammonium sulphate ((NH<sub>4</sub>)<sub>2</sub>SO<sub>4</sub>) or urea ((NH<sub>2</sub>)<sub>2</sub>CO), and all of them were prepared at 4 mg atom N/L concentration in media. Percentages of nitrogen in various media converted into cellular-nitrogen were determined by measuring productivities in dry weight of biomass nitrate, nitrite, urea and ammonia in cultures (Fidalgo

Paredes et al., 1995).

It was suggested that intracellular oxidative stress induced by increased concentration of ammonium could affect the specific activities of some enzymes and even cause deterioration of lipid peroxidation in cellular level. The primary function of microalgal pigments was to collect and convert light energy in the photosystems to generate the chemical energy required for the cultivation process. For this reason, inadequate energy induced by ammonia toxicity has been shown to block the photosynthesis of microalgal carotenoids (Li et al., 2019). Although the culture medium containing H<sub>2</sub>O<sub>2</sub>/NaOCl is known to cause oxidative stress by the formation of reactive oxygen species, the microalgal pigment of fucoxanthin was increased as 41.83±0.92 mg/g (Erdogan et al., 2022).

The nitrate transport metabolism pathway is similar to that of environmental plants, but their transport system was interesting to prove that diatoms have a metazoan-like urea cycle. Ammonia can be transported inside the cell by the nine ammonium transporters (AMTs). The nitrate transport mechanism by chloroplast using GSII-GOGAT and urea transport mechanism by mitochondrial using GSIII-GOGAT produce glutamine and glutamate, which must be transported from these organelles to replace nitrogen elsewhere in the cell (Smith et al., 2019).

Indrayani et al. (2020) reported that diatom *Amphora* sp. MUR 258 was investigated to grow over various temperatures and salinities with the aim of lipids and fatty acid profiles. The diatom obtained its highest specific growth rate (0.607 day<sup>-1</sup>) at 7% NaCl at 35°C, and its peak lipid concentration (57.69%) was observed at 7% NaCl at 25°C. In another study, *Cylindrotheca closterium*, *P. tricornutum*, *Amphora* sp., and *Thalassiosira weissflogii* were grown in photobioreactors under different physical conditions. The maximum growth rate of *C. closterium* was substantially enhanced compared to that of the other three

species at 20±1°C and a 12:12 light: dark by fluorescent light of 80 µE/m<sup>2</sup>s. Besides, the cultures of *C. closterium* was found to have increased fucoxanthin content (21 mg/g) compared to the other three diatoms (Wang et al., 2018b).

#### 4. Conclusion

In conclusion, diatoms are unicellular phytoplankton that is responsible for primary production in marine plants and plays an important role in biogeochemical cycling. The nutraceutical and cosmetic industries using diatom products have dealt with an investigation into the utilization of value-added compounds, especially fucoxanthin in the past few decades. Current study evaluated the influence of physical conditions such as aeration rate (1, 3, 5 L/min) in NaNO<sub>3</sub> containing f/2 medium as well as chemical conditions including sodium nitrite (NaNO<sub>2</sub>), urea (CH<sub>4</sub>N<sub>2</sub>O) and ammonium chloride (NH<sub>4</sub>Cl) on the biomass productivity and fucoxanthin concentration of *A. capitellata*. It is found that sodium nitrate is the potential chemical of the growth medium for *A. capitellata* to replace the nutrient supplies and growth conditions enhanced fucoxanthin productivity in the diatom with the light level of 300 µE/m<sup>2</sup>s and an airflow rate of 1 L/min.

**Acknowledgement:** This work was financial supported by Scientific and Technological Research Council of Turkey (TÜBİTAK)-COST Project number: 216Z167.

**Conflict of interest:** The authors declare that they have no conflict of interests.

**Informed consent:** The authors declare that this manuscript did not involve human or animal participants and informed consent was not collected.

#### References

- Ayre, J. M., Moheimani, N. R., & Borowitzka, M. A. (2017). Growth of microalgae on undiluted anaerobic digestate of piggery effluent with high ammonium concentrations. *Algal Research*, 24, 218-226.
- Bayu, A., Rachman, A., Noerdjito, D. R., Putra, M. Y., & Widayatno, W. B. (2020). High-value chemicals from marine diatoms: a biorefinery approach. *IOP Conference Series: Earth and Environmental Science*, West Java, Indonesia. 460(1), 012012.
- Berg, G. M., Driscoll, S., Hayashi, K., Ross, M., & Kudela, R. (2017). Variation in growth rate, carbon assimilation, and photosynthetic efficiency in response to nitrogen source and concentration in phytoplankton isolated from upper San Francisco Bay. *Journal of phycology*, 53(3), 664-679.
- Brinkmann, N., Friedl, T., Kathrin, I., & Mohr, K. I. (2011). Diatoms. In: Reitner, J., Thiel, V. (eds) *Encyclopedia of Geobiology* (pp. 1-956). Springer, Dordrecht.
- Cointet, E., Wielgosz-Collin, G., Méléder, V., & Gonçalves, O. (2019). Lipids in benthic diatoms: A new suitable screening procedure. *Algal Research*, 39, 101425.
- Demirel, Z. (2016). Identification and fatty acid composition of coccolithophore and diatom species isolated from Aegean Sea. *Romanian Biotechnological Letters*, 21(4), 11747-53.
- Erdogan, A., Demirel, Z., Dalay, M. C., & Eroglu, A. E. (2016). Fucoxanthin content of *Cylindrotheca closterium* and its oxidative stress mediated enhancement. *Turkish Journal of Fisheries and Aquatic Sciences*, 16(3), 489-497.
- Erdogan, A., Karatas, A. B., Demirel, Z., & Dalay, M. C. (2022). Purification of fucoxanthin from the diatom *Amphora capitellata* by preparative chromatography after its enhanced productivity via oxidative stress. *Journal of Applied Phycology*, 34(1), 301-309.
- Fidalgo Paredes, P., Cid, Á., Abalde, J., & Herrero, C. (1995). Culture of the marine diatom *Phaeodactylum tricornutum* with different nitrogen sources: growth, nutrient conversion and biochemical composition. *Cahiers de Biologie Marine*, 36, 165-173.
- Gómez-Loredo, A., Benavides, J., & Rito-Palomares, M. (2016). Growth kinetics and fucoxanthin production of *Phaeodactylum tricornutum* and *Isochrysis galbana* cultures at different light and agitation conditions. *Journal of Applied Phycology*, 28(2), 849-860.
- Guillard, R. R., & Ryther, J. H. (1962). Studies of marine planktonic diatoms: I. *Cyclotella nana* Hustedt, and *Detonula confervacea* (Cleve) Gran. *Canadian Journal of Microbiology*, 8(2), 229-239.
- Guo, B., Liu, B., Yang, B., Sun, P., Lu, X., Liu, J., & Chen, F. (2016). Screening of diatom strains and characterization of *Cyclotella cryptica* as a potential fucoxanthin producer. *Marine Drugs*, 14(7), 125-139.
- Hervé, V., Derr, J., Douady, S., Quinet, M., Moisan, L., & Lopez, P. J. (2012). Multiparametric analyses reveal the pH-dependence of silicon biomineralization in diatoms. *PLoS One*, 7(10), e46722.
- Indrayani, I., Moheimani, N. R., de Boer, K., Bahri, P. A., & Borowitzka, M. A. (2020). Temperature and salinity effects on growth and fatty acid composition of a halophilic diatom, *Amphora* sp. MUR258 (Bacillariophyceae). *Journal of Applied Phycology*, 32(2), 977-987.
- Jamali, A. A., Akbari, F., Ghorakhlu, M. M., de la Guardia, M., & Khosroushahi, A. Y. (2012). Applications of diatoms as potential microalgae in nanobiotechnology. *BioImpacts: BI*, 2(2), 83.
- Kaspar, H. F., Keys, E. F., King, N., Smith, K. F., Kesarcodi-Watson, A., & Miller, M. R. (2014). Continuous production of *Chaetoceros calcitrans* in a system suitable for commercial hatcheries. *Aquaculture*, 420, 1-9.
- Kumar, A., & Bera, S. (2020). Revisiting nitrogen utilization in algae: A review on the process of regulation and assimilation. *Bioresource Technology Reports*, 12, 100584.
- Legalov, A. A., & Reshetnikov, S. V. (2020). New records of weevils (Coleoptera, Curculionidae) from Western Siberia. *Acta Biologica Sibi-*

- rica, 6, 375.
- Li, C. L., Witkowski, A., Ashworth, M. P., Dąbek, P., Sato, S., Zgłobicka, I., ... & Kwon, C. J. (2018). The morphology and molecular phylogenetics of some marine diatom taxa within the Fragilariaceae, including twenty undescribed species and their relationship to *Nanofrustulum*, *Opephora* and *Pseudostaurosira*. *Phytotaxa*, 355(1), 1-104.
- Li, X., Li, W., Zhai, J., Wei, H., & Wang, Q. (2019). Effect of ammonium nitrogen on microalgal growth, biochemical composition and photosynthetic performance in mixotrophic cultivation. *Bioresource Technology*, 273, 368-376.
- Maeda, H. (2013). Anti-obesity and anti-diabetic activities of algae. In: Dominguez, H. (ed) *Functional Ingredients from Algae for Foods and Nutraceuticals* (pp. 453-472). Woodhead Publishing, Elsevier.
- Markou, G., & Muylaert, K. (2016). Effect of light intensity on the degree of ammonia toxicity on PSII activity of *Arthrospira platensis* and *Chlorella vulgaris*. *Bioresource Technology*, 216, 453-461.
- Mata, T. M., Martins, A. A., & Caetano, N. S. (2010). Microalgae for biodiesel production and other applications: a review. *Renewable and Sustainable Energy Reviews*, 14(1), 217-232.
- Mohamadnia, S., Tavakoli, O., & Faramarzi, M. A. (2022). Production of fucoxanthin from the microalga *Tisochrysis lutea* in the bubble column photobioreactor applying mass transfer coefficient. *Journal of Biotechnology*, 348, 47-54.
- Nigam, H., Jain, R., Malik, A., & Singh, V. (2022). Comparative Life-Cycle assessment of microalgal biomass production in conventional growth media versus newly developed nanoemulsion media. *Bioresource Technology*, 352, 127069.
- Ruckert, G. V., & Giani, A. (2004). Effect of nitrate and ammonium on the growth and protein concentration of *Microcystis viridis* Lemmermann (Cyanobacteria). *Brazilian Journal of Botany*, 27(2), 325-331.
- Roychoudhury, P., Nandi, C., & Pal, R. (2016). Diatom-based biosynthesis of gold-silica nanocomposite and their DNA binding affinity. *Journal of Applied Phycology*, 28(5), 2857-2863.
- Roychoudhury, P., Dąbek, P., Gloc, M., Golubeva, A., Dobrucka, R., Kurzydowski, K., & Witkowski, A. (2021). Reducing efficiency of fucoxanthin in diatom mediated biofabrication of gold nanoparticles. *Materials*, 14(15), 4094.
- Sato, S., Tamotsu, N., & Mann, D. G. (2013). Morphology and life history of *Amphora commutata* (Bacillariophyta) I: the vegetative cell and phylogenetic position. *Phycologia*, 52(3), 225-238.
- Smith, S. R., Dupont, C. L., McCarthy, J. K., Broddrick, J. T., Oborník, M., Horák, A., ... & Allen, A. E. (2019). Evolution and regulation of nitrogen flux through compartmentalized metabolic networks in a marine diatom. *Nature Communications*, 10(1), 1-14.
- Sun, Z., Dai, Z., Zhang, W., Fan, S., Liu, H., Liu, R., & Zhao, T. (2018). Antiobesity, antidiabetic, antioxidative, and antihyperlipidemic activities of bioactive seaweed substances. In: Qin Y. (ed) *Bioactive Seaweeds for Food Applications* (pp. 239-253). Academic Press.
- Sener, N., Demirel, Z., Imamoglu, E., & Dalay, M. (2022). Optimization of culture conditions for total carotenoid amount using response surface methodology in green microalgae/*Ankistrodesmus convolutus*. *Aquatic Sciences and Engineering*, 37(1), 29-37.
- Wang, H., Zhang, Y., Chen, L., Cheng, W., & Liu, T. (2018a). Combined production of fucoxanthin and EPA from two diatom strains *Phaeodactylum tricornutum* and *Cylindrotheca fusiformis* cultures. *Bioprocess and Biosystems Engineering*, 41(7), 1061-1071.
- Wang, S., Verma, S. K., Hakeem Said, I., Thomsen, L., Ullrich, M. S., & Kuhnert, N. (2018b). Changes in the fucoxanthin production and protein profiles in *Cylindrotheca closterium* in response to blue light-emitting diode light. *Microbial Cell Factories*, 17(1), 1-13.

**Cite as:** Demirel, Z., Erdogan, A., Karatas, A. B., & Conk Dalay, M. (2022). Effect of different abiotic conditions on biomass and fucoxanthin content of *Amphora capitellata*. *Front Life Sci RT*, 3(3), 107-112.



## Research article

# Self-assembling of surface active drug amitriptyline hydrochloride in association with additives: Role of surface activity in the pharmaceutical applications

Hasan Tolga Ozcam<sup>1,2,3</sup> , Zeynep Berna Tamer<sup>1,2</sup> , Sinem Gokturk\*<sup>1</sup> 

<sup>1</sup> Marmara University, Faculty of Pharmacy, Department of Basic Pharmaceutical Sciences, General Chemistry Division, Basibuyuk, 34854, Istanbul, Türkiye

<sup>2</sup> Marmara University, Institute of Health Sciences, Pharmaceutical Basic Sciences, General Chemistry Msc Program, Dragos, 34865 Kartal, Istanbul, Türkiye

<sup>3</sup> Camormanı Biyoteknoloji San. Tic. Ltd. Şti. Yapı Kredi Plaza, 34330, Levent, Istanbul, Türkiye

## Abstract

The self-assembling of surface active antidepressant drug amitriptyline hydrochloride (AMT) has been studied to determine the micellar solution behavior in the presence of polar (methanol and ethanol), dipolar aprotic solvents (acetone and 1,4 dioxane), salt (NaCl) and water structure-breakers (urea) at 298 K using surface tension and electrical conductivity measurements. The counterion binding parameter and the ionization degree of AMT micelles have been determined by electrical conductivity measurements. To better analyze the influences of additives on micellar behavior of AMT, surface features of AMT were defined using Gibbs Adsorption Isotherm in water and in association with various amounts of additives conducted by surface tension measurements. Both conductometric and surface tension experiments were also used to detect the critical micelle concentration (CMC) of AMT. The experimental results indicated that CMCs of AMT were influenced in the presence of additives. Self-aggregation of AMT was totally inhibited when methanol, ethanol, acetone, 1,4 dioxane, and urea concentration is attained to a certain value while the CMC of AMT reduced with the increase in concentration of NaCl.

**Keywords:** Amitriptyline hydrochloride; amphiphilic drugs; conductivity; critical micelle concentration; surface active drugs; surface tension

## 1. Introduction

Most of drug molecules are surface active and tend to aggregate in aqueous solution due to their surface activities and these features of them relate well with their pharmacological action (Attwood and Florence, 1983; Attwood et al., 1989; Attwood, 1995; Schreier et al., 2000; Taboada et al., 2000; Junquera et al., 2001; Srivastava and Nagappa, 2005; Alam et al., 2008). Amitriptyline hydrochloride (AMT), one of the surface active drugs, is a member of tricyclic antidepressant

drugs (TCA). There is an alkyl amine side chain in its molecular structure conferring on “surfactant-like” behavior with its planar tricyclic ring system (Fig. 1). Among the numerous studies of amphiphilic drugs, the study of their aggregation properties represent an area of continued research interest (Din et al., 2010; Ali et al., 2013; Rub et al., 2013, 2014; Sharma et al., 2014). Within this scope, excellent studies on micellization behavior of AMT are already available, thus this study aims to make an effort to indicate effects of additives which are contributing to the mechanism of surface activity on micelle formation of AMT

\* Corresponding author.

E-mail address: [sinengokturk@gmail.com](mailto:sinengokturk@gmail.com) (S. Gokturk).

<https://doi.org/10.51753/flsrt.1131218> Author contributions

Received 15 June 2022; Accepted 26 September 2022

Available online 20 October 2022

2718-062X © 2022 This is an open access article published by Dergipark under the [CC BY](https://creativecommons.org/licenses/by/4.0/) license.

in detail. Surface activity of AMT also relates with its pharmacological action because of exerting its activity by interacting with biological membranes. Furthermore, the mechanism of the self-assembling of amphiphilic drugs plays a crucial role in the pharmaceutically important process such as drug delivery systems. However, it is essential to have extent practice of the process about the associations of drugs since drugs are always used in combination with different additives (Erdinc et al., 2010; Alam et al., 2011; Gokturk and Var, 2012; Ozcam, 2015; Ozan and Gokturk, 2021). This study deals with describing the association of AMT with the additives in order to express the effects of additives on micellization behavior and interfacial properties of AMT using surface tension and conductivity measurements. Both of these methods were performed to observe the micelle formation of AMT alone and in the presence of various amounts of methanol (MeOH), ethanol (EtOH), acetone (Ace), dioxane (Diox), urea, and NaCl in aqueous media at 298 K. MeOH and EtOH which form H bonds with water were used to examine the effect on micelle formations of AMT. To see the influence of dipolar aprotic solvents on micelle formation of AMT Ace and Diox which form strong H bonds with water were used. Urea, known as a water structure breaker, were also used to see its effect on the micelle formation mechanism of AMT. In order to find out the effect of physiologic additives such as salt utilized in drug administration, similar experiments were employed in the presence of 0.45% (w/v), 0.9% NaCl (w/v).

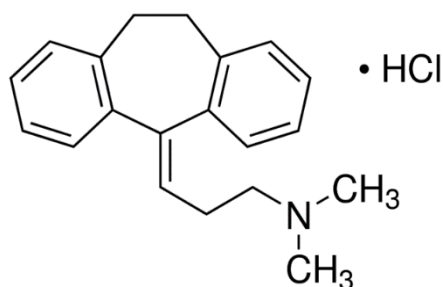


Fig. 1. Chemical structure of AMT.

## 2. Materials and methods

AMT was provided from Sigma (Germany) using without purification (>98.0% purity). Methanol (MeOH), ethanol (EtOH), acetone (Ace), dioxane (Diox), and urea were purchased from E. Merck. NaCl was supplied from Merck. The chemicals are spectroscopic grade products. All experiments were performed with doubly distilled conductivity water.

Micellization of AMT in the presence of various amount of MeOH, EtOH, Ace, Diox, urea, and NaCl have been studied and the experiments were conducted by surface tension and electrical conductivity measurement analyses at 298 K.

### 2.1. Surface tension measurements

Sigma 701 KSV Instruments computer-controlled tensiometer (Helsinki, Finland) was used to study surface tension measurements. The Wilhelmy-plate method was employed. The presented surface tension values in this study are mean quantities and all surface tension reading were taken in triplicate. The standard deviation of the mean did not deviate  $\pm 1.1\%$ . The accuracy of measurements within was 0.01 mN/m. The data of surface tension of AMT in water and the presence of

various amounts of additives were used to specify the minimum area per molecule ( $A_{min}$ ) and maximum surface excess concentration ( $\Gamma_{max}$ ) of surface active drug AMT based on a plot of the surface tension ( $\gamma$ ) against AMT concentrations in water and in the presence of additives. Gibbs Adsorption Isotherm was applied to analyze the changes of surface properties i.e.  $\Gamma_{max}$  and  $A_{min}$ . Here, C is the concentration of AMT, T is the temperature in Kelvin and R is the gas constant.

$$\Gamma_{max} = -\frac{1}{RT} \left( \frac{d\gamma}{d \ln C} \right) \quad (1)$$

$A_{min}$  ( $\text{\AA}^2$  molecule $^{-1}$ ) is determined from the value of  $\Gamma_{max}$  by the Eq.2. ( $N_A$  is the Avogadro constant);

$$A = \frac{1}{N_A \Gamma_{max}} \quad (2)$$

(Florence and Atwood 1998; Gokturk and Tamer, 2018).

### 2.2. Electrical conductivity measurements

WTW Inolab (pH/Cond 740) (automatic temperature compensated) conductivity meter were used for electrical conductivity measurements. The cell constant is  $1.0 \text{ cm}^{-1}$  with  $\pm 1\%$  uncertainty in measurement. Standard KCl solutions was used to calibrate the constant of the conductivity cell and checked at least three times during the study. The specific conductivity ( $\kappa$ ) measurements provided useful knowledge on the electrical conductivity of the AMT solutions in water and in the presence of additives. The conductometric method describes the concentration dependence of conductivity on the basis of attaining of a breaking point on the curves. The breaking point seen in the plot corresponds to micelle formation. There are two straight lines having different slopes in the concentration dependence of specific conductivity ( $\kappa$ ) plots. From these plots, the counterion binding parameter ( $\beta$ ) can be determined from the ratio of the slopes of the two intersecting lines. The values of the ionization degree of the micelles ( $\alpha$ ) can also be calculated by;

$$\beta = 1 - \alpha \quad (\text{Hiemenz and Rajogopalan, 1986; Gokturk and Aslan, 2014}).$$

## 3. Results and discussion

The CMC of amphiphilic drug AMT was determined by measuring a change in the surface tension and electrical conductivity with various concentrations of AMT in water and in the presence of additives as described in detail previously (Florence and Atwood 1998; Gokturk and Aslan, 2014; Gokturk and Tamer, 2018). The CMC of AMT obtained through different measurements are consistent with the values in literature ( $3.48 \times 10^{-2} \text{ mol/L}$ ) (Schreier et al., 2000). The CMC values of AMT determined by conductometry and tensiometry techniques in water and the presence of additives were presented in Table 1. The micellization characteristics of AMT in the absence and presence of additives in aqueous solutions have been conducted by (i) surface tension, and (ii) electrical conductivity measurements, and the effects of various concentrations of additives (MeOH, EtOH, Diox, Ace, urea and NaCl) on micellar and interfacial properties of AMT were discussed.

**3.1. Determination of surface properties of AMT ( $\Gamma_{max}$  and  $A_{min}$ )**

The influence of additives on the interfaces of AMT has been detected by using surface tension measurements. The surface excess amount of AMT was found by applying the Gibbs adsorption isotherm (Eq. 1 and Eq. 2). The effects of additives on surface properties of amphiphilic drug AMT were plotted by the surface tension ( $\gamma$ ) against AMT concentration (Fig. 2, 3, 4, 5, 6 and 7). The values of AMT obtained from tensiometry in the presence of additives were observed to be lower than those in the absence of all amount of studied additives except for urea.

As seen in Fig. 2, 3, 4 and 5, with the increase in MeOH, EtOH, Diox and Ace concentrations, micellization of AMT diminished, and inhibited at the additive concentration of 10 % (v/v). As presented in Table 1, the presence of NaCl decreased the CMC of AMT. On the other hand, the CMC of AMT increased in the presence of MeOH, EtOH, Diox and Ace. In the case of urea there was seen no significant decrease in surface tension values of AMT. However, the CMC of AMT increased depending on the urea concentration due to its modifying influence on the aqueous solution properties.

The adsorbed amount and the adsorbed area of AMT were specified based on Eq. 1. Applying Gibbs Equation to determine

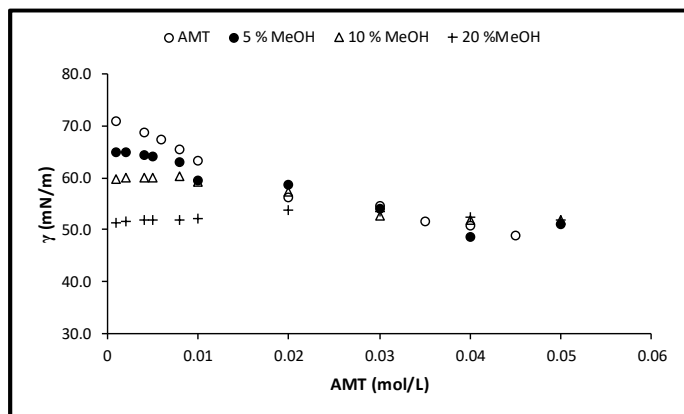


**Fig. 2.** Surface tension measurements vs. molar concentration of AMT in water and the presence of 5, 10 and 20 % (v/v) MeOH at 298 K.

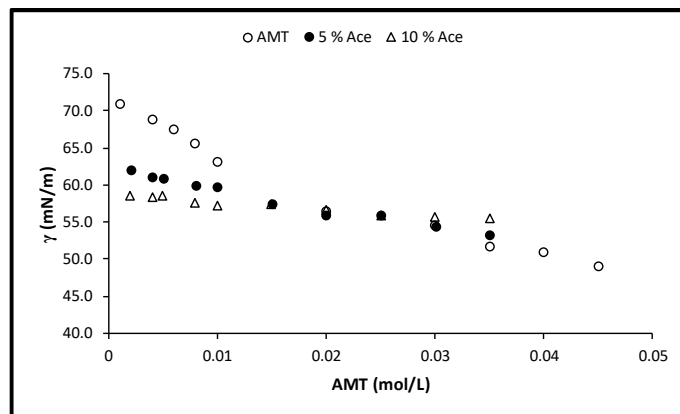


**Fig. 5.** Surface tension measurements vs. molar concentration of AMT in water and the presence of 5 and 10 % (v/v) Ace at 298 K.

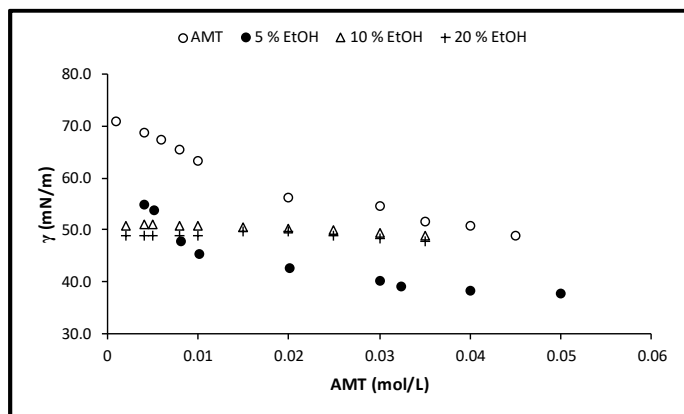


**Fig. 3.** Surface tension measurements vs. molar concentration of AMT in water and the presence of 5, 10 and 20 % (v/v) EtOH at 298 K.

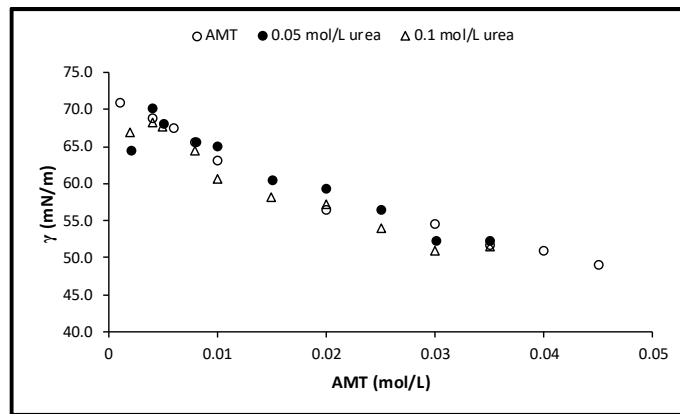


**Fig. 6.** Surface tension measurements vs. molar concentration of AMT in water and the presence of 0.05 M and 0.1 mol/L urea at 298 K.

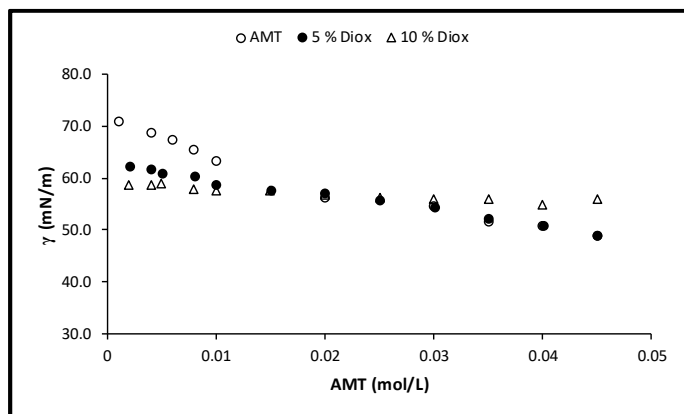


**Fig. 4.** Surface tension measurements vs. molar concentration of AMT in water and the presence of 5 and 10 % (v/v) Diox at 298 K.

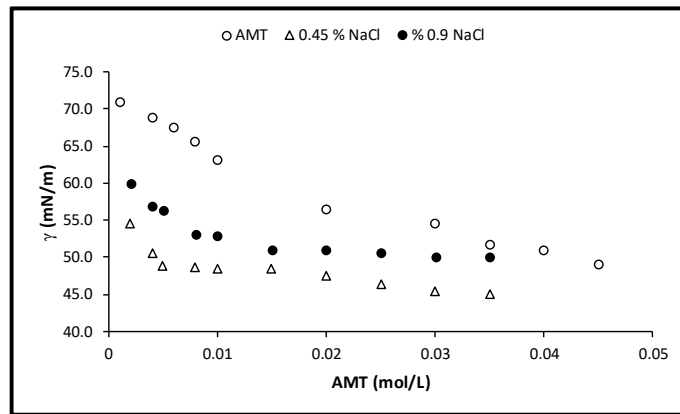


**Fig. 7.** Surface tension measurements vs. molar concentration of AMT in water and the presence of 0.45 and 0.9 (w/v) NaCl at 298 K.

quantitative surface properties was depicted in Fig. 8 and 9 for EtOH and NaCl, respectively, as representative plots. Table 1 indicates the calculated  $\Gamma_{max}$  and  $A_{min}$  values. As seen in the data given in Table 1  $\Gamma_{max}$  value of AMT was reduced and  $A_{min}$  increased in the presence of various amounts of additives. The change in tensiometry values and estimated surface parameters showed the incorporation tendency of AMT increased in the presence of additives. This can be explained by the addition of additives decreasing the electrostatic repulsion between the head groups of AMT, and thereby incorporating much more AMT molecules at the interface. This is correlated with the fact that greater value of  $A_{min}$  i.e. additives increased the penetration of AMT at the interface. No marked shift on surface parameters of AMT observed in the presence of urea which can also be explained by its superior water structure breaker properties for the interaction of AMT compared to that of MeOH, EtOH, Ace, Diox and NaCl.

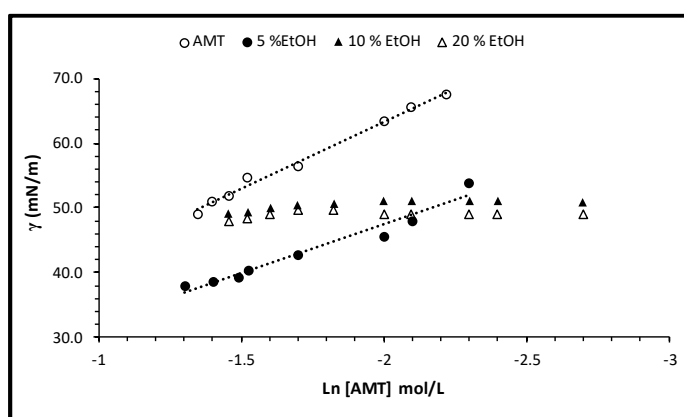


Fig. 8. Gibbs Adsorption Isotherm plots of AMT in water and the presence of 5, 10 and 20 % EtOH at 298 K.

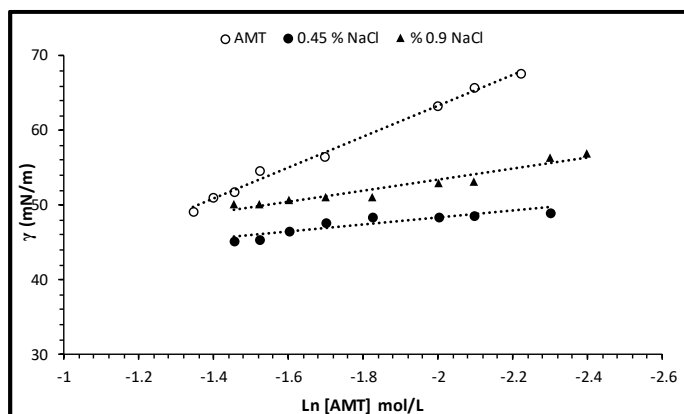


Fig. 9. Gibbs Adsorption Isotherm plots of AMT in water and the presence of 0.45 and 0.9 % (w/v) NaCl at 298 K.

### 3.2. Determination of degrees of ionization and counterion binding parameter ( $\alpha$ and $\beta$ )

In order to see the influence of electrostatic interactions on solution behavior of AMT molecules conductivity measurements were performed. For this purpose, variation of conductivity of AMT was monitored in the absence and presence of various concentrations of additives in aqueous solutions. The measured specific conductivities were plotted versus the AMT concentration. Since the same behavior was observed, only the influence of various concentrations of EtOH,

Diox and NaCl on the electrochemical properties of AMT are shown in Figs. 10, 11 12 and 13 respectively, as representative plots. As seen in these figs. there is a significant loss of ionic charges since a fraction of the counterions is limited to the micellar surface.

$\beta$  values estimated from the ratio of the slopes gives the average number of counterions per AMT ion in the micelle (Evans, 1956; Rosen, 1978; Gokturk and Aslan, 2014). Calculated  $\alpha$  and  $\beta$  values of AMT were listed in Table 1. In the presence of additives, the same behavior has been observed.  $\beta$  values increased and  $\alpha$  values decreased in comparison with the absence of additives in solutions.

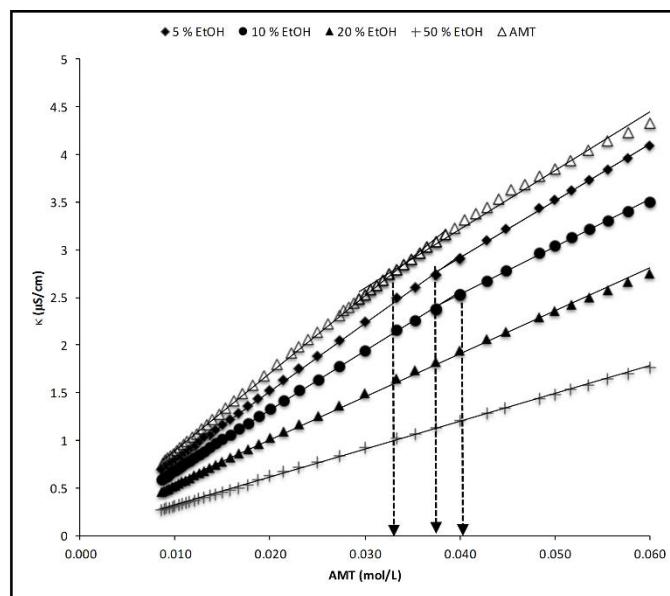


Fig. 10. Specific conductivity vs. molar concentration of AMT in water and the presence of 5, 10, 20 and 50 % (v/v) EtOH and CMC at 298 K (arrows show the CMC).

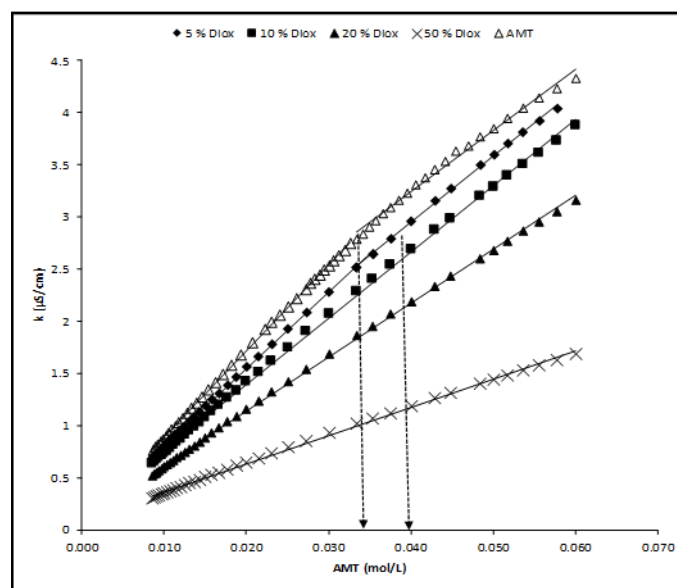
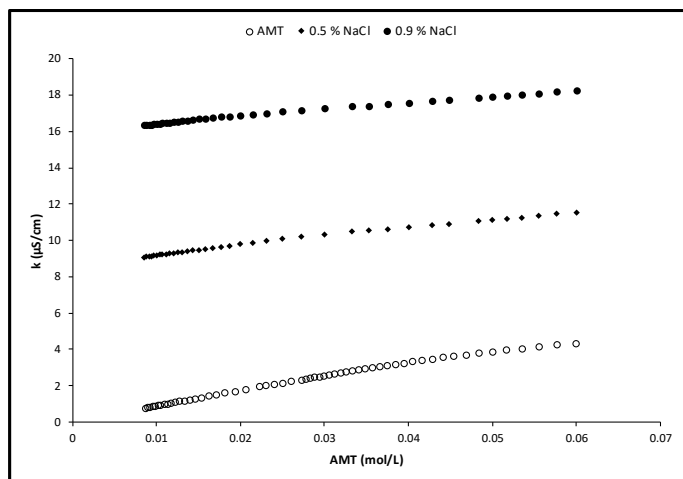


Fig. 11. Specific conductivity vs. molar concentration of AMT in water and the presence of 5, 10, 20 and 50 % (v/v) Diox and CMC at 298 K (arrows show the CMC).

The rate of neutralized charges in a micelle to the total number of surfactant molecules in the micellar phase is defined

as the incorporation degree of counterion to the micelle (Stellner and Scamehorn, 1989). The surfactant molecules show different behavior in aqueous solutions depending on their concentration. The low concentration of surfactant solutions behaves as simple electrolyte that involve free monomers in the aqueous solutions. Besides, solution behavior changes with the increase in surfactant concentration. At the concentrations above the CMC, most of the surfactant molecules aggregate to form micelles and the total monomer concentration remains almost constant. Accordingly, after the CMC the gradient of conductivity decreases which means that a larger area of micelle surface, for a certain amount of counterions and the incorporation of additives to AMT micelles occurs more remarkably.



**Fig. 12.** Specific conductivity vs. molar concentration of AMT in water and the presence of 0.45 and 0.9 % (w/v) NaCl at 298 K.

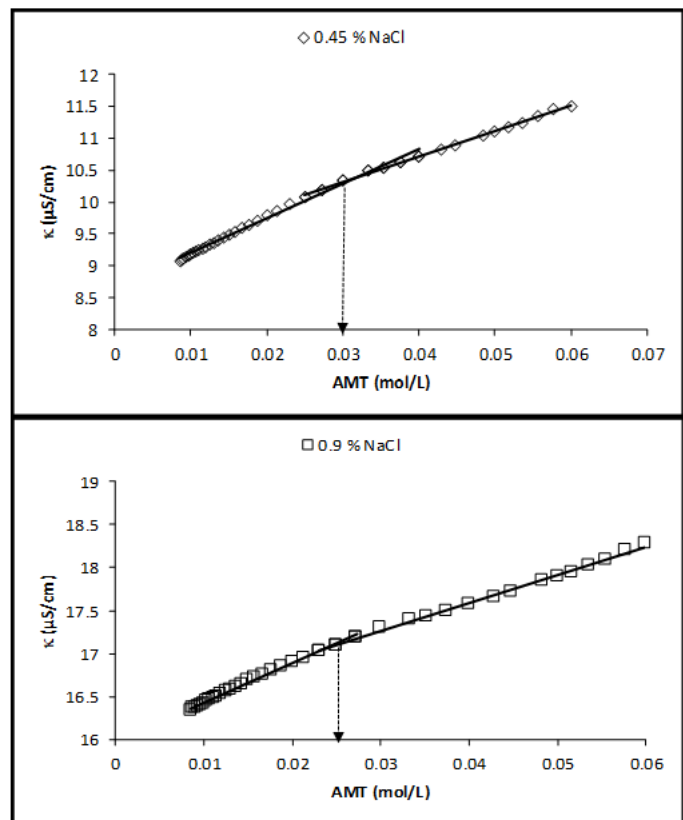


**Fig. 13.** Specific conductivity vs. molar concentration of AMT in water and the presence of 0.45 and 0.9 % (w/v) NaCl and CMC at 298 K (arrows show the CMC).

It is well known that organic and inorganic additives significantly influence the properties of surfactant solutions, especially CMC and micellization (Atwood and Florence, 1998). Studies on mixed alcohol-water systems have gained more attention due to their interest for designing of micro-emulsions (Liu and Guo, 2007). These studies reported that the association of alcohols with the micelles produces significant alteration in the micellar shape and their transport properties. The blocking effect of cosolvent and diminishing micellization at a certain concentration can be accounted for by reducing hydrophobic forces due to its destructive action on structured water molecules around the hydrophobic parts of the surfactant (Zana, 1995).

The decrease in both conductivity and surface tension values of AMT in the presence of various concentrations of MeOH, EtOH, Ace and Diox supports this assessment. Apart from preferential solvation of AMT in these cosolvents, changing water structure, alteration the polarity of the media (dielectric constant), cohesive energy changing are such responsible factors on diminishing micellization of AMT and inhibiting it at a certain concentration.

On the contrary, presence of NaCl decreased the CMC value of AMT, while the presence of urea increased the CMC of AMT (Table 1). The CMC of ionic surfactants reduces in the presence of inorganic salts. The addition of inorganic salt causes to break the hydration film and so the diffuse double is packed in the region of the ionic head groups. Monomers in the micellar surface layer can aggregate more closely, accordingly micelle formation can be formed easily at lower concentrations because of the decreasing the electrostatic repulsion with the addition of salt (Rosen, 1978).

However, as seen in Table 1, an increment in the CMC of AMT in the presence of urea can be expressed by the disruptive power of the iceberg structure, except for any big alteration in the micellar state by reducing the standard chemical potential. The increase in CMC suggests a decrease in hydrophobic attraction, followed by a great increase in the solubility of the hydrocarbon tails in the participation of urea. Based on the direct mechanism, urea increases the solubility of hydrophobic solutes which is attributed to an enhanced solvation as a result of the dislocation of the water molecules by a large number of urea molecules in the solvation layer (Kuharski and Rosky, 1984; Mizutani et al., 1989).

#### 4. Conclusions

In this study, using surface tension and conductivity measurements provided useful and important information on the effect of additives for micellization process of AMT in aqueous media. The experimental results obtained from surface tensiometry studies are compatible with electrical conductivity measurements. The CMC of AMT increased with the addition of MeOH, EtOH, Ace and Diox in different concentrations, and micellization of AMT were totally inhibited at an exact concentration of cosolvents (~10% in volume). Obtained from conductivity measurements, it was determined that the value of counterion binding parameter ( $\beta$ ) increased and  $\alpha$  values decreased. This can be supported by the data obtained from surface tension measurements.  $\Gamma_{max}$  of AMT decreased and  $A_{min}$  increased with the addition of MeOH, EtOH, Ace and Diox (v/v).

The self-aggregation of surface active molecules is expla-

**Table 1**

CMC values and estimated parameters for AMT by conductometry and surface tension measurements in water and the presence of additives at 298 K.

MeOH % (v/v)	Conductivity			Surface tension		
	$\alpha$	$\beta$	CMC (mol/L)	$\Gamma_{max}$ (mmol/m <sup>2</sup> )	$A_{min} \times 10^{-2}$ ( $\text{\AA}$ ) <sup>2</sup>	CMC (mol/L)
0	0.2776	0.7224	$3.48 \times 10^{-2}$	8.380	1.982	$3.50 \times 10^{-2}$
5	0.2133	0.7867	$3.55 \times 10^{-2}$	6.196	2.680	$3.55 \times 10^{-2}$
10	0.1788	0.8211	$3.75 \times 10^{-2}$	4.026	4.120	$4.00 \times 10^{-2}$
20	-	-	-	-	-	-
50	-	-	-	-	-	-
EtOH % (v/v)	$\alpha$	$\beta$	CMC (mol/L)	$\Gamma_{max}$ (mmol/m <sup>2</sup> )	$A_{min} \times 10^{-2}$ ( $\text{\AA}$ ) <sup>2</sup>	CMC (mol/L)
0	0.2776	0.7224	$3.48 \times 10^{-2}$	8.380	1.982	$3.50 \times 10^{-2}$
5	0.1807	0.8193	$3.75 \times 10^{-2}$	6.029	2.750	$3.70 \times 10^{-2}$
10	0.1754	0.8246	$4.00 \times 10^{-2}$	-	-	-
20	-	-	-	-	-	-
50	-	-	-	-	-	-
Acetone % (v/v)	$\alpha$	$\beta$	CMC (mol/L)	$\Gamma_{max}$ (mmol/m <sup>2</sup> )	$A_{min} \times 10^{-2}$ ( $\text{\AA}$ ) <sup>2</sup>	CMC (mol/L)
0	0.2776	0.7224	$3.48 \times 10^{-2}$	8.380	1.982	$3.50 \times 10^{-2}$
5	0.1619	0.8381	$4.20 \times 10^{-2}$	3.680	4.510	$4.0 \times 10^{-2}$
10	-	-	-	-	-	-
20	-	-	-	-	-	-
50	-	-	-	-	-	-
Diox % (v/v)	$\alpha$	$\beta$	CMC (mol/L)	$\Gamma_{max}$ (mmol/m <sup>2</sup> )	$A_{min} \times 10^{-2}$ ( $\text{\AA}$ ) <sup>2</sup>	CMC (mol/L)
0	0.2776	0.7224	$3.48 \times 10^{-2}$	8.380	1.982	$3.50 \times 10^{-2}$
5	0.1585	0.8415	$4.00 \times 10^{-2}$	3.807	4.360	$4.50 \times 10^{-2}$
10	-	-	-	-	-	-
20	-	-	-	-	-	-
50	-	-	-	-	-	-
Urea (mol/L)	$\alpha$	$\beta$	CMC (mol/L)	$\Gamma_{max}$ (mmol/m <sup>2</sup> )	$A_{min} \times 10^{-2}$ ( $\text{\AA}$ ) <sup>2</sup>	CMC (mol/L)
0	0.2776	0.7224	$3.48 \times 10^{-2}$	8.380	1.982	$3.50 \times 10^{-2}$
0.05	0.2869	0.7137	$4.00 \times 10^{-2}$	7.412	2.240	$4.00 \times 10^{-2}$
0.1	0.3025	0.6975	$4.50 \times 10^{-2}$	7.142	2.320	$4.50 \times 10^{-2}$
1.0	0.2281	0.7719	$5.00 \times 10^{-2}$	7.210	2.450	$5.0 \times 10^{-2}$
NaCl % (w/v)	$\alpha$	$\beta$	CMC (mol/L)	$\Gamma_{max}$ (mmol/m <sup>2</sup> )	$A_{min} \times 10^{-2}$ ( $\text{\AA}$ ) <sup>2</sup>	CMC (mol/L)
0	0.2776	0.7224	$3.48 \times 10^{-2}$	8.380	1.982	$3.48 \times 10^{-2}$
0.45	0.3399	0.6601	$3.00 \times 10^{-2}$	1.868	8.890	$3.00 \times 10^{-2}$
0.9	0.3000	0.6999	$2.50 \times 10^{-2}$	2.976	5.580	$2.00 \times 10^{-2}$

ined by hydrophobic association within the nonpolar hydrocarbon part, and the electrostatic attraction of the ionic polar head groups thereby forming aggregates. The tendency of micelle formation in the presence of polar solvents, instead of water, is called solvophobic interaction. The Gibbs free energy of the system decreases due to micelle formation in the aqueous media, associating the hydrophobic parts of the surfactant molecules and repelling the water molecules around them. The main factor directing micelle formation in aqueous solution is entropy. The water structure, which is organized around the surface active molecules, returns to its former disorder with the formation of micelles. Based on these statements reduction in conductivity values of AMT in the presence of MeOH, EtOH, Ace and Diox can be explained by solvophobic interaction. As a matter of fact, the same solvents rise the CMC of AMT up to a certain concentration and then diminished micelle formation which can be explained by decreasing the intermolecular attraction density of water or the solubility parameter. The presence of MeOH, EtOH, Ace, and Diox lower the dielectric constant of the medium, increasing the repulsion between the ionic head groups in the ionic AMT micelles, thus increasing

CMC and making micelle formation difficult. It is also well known that entropy change is an important factor in micelle formation in aqueous media. Therefore, urea was used as a water structure breaker in order to see its influence on the structure of water. The presence of urea also increased the CMC of AMT due to increased hydration of the hydrophilic group with the breaking down of the water structure and making micellization difficult. The presence of electrolytes in aqueous media caused a reduction in the CMC of AMT, since especially ionic surface active agents are very sensitive to small changes in the ionic strength of aqueous solutions as in the case of cationic amphiphilic drug AMT. The presence of NaCl in the environment decreases the CMC by decreasing the electrostatic repulsion between the head groups of AMT due to the screening effect. Thereby, adding different concentrations of NaCl to ionic AMT solutions reduced the CMC since less electricity is required for micelle formation. In case of NaCl, the rise in conductivity values of AMT can be explained by an increase the salt concentration decreasing the electrical repulsions and affecting the balance of the forces on which the micelle size is dependent and causing the micelle size to grow.

Surface tension measurements provided very useful information on the surface activity of amphiphilic drug molecule AMT at surfaces and interfaces that elucidate the penetration behavior of AMT molecules at air-liquid interface in the absence and presence of additives. Decreasing  $\Gamma_{max}$  values and increasing  $A_{min}$  values can be attributed to the presence of additives increasing the incorporation of AMT at the interface. The higher  $A_{min}$  and the lower  $\Gamma_{max}$  values are consistent with  $\beta$  and  $\alpha$  parameters obtained from conductivity measurements. All parameters obtained from both experimental techniques supported that amphiphilic AMT molecules can be incorporated at the interface.

The results presented in this study can provide important knowledge in elucidating the role of additives that contribute to their practice in the relevant pharmaceutical processes as active pharmaceutical additives. The determination of interfacial properties of amphiphilic drugs and their associations with pharmaceutically important additives are considered significant

## References

- Alam, M. S., Ghosh, G., & Din, K. (2008). Light scattering studies of amphiphilic drugs promethazine hydrochloride and imipramine hydrochloride in aqueous electrolyte solutions. *The Journal of Physical Chemistry B*, 112(41), 12962-12967.
- Alam, S., Mandal, A., & Mandal, A. B. (2011). Thermodynamics of amphiphilic drug imipramine hydrochloride in presence of additives. In: Moreno-Piraján J. C. (ed) *Thermodynamics-Systems in Equilibrium and Non-Equilibrium* (pp. 229-254). IntechOpen.
- Ali, M. S., Rub, M. A., Khan, F., & Al-Lohedan, H. A. (2013). Thermodynamic, interfacial and hydrodynamic aspects of interaction of cationic drug amitriptyline hydrochloride with anionic and nonionic polymers. *Journal of Molecular Liquids*, 180, 200-206.
- Attwood, D., & Florence, A. T. (1983). *Surfactant systems: Their chemistry, pharmacy and biology*. (pp. 1-794). New York, Chapman and Hall.
- Attwood, D. (1995). The mode of association of amphiphilic drugs in aqueous solution. *Advances in colloid and interface science*, 55, 271-303.
- Attwood, D., Mosquera, V., & Villar, V. P. (1989). Thermodynamic properties of amphiphilic drugs in aqueous solution. *Journal of the Chemical Society, Faraday Transactions 1: Physical Chemistry in Condensed Phases*, 85(9), 3011-3017.
- Din, K., Rub, M. A., & Naqvi, A. Z. (2010). Mixed micelle formation between amphiphilic drug amitriptyline hydrochloride and surfactants (conventional and gemini) at 293.15–308.15 K. *The Journal of Physical Chemistry B*, 114(19), 6354-6364.
- Erdinc, N., Gokturk, S., & Tuncay, M. (2010). A study on the adsorption characteristics of an amphiphilic phenothiazine drug on activated charcoal in the presence of surfactants. *Colloids and Surfaces B: Biointerfaces*, 75(1), 194-203.
- Evans, H. C. (1956). 117. Alkyl sulphates. Part I. Critical micelle concentrations of the sodium salts. *Journal of the Chemical Society (Resumed)*, 78, 579-586.
- Florence, A. T., & Atwood, D. (1998). *Physicochemical principles of pharmacy*. (pp. 1-564). Pharmaceutical Press.
- Gokturk, S., & Aslan, S. (2014). Study on binding properties of poorly soluble drug trimethoprim in anionic micellar solutions. *Journal of Dispersion Science and Technology*, 35(1), 84-92.
- Gokturk, S., & Tamer, Z. B. (2018). Interactions and solubilization of poorly soluble drugs in aerosol-ot micelles. *Journal of Surfactants and Detergents*, 21(6), 889-898.
- Gokturk, S., & Var, U. (2012). Effect of pharmaceutically important cosolvents on the interaction of promethazine and trifluopromazine hydrochloride with sodium dodecyl sulfate micelles. *Journal of Dispersion Science and Technology*, 33(4), 527-535.
- Hiemenz, P. C., & Rajogopalan, R. (1986). *Principles of colloid and surface chemistry*. (pp. 1-671). Marcel Dekker.
- Junquera, E., Romero, J. C., & Aicart, E. (2001). Behavior of tricyclic antidepressants in aqueous solution: Self-aggregation and association with  $\beta$ -cyclodextrin. *Langmuir*, 17(6), 1826-1832.
- Kuharski, R. A., & Rosky, P. J. (1984). Solvation of hydrophobic species in aqueous urea solution: a molecular dynamics study. *Journal of the American Chemical Society*, 106(20), 5794-5800.
- Liu, Y., & Guo, R. (2007). Microenvironment effect on the location distribution of phenothiazine in cetyltrimethylammonium bromide/n-pentanol/H<sub>2</sub>O W/O and bi-continuous microemulsions. *Journal of Solution Chemistry*, 36(9), 1079-1092.
- Mizutani, Y., Kamogawa, K., & Nakanishi, K. (1989). Effect of urea on hydrophobic interaction: Raman difference spectroscopy on the carbon-hydrogen stretching vibration of acetone and the carbon-nitrogen stretching vibration of urea. *The Journal of Physical Chemistry*, 93(15), 5650-5654.
- Ozan, M., & Gokturk, S. (2021). Effect of ionic liquids as active pharmaceutical ingredients on the micellar binding of an amphiphilic drug trifluopromazine hydrochloride. *Journal of Dispersion Science and Technology*, 42(2), 214-222.
- Ozcam, H. T. (2015). A study on micelle formation of amphiphilic drug amitriptyline hydrochloride, Master Dissertation, (pp. 1-102). Marmara University, İstanbul, Türkiye.
- Rosen, M. J. (1978). *Surfactants and interfacial phenomena*. (pp. 1-431). John Wiley and Sons.
- Rub, M. A., Asiri, A. M., Sheikh, M. S., Azum, N., Khan, A., Khan, A. A. P., & Rahman, M. M. (2014). Aggregation and phase separation phenomenon of amitriptyline hydrochloride under the influence of pharmaceutical excipients. *Journal of Surfactants and Detergents*, 17(1), 37-48.
- Rub, M. A., Asiri, A. M., Khan, A., Khan, A. A. P., Azum, N., & Khan, S. B. (2013). Investigation of micellar and phase separation phenomenon of the amphiphilic drug amitriptyline hydrochloride with cationic hydrotropes. *Journal of Solution Chemistry*, 42(2), 390-411.
- Schreier, S., Malheiros, S. V., & de Paula, E. (2000). Surface active drugs: self-association and interaction with membranes and surfactants. Physicochemical and biological aspects. *Biochimica et Biophysica Acta (BBA)-Biomembranes*, 1508(1-2), 210-234.
- Sharma, R., Nandni, D., & Mahajan, R. K. (2014). Interfacial and micellar properties of mixed systems of tricyclic antidepressant drugs with polyoxyethylene alkyl ether surfactants. *Colloids and Surfaces A: Physicochemical and Engineering Aspects*, 451, 107-116.
- Srivastava, R. C., & Nagappa, A. N. (2005). *Surface activity in drug action*. (pp.1-327). Amsterdam, Elsevier.
- Stellner, K. L., & Scamehorn, J. F. (1989). Hardness tolerance of anionic surfactant solutions. 1. Anionic surfactant with added monovalent electrolyte. *Langmuir*, 5(1), 70-77.
- Taboada, P., Attwood, D., Ruso, J. M., García, M., & Mosquera, V. (2000). Static and dynamic light scattering study on the association of some antidepressants in aqueous electrolyte solutions. *Physical Chemistry Chemical Physics*, 2(22), 5175-5179.
- Zana, R. (1995). Aqueous surfactant-alcohol systems: a review. *Advances in Colloid and Interface Science*, 57, 1-64.

**Cite as:** Ozcam, H. T., Tamer, Z. B., & Gokturk, S. (2022). Self-assembling of surface active drug amitriptyline hydrochloride in association with additives: Role of surface activity in the pharmaceutical applications. *Front Life Sci RT*, 3(3), 113-120.



Araştırma makalesi / Research article

## Antiviral peptidlerin SARS COV-2 ana proteaz yapısına bağlanma etkinliklerinin protein-yanaştırma yöntemi ile incelenmesi: *In silico* bir çalışma

İlter Demirhan<sup>\*1</sup> , Erkan Oner<sup>2</sup> , Ergul Belge Kurutas<sup>3</sup> 

<sup>1</sup> Harran University, Health Services Vocational School, Biomedical Device Technology Program, 63300, Sanliurfa, Türkiye

<sup>2</sup> Mersin University, Faculty of Pharmacy, Department of Biochemistry, 33169, Mersin, Türkiye

<sup>3</sup> Kahramanmaraş Sutcu Imam University, Faculty of Medicine, Department of Medical Biochemistry, 46040, Kahramanmaraş, Türkiye

### Öz

Virüsler günümüzde hastalıklarının önemli etkenleri arasında yer almaktadır. Viral hastalıklar için tasarlanan tedavilerin yetersizliği yeni tedavi yöntemlerinin tasarlanması ihtiyacını doğurmaktadır. 2019 yılında ortaya çıkan COVID-19 (SARS COV-2) de yeni antiviral ajanların ihtiyacı olduğu görülmüştür. Yapılan çalışmalar sonucu sunulan raporlarda viral direncin arttığı görülmektedir. Bu çalışmanın amacı, antiviral/antimikrobiyal etkinliğe sahip peptidlerin SARS COV-2 ana proteaz yapısında protein-peptid yanaştırma yöntemiyle araştırılmasıdır. Antiviral aktiviteye sahip antimikrobiyal peptidlerin sayısı hala düşük olsada, hali hazırda farmasötik olarak temin edilebilen antiviral ilaçlar olma yolunda muazzam bir potansiyel göstermektedir. Antiviral etkinliğe sahip alloferon 1, e ctry2801, temporin 1ta, dermaseptin s4, clavanin b, magainin b2 ve magainin b1 peptidlerinin SARS COV-2 ana proteaz (PDB ID:6LU7) yapısında protein çalışması CABSDOCK ile yapılmıştır. Magainin b2 ve peptid ctyr2801 peptidleri bağlanmalarının yüksek düzeyde olduğu, alloferon 1 ve magainin b1 in orta düzeyde bağlanma afinitesinin olduğu, termorin 1ta, dermaseptin s4 ve clavanin b'nin düzey düzeyde bağlanma afinitesine sahip olduğu gözlemlenmiştir. Sonuçlarımıza göre; peptid ctyr2801 ve magainin b2'nin, SARS COV-2 ana proteaz yapısında *in vivo* çalışmalara ve diğer çalışmalara öncülük edeceği düşünülmektedir.

**Anahtar kelimeler:** Antiviral peptid; CABSDOCK; protein peptid yanaştırma; SARS COV-2 Mpro

## Investigation of antiviral peptides in SARS COV-2 major protease structure by protein-e docking method: An *in silico* study

### Abstract

Viruses are among the important factors of diseases today. The inadequacy of the treatments designed for viral diseases necessitates the design of new treatment methods. It has been seen that there is a need for new antiviral agents in COVID-19. In the reports presented as a result of the studies, it was seen that the viral resistance has increased. The aim of this study is to investigate peptides with antiviral/antimicrobial activity in the main protease (Mpro) structure of SARS COV-2 by protein-peptide docking method. Although the number of antimicrobial peptides with antiviral activity is still low, they still show enormous potential as pharmaceutically available antiviral drugs. Protein analysis of alloferon 1, ctry2801, temporin 1ta, dermaceptin-s4, clavanin b, magainin b2 and magainin b1 peptides with antiviral activity in the SARS COV-2 Mpro (PDB ID: 6LU7) structure was performed

\* Sorumlu yazar / Corresponding author.

E-mail: [ilterdemirhan@harran.edu.tr](mailto:ilterdemirhan@harran.edu.tr) (I. Demirhan).

<https://doi.org/10.51753/flsrt.1092767> Yazar katkıları / Author contributions

Geliş tarihi / Received 24 Mart 2022 / 24 March 2022; Kabul tarihi / Accepted 27 Eylül 2022/ 27 September 2022

Çevrimiçi yayın / Available online 26 Aralık 2022 / 26 December 2022

2718-062X © 2022 This is an open access article published by Dergipark under the [CC BY](https://creativecommons.org/licenses/by/4.0/) license.

with CABSDOCK. It has been observed that the binding affinity of magainin b2 and peptide ctyr2801 is high, alloferon 1 and magainin b1 have a moderate binding affinity, and thermorin-1ta, dermaseptin s4 and clavanin b have a high level of binding affinity. According to our results; Peptide ctyr2801 and magainin b2 are thought to lead to *in vivo* studies and other studies on the SARS COV-2 Mpro structure.

**Keywords:** Antiviral peptide; CABSDOCK; protein peptide docking; SARS COV-2 Mpro

## 1. Giriş / Introduction

Viral enfeksiyonlar eski zamanlardan bu yana bildirilmiş olsa da bilim insanlarının daha sonra virüs olarak adlandırılan "filtrelenabilir parçacıkları" izole edebilmeleri ancak on dokuzuncu yüzyılda mümkün olmuştur. O zamandan günümüze, viral çoğalma, enfeksiyon ve aşı üretiminin kontrolü ile ilgili büyük atılımlar, çiçek hastalığının eradikasyonu, kızamık ve çocuk felci bulaşmasının kontrolü gibi insan-virüs etkileşiminde dikkate değer ilerlemelere yol açmıştır. Bununla birlikte, virüsler hala insan hastalıklarının ana nedenlerinden biri olmaya devam etmektedir. Bunun sebebi olarak yeni aşılardan keşfinin ve geliştirilmesinin genellikle zorlu ve zaman alıcı olması söylenebilir (Mahmoud, 2016). Viral kontrol için en yaygın kullanılan tedavi yöntemi antiviral ilaç tedavisi olmuştur (Lou, 2014).

Genel bir bakış açısıyla, antiviral ilaçlar için en yaygın etki mekanizmaları, virüs hedefli antiviraller ve konakçı hedefli antivirallerdir. Virüs hedefli antiviraller, proteazlar ve polimerazlar gibi önemli transkripsiyon ve replikasyon enzimlerinin inhibisyonuna veya viral yapısal proteinlerin doğrudan inaktivasyonuna odaklanır (Kiser ve Flexner, 2013). Bunun aksine, konakçı hücreyi hedefleyen antiviraller ise replikasyon döngüsü sırasında bazı virüsler tarafından kaçırılan önemli hücresel faktörler olduğu bilinen inhibisyon siklofilinleri (Lou, 2014), interferonlar gibi immünomodülatörlerin kullanımı ve gama globülinlere odaklanmaktadır (El Raziky ve ark., 2013; Lin ve Young, 2014).

Birinci nesil antiviral moleküller (60'larda ve 70'lerin başında tanımlanmıştır), zayıf özgüllüklerinden dolayı insanlar üzerinde ciddi yan etkilere sahiptir. Örneğin, bir replikasyon inhibitörü olarak kullanılan bir adenosin analogu olan vidarabin, sadece viral DNA polimerazı değil, aynı zamanda ökaryotik analogu da etkileyebilmektedir. Bu alandaki araştırmaların ilerlemesi, herpes simplex virüsü (HSV) ve varicella zoster virüsü (VZV) enfeksiyonlarının tedavisinde başarılı olarak kabul edilen asiklovir, ilk nükleozid analogu ve antiviral ilaç gibi daha iyi moleküllerin tanımlanmasına yol açmıştır. Spesifikliği nedeniyle (viral bir proteinin aracılık ettiği bir fosforilasyon adımı gerektirir) bu molekül, daha önce kullanılan tedavilere kıyasla konakçı için daha düşük toksisiteye neden olur (Thompson ve Whitley, 2011).

H1N1, Ebola ve zika virüsü (ZIKV) viral salgınlarının ortaya çıktıktan sonraki ilk 5 yılında yapılan çalışmalarda gözlemlendiği gibi kullanılan antiviral tedavilerin düşük etkinliği, viral direnç ve artan viral enfeksiyonlar yeni raporlar ile kanıtlanmıştır (Deming ve McNicholl, 2011; Le Page ve ark., 2013; Hui ve ark., 2017; Marston ve ark., 2017; De Souza ve ark., 2018). Bu nedenle, geniş spektrumlu aktivite sunabilen moleküller için artan tercihle birlikte yeni antiviral ilaçların üretimine olan talep her zamankinden daha fazladır (Lowe ve ark., 2018). Bu yeni moleküllerin araştırılması, önemli viral yapılar veya enzimler ile molekül etkileşimine (Jesus ve ark.,

2012; Elshabrawy ve ark., 2014) ve doğal kaynaklardan elde edilen yeni bileşiklerin izolasyonuna (Cantatore ve ark., 2013; Rothan ve ark., 2014) dayanan biyoinformatik destekli tahminler gibi farklı yaklaşımları içerir. Bu tür teknikler kullanılarak şimdiye kadar birçok yeni molekül tanımlanmıştır ve son zamanlarda antimikrobiyal peptidlerin tanımı dikkat çekmektedir (Hakim ve ark., 2013; Ishaq ve ark., 2013).

Son kanıtlar, bir savunma bariyeri olarak antiviral proteinli bileşiklerin işlevini vurgulamaktadır ve bazı antimikrobiyal peptidlerin ayrıca geniş bir virüs yelpazesine karşı aktivite gösterebildiği ve bu nedenle antiviral peptidler (AVP'ler) olarak adlandırıldığı gösterilmiştir (Chen ve ark., 2017; Altmann ve ark., 2012). Bu moleküller ayrıca biyoinformatik araçların kullanılmasıyla da elde edilebilmektedir ve daha sonra tasarlanmış veya yapay AVP'ler olarak adlandırılmaktadır. Yapay bir peptidin, bir yüzey glikoproteini veya önemli bir viral enzim gibi belirli bir hedefe karşı etkileşim için test edildiği yem çalışmalarından elde edilebilmektedir (Okazaki ve Kida, 2004). Peptidlerin tahmini için tasarlanmış özel yazılım kullanılarak *in silico*'da elde edilmektedir (Mooney ve ark., 2012). Her iki durumda da topoloji, amino asit bileşimi, yük ve bir in antiviral aktivitesini etkileyebilecek diğer birçok kimyasal ve yapısal özellik gibi birçok ayar dikkate alınır (Maccari ve ark., 2013; Sharma ve ark., 2014).

AVP'lerin incelenmesi, son yıllarda çok sayıda araştırma projesinin odak noktası olmuştur ve bu tür moleküllerin yapıları ve etki mekanizmaları daha önce gözden geçirilmiş ve hatta antiviral peptid veritabanı (AVPdb—<http://crdd.osdd.net/servers/avpdb/>) gibi çevrimiçi veri tabanlarında derlenmiştir. İlgili sunucuda 2683 deneysel olarak test edilmiş peptid girişi olduğu görülmektedir (Barlow ve ark., 2014; Mulder ve ark., 2014; Qureshi ve ark., 2014). Etki mekanizmaları ile ilgili olarak (Şekil 1), AVP'lerin viral partikülü doğrudan inhibe ederek hareket ettiklerinde çoğunlukla virüsidal olarak adlandırılırlar veya konakçı hücre zarındaki protein bağlantı bölgesi için rekabet ederler. Bununla birlikte, viral gen ekspresyonunun baskılanmasına neden olarak viral döngünün diğer aşamalarında da etkili olabilmektedir (Zapata ve ark., 2016).

CABSDOCK modelleme yöntemi, CABS kaba taneli modeli kullanılarak bir peptidin birleştirilmiş bağlanması ve katlanması için etkin simülasyon şemasına dayanmaktadır. CABS, içsel olarak düzensiz bir peptidin katlanma ve bağlanma mekanizması, denatüre edilmiş durumdan katlanmış duruma küresel proteinlerin katlanma mekanizmaları (Jamroz ve ark., 2014; Zambrano ve ark., 2015) protein dinamiklerinin simülasyonu, neredeyse- doğal yapı dalgalanmaları (Steczkiewicz ve ark., 2014) ve protein yapısı tahminine dayanmaktadır (Kurcinski ve Kolinski, 2007). CABSDOCK otomatik protokolünde (Nielsen ve ark., 2007), CABS kaba taneli simülasyonu, seçilen yeniden yapılandırılmış modellerin tüm atomlu yerel optimizasyonu ile birleştirilir.

Bu çalışmanın amacı peptidlerin antiviral aktivitesini gösteren çalışmaların sayısının artması ve yeni antiviral ilaçlara

yönelik acil ihtiyaç nedeniyle etkili ilaçlar haline gelebilecek ve halen üzerinde çalışılmakta olan en umut verici antiviral peptidlerden protein-docking (yanaştırma) yöntemi ile SARS COV-2 ana proteaz yapısına bu peptidlerin ilgisini belirlemektir.

## 2. Gereç ve yöntemler / Materials and methods

Modelleme, esnek protein-yanaştırma için CABSDOCK web sunucusu kullanılarak (<http://biocomp.chem.uw.edu.pl/CABSDOCK/>) bağlanma bölgesi hakkında önceden bilgi sahibi olmadan gerçekleştirilmiştir. CABSDOCK bir bağlanma bölgesi için kör arama sırasında peptid yapısının tam esnekliğini ve protein fragmanlarının büyük ölçekli esnekliğini sağlar. CABSDOCK sunucusunun ayrıntılı açıklaması ve kıyaslama testleri yakın zamanda açıklanmıştır. CABSDOCK uygulamalarının ve uzantılarının birkaç örneğini de ifade eden literatür çalışması mevcuttur (Nielsen ve ark., 2007).

### 2.1. Giriş verileri / Input data

SARS COV-2 ana proteaz yapısı (PDB ID: 6LU7) protein data bankdan (<https://www.rcsb.org/>) alındı. Antiviral peptidlerden alloferon 1, e ctry2801, temporin 1ta, dermaseptin s4, cavanin b, magainin b2 ve magainin b1 yapılarının amino asit dizileri Uniprot'dan (<https://www.uniprot.org/>) alındı. Anti viral peptidlerin biyokimyasal özelliklerine bakıldığında, kationik ve amfipatik özellikler ve pozitif net yükler olup, bunların tümü bu peptidlerin antiviral ajan olarak çalışması için önemli bir özelliktir. Ayrıca antiviral peptidlerdeki hidrofobik olan yapıları zarflı virüslere karşı önemli aktiviteler gösterdiği bilinmektedir (Badani ve ark., 2014).

## 3. Bulgular / Results

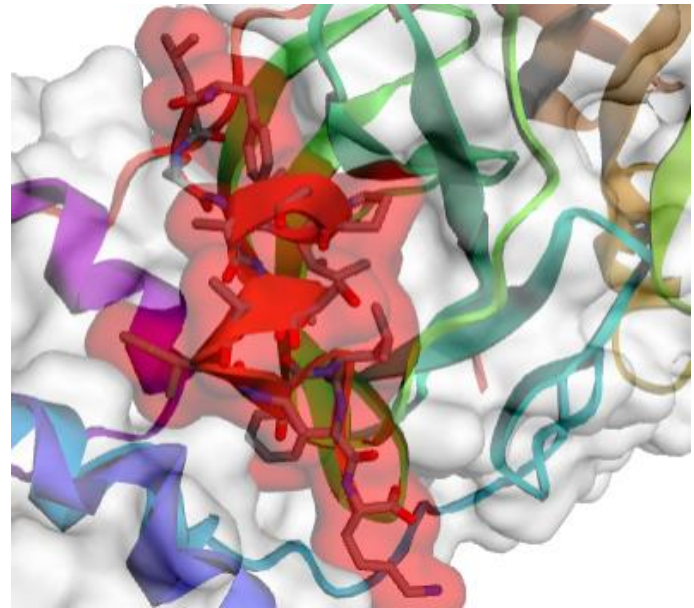
Antiviral peptidlerin protein-peptid etkileşimleri için proteinin peptide olan bağlanma ilgisi (RMSD değeri) Tablo 1 de verilmiştir. Antiviral peptidlerin SARS COV-2 Mpro (PDB ID:6LU7) yapısı ile birlikte yaptığımız protein-peptid docking sonuçlarına göre en iyi bağlanma modelleri Şekil 1-2-3-4-5-6-7'de gösterildi. Şekil 1-2-3-4-5'de 6LU7 protein yapısının aktif bölgesine hedeflendiği de gözükmektedir. RMSD sonuçlarına göre en iyi bağlanma Şekil 2'de görülen e ctry2801 de ve Şekil 5'de görülen magainin b2 de olduğu belirlendi. En iyi bağlanma

modeli tahminleri de Ek Şekil 1-2-3-4-5-6-7'de gösterilmiştir.

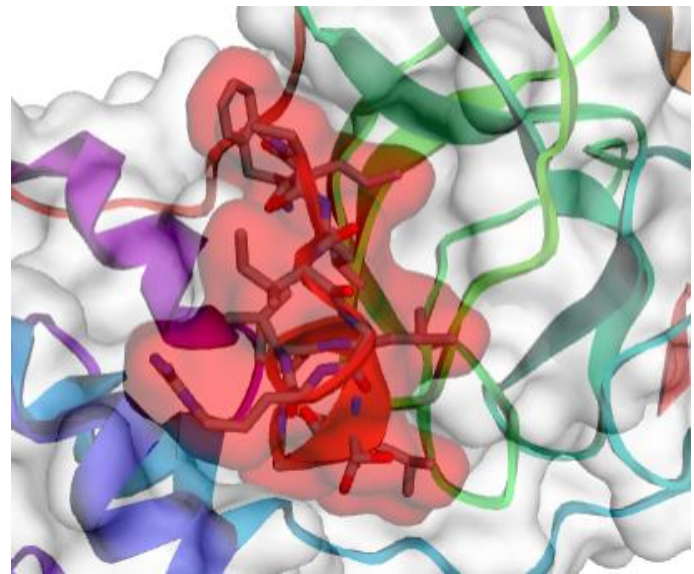
**Tablo 1 / Table 1**

Protein-peptid etkileşimlerinin RMSD değerleri, küme yoğunlukları ve kümede bulunan toplam element sayıları / RMSD values of protein-peptide interactions, cluster densities and total number of elements in the cluster.

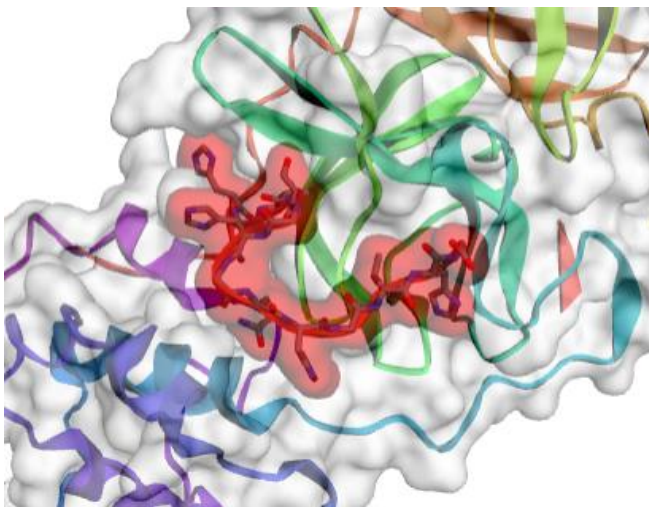
Peptidler	RMSD Değeri	Küme Yoğunluğu	Kümede Bulunan Toplam Element Sayısı
Alloferon 1	3.60	39.40	142
E ctry2801	2.82	38.19	108
Temporin 1ta	7.30	29.01	212
Dermaseptin s4	8.64	25.22	218
Clavanin b	7.83	26.80	210
Magainin b2	2.85	38.53	110
Magainin b1	5.01	25.50	128



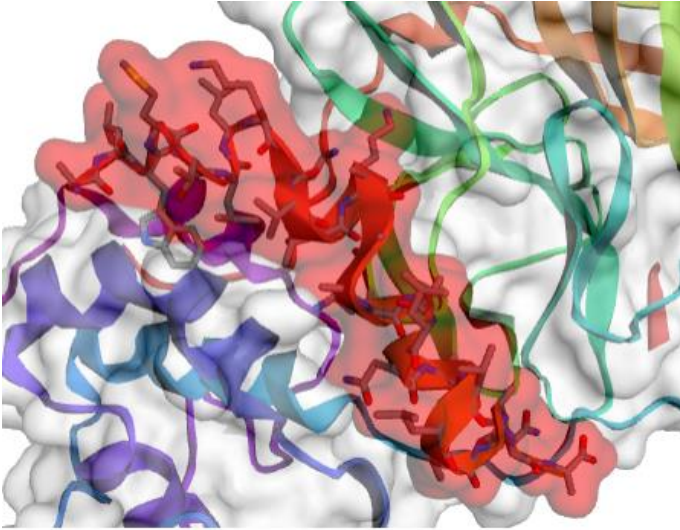
**Şekil 2 / Figure 2.** Peptid ctry2801 in SARS COV-2 (6LU7) yapısına bağlanma modeli / Binding model of the peptide Ctry2801 to the SARS COV-2 (6LU7) structure.



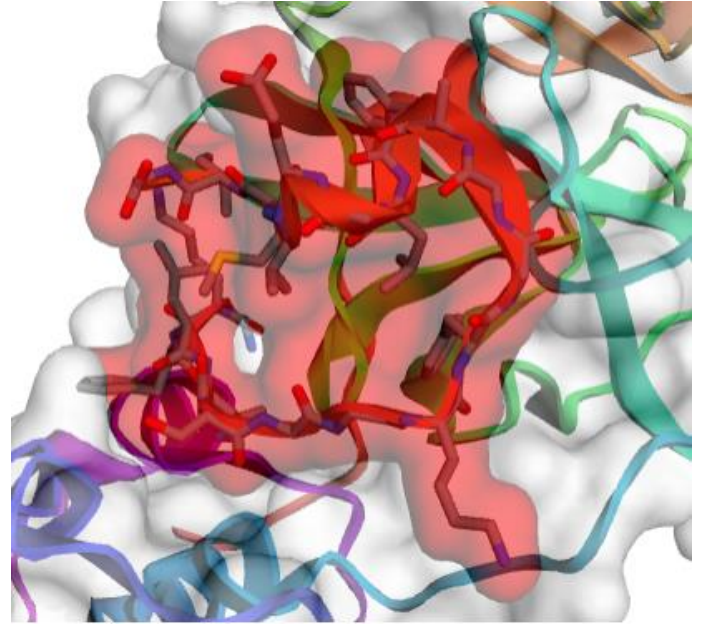
**Şekil 3 / Figure 3.** Temporin 1ta'nın SARS COV-2 (6LU7) yapısına bağlanma modeli / Binding model of the temporin 1ta to the SARS COV-2 (6LU7) structure.



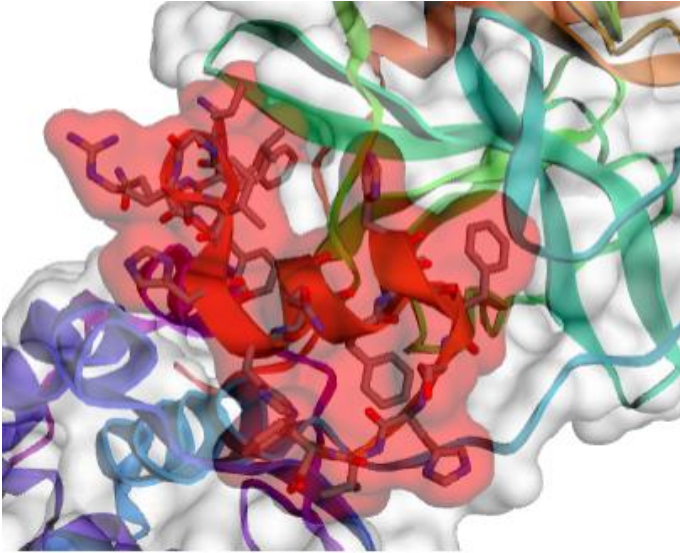
**Şekil 1 / Figure 1.** Alloferon 1 in SARS COV-2 (6LU7) yapısına bağlanma modeli / Binding model of alloferon 1 to the SARS COV-2 (6LU7) structure.



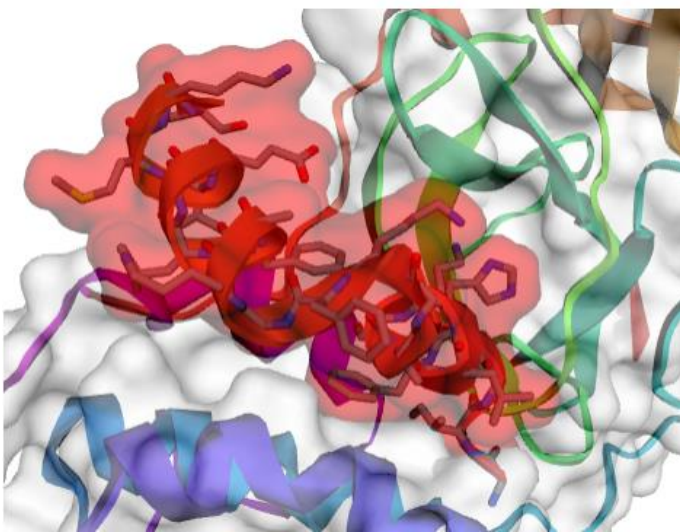
**Şekil 4 / Figure 4.** Dermaseptin s4'ün SARS COV-2 (6LU7) yapısına bağlanma modeli / Binding model of the tempoin 1ta to the SARS COV-2 (6LU7) structure.



**Şekil 7 / Figure 7.** Magainin b1'in SARS COV-2 (6LU7) yapısına bağlanma modeli / Binding model of the magainin b1 to the SARS COV-2 (6LU7) structure.



**Şekil 5 / Figure 5.** Clavanin b'nin SARS COV-2 (6LU7) yapısına bağlanma modeli / Binding model of the clavanin b to the SARS COV-2 (6LU7) structure.



**Şekil 6 / Figure 6.** Magainin b2'nin SARS COV-2 (6LU7) yapısına bağlanma modeli / Binding model of the magainin b2 to the SARS COV-2 (6LU7) structure.

#### 4. Tartışma / Discussion

COVID-19, 2020'de küresel bir salgın haline geldi ve etkili bir antiviral ilaç veya aşı tam anlamıyla oluşturulamadı (Genc, 2020). Ayrıca, virüsün delta ve omikron gibi farklı SARS COV-2 varyantlarının ortaya çıkması, dünya çapında küresel sağlık için ciddi bir tehdit oluşturmuştur (Li, 2021; Araf, 2022). Salgınlar ve pandemilerle ilişkili ortaya çıkan bulaşıcı hastalıklara yanıt vermede önceliklendirme ve acil durum hazırlığı son derece elzemdir. COVID-19'a karşı etkili bir antiviral arayışı içinde, AVP'lerin SARS COV-2'ye karşı potansiyel yeni antiviral ajan sınıflarından birini temsil edebileceğine inanıyoruz. Bu çalışma daha önce SARS COV-2 yapısında bilgisayar destekli modelleme çalışmalarıyla incelenmemiş olup ilk kez yapılmaktadır. Çalışma bulgularımıza göre magainin b2 ve peptid ctyr2801 peptidleri bağlanmalarının yüksek düzeyde olduğu, alloferon 1 ve magainin b1 in orta düzeyde bağlanma affinitesinin olduğu, termorin 1ta, dermaseptin s4 ve clavanin b'nin düşük düzeyde bağlanma affinitesinin olduğu belirlenmiştir.

Moleküler yanıştırma süreci, güvenilir çevrimiçi tabanlı veri tabanında bulunan çeşitli peptid dizileri arasında güvenilir antiviral terapötiklerin belirlenmesi için uygun bir yaklaşım olarak kabul edilir. Özellikle, bir protein substratı ve bir peptid ligandı arasındaki etkileşimin bağ mesafesi ile bağlantılı olarak etkileşim tipi ve bağlanma enerjisi, moleküler kenetlenmenin kullanımı yoluyla değerlendirilebilir. Bu nedenle, bağlanma enerjisi değerlendirmesine dayalı olarak çok sayıda peptid dizisi arasında makul bir peptid taraması, en yüksek peptid adaylarını yanıştırma etkileşimine göre değerlendirmek için moleküler yanıştırma çalıştırılarak minimum süre içinde uygulanabilir. Ayrıca, doğruluk elde etmek için hesaplama şemasına dahil olmak için çeşitli yanıştırma programları uyumludur (Shoichet, 2006; Hengphatporn ve ark., 2020). Sonuç olarak, hesaplama dayalı bir yaklaşımın, SARS COV-2'ye karşı antiviral peptid adayının yakalanması için güvenilir bir teknik olduğu düşünülmektedir.

COVID-19'da spike proteinin bağlanma alanında mutasyon gösteren birkaç SARS COV-2 varyantı ortaya çıktı. Gupta, 2021 tarafından belirlenmiştir. Mpro homodimerik sistein proteaz yapısındadır. Subsrat bağlanma bölgesi 3 cepten oluşur. İlk cep olarak tanımlanan P1 cebinde Phe140, Asn142, Glu166, His163 ve His172 amino asit kalıntıları oluşur. P2 cebi daha derinde ve His41, Met49, Tyr54, Met165 ve Asp187 kalıntıları oluşur. P3 cebinde ise Leu168, Glu166, Pro168, Gly170 kalıntıları oluşur. Ama en önemlisi Cys15 ve His41 amino asitleri katalitik özelliği sebebiyle proteolize etki eder. Enzim yapısındaki bölünme genellikle Leu/Phe/Met-Gln ↓ Gly/Ser/Ala modelini takip eder (↓ bölünme bölgesini belirtir). P1 pozisyonundaki glutamin, proteolizin gerçekleşmesi için çok önemlidir. Bu tür bölünme bölgelerine sahip bilinen doğal insan enzimleri olmadığı için, konak hücreler üzerinde toksik etkiler için düşük bir risk olduğundan Mpro ideal bir ilaç hedefi gibi görünmektedir (Hilgenfeld ve ark., 2014; Zhang ve ark., 2020; Zhang ve ark., 2021). Virüsün tüm varyantlarında mutasyon gözlenirken Mpro geninde mutasyon gözlenmediği Jukic ve ark., 2021, tarafından bildirilmiştir. Bu sonuç Mpro'nun hedef gen olabileceğini göstermektedir.

AVP'lerin antiviral aktivitelerini uygulamak için varsayılan etki mekanizması şöyle görünmektedir: (i) yüzey karbonhidrat etkileşimi ile viral girişin erken aşamalarını bloke etmek, (ii) spesifik hücre reseptörlerle etkileşimler yoluyla viral bağlanmayı veya konakçı hücrelere penetrasyonu bloke etmek, (iii) viral zarf glikoproteinlerinin etkileşimi ve inaktivasyonu, (iv) konakçı hücre antiviral tepkilerinin modülasyonu ve (v) viral genlerin hücre içi ekspresyonunun ve/veya viral proteinlerin üretiminin bloke edilmesi. Bununla birlikte, şimdiye kadar AVP yapıları ile viral inhibisyon arasında kesin bir ilişki ortaya çıkmamıştır. Aslında, peptidten peptide çarpıcı farklılıklar genellikle gözlenir. Mekanik olarak, birçok AVP, virüs partikülünün dış yüzey zarının doğrudan bozulmasıyla virüsidal etkilerini gösterir.

Zhao ve ark. (2012), peptid ctyr2801'in Hepatit B virüsünün replikasyonunu % 40 oranda engellediğini ve hepatit B virüsü için zayıf bir inhibitör olacağını bulmuşlardır. El Bitar ve ark. (2015) akrep zehirlerinden elde edilen magainin b1'in hepatit c virüsüne karşı öldürücü aktivitesini bulmuşlardır.

Farklı bir çalışmada antimikrobiyal etkisi olan dermaseptin s4'ün HIV-1 viral enfektesini *in vivo* olarak inhibe ettiği gösterildi (Lorin ve ark., 2005). Antimikrobiyal etkide bulunan clavanin b'nin HIV-1 viral enfektesinin inhibitörü olabileceğini vurgulayan çalışmalar literatürde kayıtlıdır (Wang ve ark., 2004). Wachinger ve ark. (1992), alloferon 1 in HIV-1'in inhibitörü olabileceğini ayrıca alloferon 1'in herpes simpleks virüsüne karşı etkili bir inhibitör olacağını savunan çalışmalar bulunmaktadır (Wachinger ve ark., 1992; Egal ve ark., 1999).

## Kaynaklar / References

- Altmann, S. E., Brandt, C. R., Jahrling, P. B., & Blaney, J. E. (2012). Antiviral activity of the EB peptide against zoonotic poxviruses. *Virology Journal*, 9(1), 1-6.
- Araf, Y., Akter, F., Tang, Y. D., Fatemi, R., Parvez, M. S. A., Zheng, C., & Hossain, M. G. (2022). Omicron variant of SARS-COV-2: genomics, transmissibility, and responses to current COVID-19 vaccines. *Journal of Medical Virology*, 94(5), 1825-1832.
- Badani, H., Garry, R. F., & Wimley, W. C. (2014). Peptide entry inhibitors of enveloped viruses: the importance of interfacial hydrophobicity. *Biochimica et Biophysica Acta (BBA)-Biomembranes*, 1838(9), 2180-2197.
- Barlow, P. G., Findlay, E. G., Currie, S. M., & Davidson, D. J. (2014). Antiviral potential of cathelicidins. *Future Microbiology*, 9(1), 55-73.

Mohan ve ark., Vaccinia virüsü zarlarına karşı AVP yapısında bulunan PD3, PD4 ve RW3'ün virüsidal aktivitesini %100'e yakın buldular (Mohan ve ark., 2010). Benzer çalışmada temporin 1ta'nın vaccina virüsüne karşı inhibitör etkisinin olduğu, AVP yeteneğinin oldukça güçlü olduğu vurgulanmaktadır (Wang ve ark., 2004).

Yu ve ark. (2017), hamile farelerde zika virüsü enfeksiyonunu bazlı bir viral inaktivatörle engellediklerini gösterdiler. Lok ve ark. (2012) dang virüsünün genomunun salımını ile inhibe ettiğini gösterdi. Hrobowski ve ark. (2005) Dang ve batı Nil virüsü enfektesini ile inhibe ettiğini gösterdi. Literatür araştırmaları değerlendirildiğinde çeşitli peptid yapılarının anti viral inhibitör olabileceği göstermektedir.

## 4. Sonuç / Conclusion

Sonuç olarak, AVP'ler basit birincil yapıları nedeniyle yapısal ve işlevsel olarak çok yönlüdür ve öngörülemeden gelecekte ciddi halk sağlığı tehditleri oluşturan COVID-19 veya ortaya çıkan salgınlar karşısında hızlı terapötik adayların oluşturulması için moleküler şablonlar olarak hizmet edebilir. Yapmış olunan çalışma sonuçlarına göre bağlanma tahminin değerlendirilmesi Yüksek kaliteli tahmin:  $rmsd < 3 \text{ \AA}$  , Orta kalitede tahmin:  $3 \text{ \AA} \leq rmsd \leq 5,5 \text{ \AA}$  , Düşük kaliteli tahmin:  $rmsd > 5,5 \text{ \AA}$  olarak tanımlanmaktadır. Buna göre magainin b2 ve peptid ctyr2801 peptidleri bağlanmalarının yüksek düzeyde olduğu, alloferon 1 ve magainin b1 in orta düzeyde bağlanma affinitesinin olduğu, termorin 1ta, dermaseptin s4 ve clavanin B'nin düzey düzeyde bağlanma affinitesinin olduğu belirlenmiştir. Sonuçlarımız değerlendirildiğinde alloferon 1 ve magainin b2'nin SARS COV-2 ana proteaz yapısında *in vivo* çalışmalarda değerlendirilebileceği ve diğer çalışmalara öncülük edeceği kanaatindeyiz.

**Teşekkür / Acknowledgments:** Bu çalışmanın hazırlanması aşamasında bizlerden yardımlarını esirgemeyen Prof. Dr. Ergül BELGE KURUTAŞ hocamıza teşekkürlerimizi sunarız. / We would like to thank Prof. Dr. Ergül BELGE KURUTAŞ for her assistance during the preparation of this study.

**Çıkar çatışması / Conflict of interest:** Yazarlar herhangi bir çıkar çatışması olmadığını beyan eder / The authors declare that they have no conflict of interests.

**Etik beyanı / Informed consent:** Bu çalışmada, yazarlar, hiçbir insan ya da hayvan denek kullanılmadığını ve Etik Kurul iznine gerek olmadığını beyan eder / The authors declare that this manuscript did not involve human or animal participants and informed consent was not collected.

- Cantatore, A., Randall, S. D., Traum, D., & Adams, S. D. (2013). Effect of black tea extract on herpes simplex virus-1 infection of cultured cells. *BMC Complementary and Alternative Medicine*, 13(1), 1-10.
- Chen, L., Liu, Y., Wang, S., Sun, J., Wang, P., Xin, Q., ... & Wang, W. (2017). Antiviral activity of peptide inhibitors derived from the protein E stem against Japanese encephalitis and Zika viruses. *Antiviral Research*, 141, 140-149.
- Deming, P., & McNicholl, I. R. (2011). Coinfection with Human Immunodeficiency Virus and Hepatitis C Virus: Challenges and Therapeutic Advances: Insights from the Society of Infectious Diseases Pharmacists. *Pharmacotherapy: The Journal of Human Pharmacology and Drug Therapy*, 31(4), 357-368.
- De Souza, W. V., Albuquerque, M. D. F. P. M. D., Vazquez, E., Bezerra,

- L. C. A., Mendes, A. D. C. G., Lyra, T. M., ... & Martelli, C. M. T. (2018). Microcephaly epidemic related to the Zika virus and living conditions in Recife, Northeast Brazil. *BMC Public Health*, 18(1), 1-7.
- Egal, M., Conrad, M., MacDonald, D. L., Maloy, W. L., Motley, M., & Genco, C. A. (1999). Antiviral effects of synthetic membrane-active peptides on herpes simplex virus, type 1. *International Journal of Antimicrobial Agents*, 13(1), 57-60.
- El-Bitar, A. M., Sarhan, M. M., Aoki, C., Takahara, Y., Komoto, M., Deng, L., ... & Hotta, H. (2015). Virocidal activity of Egyptian scorpion venoms against hepatitis C virus. *Virology Journal*, 12(1), 1-9.
- El Raziky, M., Fathalah, W. F., El-Akel, W. A., Salama, A., Esmat, G., Mabrouk, M., ... & Khatib, H. M. (2013). The effect of peginterferon alpha-2a vs. peginterferon alpha-2b in treatment of naive chronic HCV genotype-4 patients: a single centre Egyptian study. *Hepatitis Monthly*, 13(5).
- Elshabrawy, H. A., Fan, J., Haddad, C. S., Ratia, K., Broder, C. C., Caffrey, M., & Prabhakar, B. S. (2014). Identification of a broad-spectrum antiviral small molecule against severe acute respiratory syndrome coronavirus and Ebola, Hendra, and Nipah viruses by using a novel high-throughput screening assay. *Journal of Virology*, 88(8), 4353-4365.
- Genc, B. N. (2020). Critical management of COVID-19 pandemic in Turkey. *Frontiers in Life Sciences and Related Technologies*, 1(2), 69-73.
- Gupta, R.K. (2021). Will SARS COV-2 variants of concern affect the promise of vaccines? *Nature Reviews Immunology*, 21, 340-341.
- Hakim, A., Nguyen, J. B., Basu, K., Zhu, D. F., Thakral, D., Davies, P. L., ... & Meng, W. (2013). Crystal structure of an insect antifreeze protein and its implications for ice binding. *Journal of Biological Chemistry*, 288(17), 12295-12304.
- Hilgenfeld, R. (2014). From SARS to MERS: crystallographic studies on coronaviral proteases enable antiviral drug design. *The FEBS Journal*, 281(18), 4085-4096.
- Hengphasatporn, K., Garon, A., Wolschann, P., Langer, T., Yasuteru, S., Huynh, T. N., ... & Rungrotmongkol, T. (2020). Multiple virtual screening strategies for the discovery of novel compounds active against dengue virus: A hit identification study. *Scientia Pharmaceutica*, 88(1), 2-19.
- Hrobowski, Y. M., Garry, R. F., & Michael, S. F. (2005). Peptide inhibitors of dengue virus and West Nile virus infectivity. *Virology Journal*, 2(1), 1-10.
- Hui, D. S., Lee, N., & Chan, P. K. (2017). A clinical approach to the threat of emerging influenza viruses in the Asia-Pacific region. *Respirology*, 22(7), 1300-1312.
- Ishag, H. Z., Li, C., Huang, L., Sun, M. X., Ni, B., Guo, C. X., & Mao, X. (2013). Inhibition of Japanese encephalitis virus infection in vitro and in vivo by pokeweed antiviral protein. *Virus Research*, 171(1), 89-96.
- Jamroz, M., Kolinski, A., & Kmiecik, S. (2014). CABS-flex predictions of protein flexibility compared with NMR ensembles. *Bioinformatics*, 30(15), 2150-2154.
- Jesus, T., Rogelio, L., Abraham, C., Uriel, L., Garcia, J., Alfonso, M. T., & Lilia, B. B. (2012). Prediction of antiviral peptides derived from viral fusion proteins potentially active against herpes simplex and influenza A viruses. *Bioinformatics*, 8(18), 870.
- Jukic, M., Škrlić, B., Tomšič, G., Pleško, S., Podlipnik, Č., & Bren, U. (2021). Prioritisation of compounds for 3CLpro inhibitor development on SARS-COV-2 variants. *Molecules*, 26(10), 300-303.
- Kurcinski, M., & Kolinski, A. (2007). Hierarchical modeling of protein interactions. *Journal of Molecular Modeling*, 13(6), 691-698.
- Kiser, J. J., & Flexner, C. (2013). Direct-acting antiviral agents for hepatitis C virus infection. *Annual Review of Pharmacology and Toxicology*, 53, 427-449.
- Le Page, A. K., Jager, M. M., Iwasenko, J. M., Scott, G. M., Alain, S., & Rawlinson, W. D. (2013). Clinical aspects of cytomegalovirus antiviral resistance in solid organ transplant recipients. *Clinical Infectious Diseases*, 56(7), 1018-1029.
- Li, M., Lou, F., & Fan, H. (2021). SARS-COV-2 Variants of Concern Delta: a great challenge to prevention and control of COVID-19. *Signal Transduction and Targeted Therapy*, 6(1), 1-3.
- Lin, F. C., & Young, H. A. (2014). Interferons: success in anti-viral immunotherapy. *Cytokine & Growth Factor Reviews*, 25(4), 369-376.
- Lok, S. M., Costin, J. M., Hrobowski, Y. M., Hoffmann, A. R., Rowe, D. K., Kukkaro, P., ... & Michael, S. F. (2012). Release of dengue virus genome induced by a peptide inhibitor. *PLoS One*, 7(11), e50995.
- Lou, Z., Sun, Y., & Rao, Z. (2014). Current progress in antiviral strategies. *Trends in Pharmacological Sciences*, 35(2), 86-102.
- Lowe, R., Barcellos, C., Brasil, P., Cruz, O. G., Honório, N. A., Kuper, H., & Carvalho, M. S. (2018). The Zika virus epidemic in Brazil: from discovery to future implications. *International Journal of Environmental Research and Public Health*, 15(1), 96.
- Maccari, G., Di Luca, M., Nifosi, R., Cardarelli, F., Signore, G., Boccardi, C., & Bifone, A. (2013). Antimicrobial peptides design by evolutionary multiobjective optimization. *PLoS Computational Biology*, 9(9), e1003212.
- Mahmoud, A. (2016). New vaccines: Challenges of discovery. *Microbial Biotechnology*, 9(5), 549-552.
- Marston, B. J., Dokubo, E. K., van Steelandt, A., Martel, L., Williams, D., Hersey, S., ... & Redd, J. T. (2017). Ebola response impact on public health programs, West Africa, 2014-2017. *Emerging Infectious Diseases*, 23(Suppl 1), S25.
- Mohan, K. V., Rao, S. S., & Atreya, C. D. (2010). Antiviral activity of selected antimicrobial peptides against vaccinia virus. *Antiviral Research*, 86(3), 306-311.
- Mooney, C., Haslam, N.J., Pollastri, G., & Shields, D.C. (2012). Towards the improved discovery and design of functional es: common features of diverse classes permit generalized prediction of bioactivity. *PLoS One*, 7, 1-12.
- Mulder, K. C., Lima, L. A., Miranda, V. J., Dias, S. C., & Franco, O. L. (2013). Current scenario of peptide-based drugs: the key roles of cationic antitumor and antiviral peptides. *Frontiers in Microbiology*, 4, 321-344.
- Nielsen, M., Lundegaard, C., Blicher, T., Lamberth, K., Harndahl, M., Justesen, S., ... & Buus, S. (2007). NetMHCpan, a method for quantitative predictions of peptide binding to any HLA-A and-B locus protein of known sequence. *PLoS One*, 2(8), e796.
- Okazaki, K., & Kida, H. (2004). A synthetic peptide from a heptad repeat region of herpesvirus glycoprotein B inhibits virus replication. *Journal of General Virology*, 85(8), 2131-2137.
- Qureshi, A., Thakur, N., Tandon, H., & Kumar, M. (2014). AVpdb: a database of experimentally validated antiviral peptides targeting medically important viruses. *Nucleic Acids Research*, 42(D1), D1147-D1153.
- Rothan, H. A., Bahrani, H., Rahman, N. A., & Yusof, R. (2014). Identification of natural antimicrobial agents to treat dengue infection: In vitro analysis of laticin peptide activity against dengue virus. *BMC Microbiology*, 14(1), 1-10.
- Sharma, A., Singla, D., Rashid, M., & Raghava, G. P. S. (2014). Designing of peptides with desired half-life in intestine-like environment. *BMC Bioinformatics*, 15(1), 1-8.
- Shoichet, B. K. (2006). Interpreting steep dose-response curves in early inhibitor discovery. *Journal of Medicinal Chemistry*, 49(25), 7274-7277.
- Steczkiwicz, K., Zimmermann, M. T., Kurcinski, M., Lewis, B. A., Dobbs, D., Kloczkowski, A., ... & Ginalski, K. (2011). Human telomerase model shows the role of the TEN domain in advancing the double helix for the next polymerization step. *Proceedings of the National Academy of Sciences*, 108(23), 9443-9448.
- Thompson, C., & Whitley, R. (2011). Neonatal herpes simplex virus infections: where are we now?. *Hot Topics in Infection and Immunity in Children VII*, 221-230.
- Wang, W., Owen, S. M., Rudolph, D. L., Cole, A. M., Hong, T., Waring, A. J., ... & Lehrer, R. I. (2004). Activity of  $\alpha$ - and  $\theta$ -defensins against primary isolates of HIV-1. *The Journal of Immunology*, 173(1), 515-520.
- Yu, Y., Deng, Y. Q., Zou, P., Wang, Q., Dai, Y., Yu, F., ... & Lu, L. (2017). A peptide-based viral inactivator inhibits Zika virus infection in pregnant mice and fetuses. *Nature Communications*, 8(1), 1-12.
- Zambrano, R., Jamroz, M., Szczasiuk, A., Pujols, J., Kmiecik, S., & Ventura, S. (2015). AGGRESCAN3D (A3D): server for prediction of aggregation properties of protein structures. *Nucleic Acids Research*, 43(W1), W306-W313.
- Zapata, W., Aguilar-Jiménez, W., Feng, Z., Weinberg, A., Russo, A., Potenza, N., ... & Rugeles, M. T. (2016). Identification of innate immune antiretroviral factors during in vivo and in vitro exposure to HIV-1. *Microbes and Infection*, 18(3), 211-219.
- Zhang, C. H., Stone, E. A., Deshmukh, M., Ippolito, J. A., Ghahremanpour, M. M., Tirado-Rives, J., ... & Jorgensen, W. L. (2021). Potent noncovalent inhibitors of the main protease of SARS-COV-2 from

- molecular sculpting of the drug perampanel guided by free energy perturbation calculations. *ACS central science*, 7(3), 467-475.
- Zhang, L., Lin, D., Kusov, Y., Nian, Y., Ma, Q., Wang, J., ... & Hilgenfeld, R. (2020).  $\alpha$ -Ketoamides as broad-spectrum inhibitors of coronavirus and enterovirus replication: structure-based design, synthesis, and activity assessment. *Journal of Medicinal Chemistry*, 63(9), 4562-4578.
- Zhao, Z., Hong, W., Zeng, Z., Wu, Y., Hu, K., Tian, X., ... & Cao, Z. (2012). Mucroporin-M1 inhibits hepatitis B virus replication by activating the mitogen-activated protein kinase (MAPK) pathway and down-regulating HNF4 $\alpha$  in vitro and in vivo. *Journal of Biological Chemistry*, 287(36), 30181-30190.

**Cite as / Atf şekli:** Demirhan, I., Oner, E., & Belge Kurtulus, E. (2022). Antiviral peptidlerin SARS COV-2 ana proteaz yapısına bağlanma etkinliklerinin protein-yanıştırma yöntemi ile incelenmesi: *In silico* çalışma. *Front Life Sci RT*, 3(3), 121-127.

## Ek / Supplementary

Receptor residue	Peptide residue	Receptor residue	Peptide residue	Receptor residue	Peptide residue
ASP A 295	GLY B 2	ARG A 298	HIS B 1	ASP A 295	HIS B 1
PHE A 294	GLY B 2	PHE A 294	HIS B 6	PHE A 294	HIS B 1
THRA A 292	GLY B 2	THRA A 292	GLN B 8	ILE A 249	GLY B 7
VAL A 202	GLN B 8	GLUA A 240	HIS B 9	ILE A 200	HIS B 9
GLY A 183	HIS B 12	ILE A 200	GLN B 8	TYR A 182	HIS B 12
CYS A 160	VAL B 3	TYR A 182	VAL B 11	SERA A 158	SER B 4
ASNA A 151	SER B 4	ILE A 152	HIS B 1	ASNA A 151	VAL B 3
ASNA A 151	HIS B 1	ASNA A 151	GLY B 2	PHE A 134	HIS B 12
PHE A 112	HIS B 1	PHE A 112	VAL B 3	THRA A 111	VAL B 3
THRA A 111	HIS B 1	THRA A 111	GLY B 2	GLNA A 110	GLY B 5
GLNA A 110	VAL B 3	GLNA A 110	SER B 4	GLNA A 110	GLY B 2
GLY A 109	GLN B 8	GLY A 109	HIS B 9	PRO A 108	VAL B 11
PRO A 108	HIS B 9	PRO A 108	GLY B 10	GLNA A 107	GLY B 10
GLNA A 107	GLN B 8	GLNA A 107	HIS B 9	GLNA A 107	HIS B 6
GLNA A 107	SER B 4	GLNA A 107	GLY B 5	ILE A 106	VAL B 11
ARG A 105	VAL B 11	ARG A 105	HIS B 12	ARG A 105	GLY B 5
VAL A 104	GLY B 5	ARG A 105	SER B 4	VAL A 104	SER B 4
MET A 6	HIS B 1	PHE A 8	HIS B 1		

**Ek Şekil 1 / Supplement Figure 1.** Alloferon 1 in SARS COV-2 (6LU7) yapısındaki bağlanma bölgesi tahminleri / Binding site predictions in the SARS COV-2 (6LU7) structure of alloferon 1.

Receptor residue	Peptide residue	Receptor residue	Peptide residue	Receptor residue	Peptide residue
ARG A 298	PHE B 1	ARG A 298	LEU B 2	ARG A 298	SER B 3
ASP A 295	SER B 3	VAL A 297	ALA B 8	VAL A 297	ILE B 12
PHE A 294	ALAB B 8	PHE A 294	ILE B 9	PHE A 294	SER B 14
PHE A 294	LEU B 2	PHE A 294	SER B 3	PHE A 294	LEU B 4
PRO A 293	SER B 14	PRO A 293	PHE B 16	PHE A 294	PHE B 1
PRO A 252	ILE B 12	LEU A 253	ILE B 12	THRA A 292	PHE B 16
ILE A 249	ALAB B 13	ILE A 249	SER B 14	LEU A 250	ILE B 12
ILE A 200	PHE B 16	VAL A 202	PHE B 16	ILE A 249	ILE B 12
ASP A 153	GLY B 7	TYR A 154	PHE B 1	SERA A 158	PRO B 6
ILE A 152	ILE B 5	ASP A 153	PHE B 1	ASP A 153	PRO B 6
ILE A 152	PHE B 1	ILE A 152	LEU B 2	ILE A 152	LEU B 4
ASNA A 151	LEU B 4	ASNA A 151	ILE B 5	ASNA A 151	PRO B 6
PHE A 112	LEU B 4	SERA A 113	LEU B 4	PHE A 150	LEU B 4
THRA A 111	SER B 3	THRA A 111	LEU B 4	THRA A 111	ILE B 5
GLNA A 110	SER B 14	GLNA A 110	LEU B 15	GLNA A 110	PHE B 16
GLY A 109	PHE B 16	GLNA A 110	LEU B 4	GLNA A 110	ILE B 5
GLNA A 107	PHE B 16	GLNA A 107	LYS B 17	GLY A 109	LEU B 15
PRO A 9	LEU B 2	ILE A 106	ILE B 5	ILE A 106	LEU B 15
PHE A 8	LEU B 2	PHE A 8	SER B 3	PHE A 8	LEU B 4
MET A 6	SER B 3	ALAA 7	SER B 3	PHE A 8	PHE B 1

**Ek Şekil 2 / Supplement Figure 2.** Peptid ctyr2801 in SARS COV-2 (6LU7) yapısındaki bağlanma bölgesi tahminleri / Binding site predictions in the SARS COV-2 (6LU7) structure of peptid ctyr2801.

Receptor residue	Peptide residue	Receptor residue	Peptide residue	Receptor residue	Peptide residue
PHE A 294	ILE B 12	ASP A 295	PHE B 1	ARG A 298	PHE B 1
PHE A 294	LEU B 2	PHE A 294	PRO B 3	PHE A 294	VAL B 8
THR A 292	ILE B 12	PRO A 293	ILE B 12	PHE A 294	PHE B 1
ASP A 248	ARG B 7	ILE A 249	ARG B 7	ILE A 249	VAL B 8
GLU A 240	LEU B 13	ASP A 245	ARG B 7	HIS A 246	GLY B 11
VAL A 202	GLY B 11	ASN A 203	ILE B 12	GLU A 240	GLY B 11
ASP A 153	LEU B 2	ILE A 200	ILE B 12	ILE A 200	LEU B 13
ASN A 151	LEU B 2	ILE A 152	PHE B 1	ASP A 153	PHE B 1
GLN A 110	ILE B 12	THR A 111	PHE B 1	ASN A 151	PHE B 1
GLN A 110	LEU B 2	GLN A 110	LEU B 4	GLN A 110	VAL B 8
GLY A 109	ILE B 12	GLY A 109	LEU B 13	GLN A 110	PHE B 1
GLN A 107	LEU B 9	GLN A 107	LEU B 13	PRO A 108	LEU B 13
VAL A 104	LEU B 2	ILE A 106	LEU B 2	ILE A 106	LEU B 9

**Ek Şekil 3 / Supplement Figure 3.** Temporin 1ta'nın SARS COV-2 (6LU7) yapısındaki bağlanma bölge tahminleri / Binding site predictions in the SARS COV-2 (6LU7) structure of temporin 1ta.

Receptor residue	Peptide residue	Receptor residue	Peptide residue	Receptor residue	Peptide residue
VAL A 297	TRP B 3	SER A 301	ALA B 1	SER A 301	LEU B 2
PHE A 294	LEU B 7	PHE A 294	LYS B 9	PHE A 294	LEU B 11
PRO A 293	TRP B 3	PRO A 293	LEU B 11	PHE A 294	LEU B 6
PRO A 252	THR B 5	LEU A 253	TRP B 3	THR A 292	LEU B 11
LEU A 250	TRP B 3	PRO A 252	ALA B 1	PRO A 252	TRP B 3
ILE A 249	VAL B 10	ILE A 249	LEU B 11	ILE A 249	ALA B 15
ASP A 245	ALA B 15	ILE A 249	TRP B 3	ILE A 249	LEU B 6
PRO A 241	VAL B 23	THR A 243	ASN B 19	THR A 243	LEU B 22
GLU A 240	ALA B 20	GLU A 240	VAL B 23	PRO A 241	ASN B 19
ASN A 203	LYS B 16	GLU A 240	LYS B 16	GLU A 240	ASN B 19
THR A 196	ALA B 27	THR A 198	ALA B 25	VAL A 202	LYS B 16
GLY A 195	ASN B 26	GLY A 195	ALA B 27	THR A 196	ASN B 26
ASN A 133	ASN B 26	ASN A 151	LYS B 9	SER A 158	LYS B 12
PRO A 132	ALA B 25	PRO A 132	ASN B 26	ASN A 133	ALA B 25
PRO A 108	ALA B 17	PRO A 108	ALA B 20	GLY A 109	LYS B 16
GLN A 107	LYS B 16	GLN A 107	ALA B 17	PRO A 108	LYS B 16
GLN A 107	LYS B 12	GLN A 107	ALA B 13	GLN A 107	ALA B 14
VAL A 104	LYS B 12	ILE A 106	LYS B 12	GLN A 107	LEU B 11

**Ek Şekil 4 / Supplement Figure 4.** Dermaseptin s4'ün SARS COV-2 (6LU7) yapısındaki bağlanma bölge tahminleri / Binding site predictions in the SARS COV-2 (6LU7) structure of dermaseptin s4.

Receptor residue	Peptide residue	Receptor residue	Peptide residue	Receptor residue	Peptide residue
THR A 292	PHE B 4	PHE A 294	PHE B 2	ILE A 249	ILE B 9
ASP A 245	ILE B 9	ASP A 245	HIS B 10	ASP A 245	ILE B 8
THR A 243	HIS B 11	ASP A 245	ARG B 7	PRO A 241	PHE B 23
PRO A 241	HIS B 11	PRO A 241	VAL B 22	GLU A 240	VAL B 12
GLU A 240	ILE B 9	GLU A 240	HIS B 11	TYR A 239	VAL B 22
ILE A 200	VAL B 12	MET A 235	VAL B 22	THR A 198	PHE B 15
GLY A 183	PHE B 19	PRO A 184	PHE B 19	TYR A 182	VAL B 16
ASNA 151	PHE B 2	ASP A 153	VAL B 1	PHE A 134	VAL B 16
PRO A 132	VAL B 16	ASNA 133	PHE B 15	PRO A 132	PHE B 15
PHE A 112	PHE B 2	ARG A 131	VAL B 16	THR A 111	PHE B 2
GLNA 110	PHE B 2	GLNA 110	PHE B 4	GLY A 109	VAL B 12
PRO A 108	VAL B 16	GLY A 109	PHE B 4	PRO A 108	GLY B 13
PRO A 108	PHE B 4	PRO A 108	VAL B 12	GLNA 107	GLY B 13
GLNA 107	ILE B 8	GLNA 107	VAL B 12	GLNA 107	LEU B 5
ILE A 106	LEU B 5	GLNA 107	PHE B 4	ILE A 106	PHE B 2
VAL A 104	LEU B 5	ARG A 105	LEU B 5		

**Ek Şekil 5 / Supplement Figure 5.** Clavanin B'nin SARS COV-2 (6LU7) yapısındaki bağlanma bölge tahminleri / Binding site predictions in the SARS COV-2 (6LU7) structure of Clavanin B.

Receptor residue	Peptide residue	Receptor residue	Peptide residue	Receptor residue	Peptide residue
SER A 301	VAL B 20	GLY A 302	LEU B 17	GLY A 302	MET B 21
ARG A 298	VAL B 20	ARG A 298	SER B 23	SERA 301	LEU B 17
VAL A 297	PHE B 16	VAL A 297	VAL B 20	ARG A 298	GLU B 19
PHE A 294	SER B 8	PHE A 294	PHE B 16	VAL A 297	SER B 8
PRO A 293	PHE B 5	PRO A 293	SER B 8	PHE A 294	PHE B 5
PHE A 291	ILE B 2	THR A 292	ILE B 2	PRO A 293	ILE B 2
PRO A 252	GLY B 13	LEU A 253	PHE B 5	GLNA 256	LEU B 17
ASP A 245	LEU B 6	ILE A 249	ILE B 2	ILE A 249	PHE B 5
VAL A 202	GLY B 1	VAL A 202	ILE B 2	ASNA 203	ILE B 2
PHE A 112	LYS B 4	ASNA 151	LYS B 4	TYR A 154	LYS B 22
GLNA 110	LYS B 4	GLNA 110	HIS B 7	THR A 111	LYS B 4
GLY A 109	ILE B 2	GLNA 110	ILE B 2	GLNA 110	GLY B 3
PRO A 108	ILE B 2	PRO A 108	GLY B 3	GLY A 109	GLY B 1
GLNA 107	GLY B 3	GLNA 107	LEU B 6	PRO A 108	GLY B 1

**Ek Şekil 6 / Supplement Figure 6.** Magainin b2'nin SARS COV-2 (6LU7) yapısındaki bağlanma bölge tahminleri / Binding site predictions in the SARS COV-2 (6LU7) structure of magainin b2.

Receptor residue	Peptide residue
PHE A 294	PHE B 3
PRO A 293	PHE B 3
THR A 292	GLY B 1
ASP A 245	SER B 6
GLU A 240	SER B 6
ILE A 200	HIS B 5
GLY A 183	LYS B 12
TYR A 182	LEU B 15
ASNA 180	PHE B 14
ASP A 176	LYS B 12
PHE A 134	PHE B 10
ASNA 133	GLY B 8
THR A 111	GLY B 1
GLNA 110	LEU B 4
GLY A 109	HIS B 5
PRO A 108	ALAB 7
GLNA 107	VAL B 18
GLNA 107	HIS B 5
ARGA 105	GLY B 21
ARGA 105	PHE B 14

Receptor residue	Peptide residue
ASP A 295	GLY B 1
PHE A 294	GLY B 1
THR A 292	PHE B 3
ILE A 249	PHE B 3
GLU A 240	ALA B 7
VAL A 202	HIS B 5
PRO A 184	PHE B 10
GLY A 183	PHE B 10
PHE A 181	LYS B 12
ASP A 176	PHE B 14
ASNA 151	GLY B 1
ASNA 133	LYS B 9
ARG A 131	PHE B 10
GLNA 110	HIS B 5
GLNA 110	GLY B 1
PRO A 108	PHE B 10
GLNA 107	MET B 19
GLNA 107	SER B 6
ILE A 106	MET B 19
ARG A 105	MET B 19

Receptor residue	Peptide residue
VALA 297	PHE B 3
PHE A 294	LYS B 2
THR A 292	HIS B 5
ILE A 249	LEU B 4
THR A 243	SER B 6
ASNA 203	HIS B 5
PRO A 184	GLY B 11
GLY A 183	GLY B 11
TYR A 182	LYS B 12
ASNA 180	LYS B 12
ASNA 151	LYS B 2
ASNA 133	PHE B 10
PRO A 132	PHE B 10
GLNA 110	ILE B 20
GLNA 110	LYS B 2
PRO A 108	LEU B 15
PRO A 108	HIS B 5
GLNA 107	ALAB 7
GLNA 107	LEU B 4
ARG A 105	ILE B 20

**Ek Şekil 7 / Supplement Figure 7.** Magainin b1'in SARS COV-2 (6LU7) yapısındaki bağlanma bölge tahminleri / Binding site predictions in the SARS COV-2 (6LU7) structure of magainin b1.



Araştırma makalesi / Research article

## Üretkenlik karşıtı iş davranışlarının iş kazalarına olan etkisinde güvenlik ikliminin düzenleyici rolü; makine ve ekipman imalatı sektörü örneği

Fahri Oluk<sup>\*1</sup> , Ahmet Gokcan<sup>2</sup> , Goksel Demir<sup>2</sup> 

<sup>1</sup> Cankiri Karatekin University, Yapraklı Technical and Business Collage, Department of Property Protection and Security, Program of Occupational Health and Safety, 18200, Cankiri, Türkiye

<sup>2</sup> University of Health Sciences Turkey, Hamidiye Faculty of Health Sciences, Department of Occupational Health and Safety, 34668, Uskudar, Istanbul, Türkiye

### Öz

Güvenlik iklimi, örgütlerde çalışanların iş kazalarına karşı davranış ve tutumlarını olumlu veya olumsuz yönde şekillendiren belirleyici etki olarak görülmektedir. Çalışanların sergilemiş oldukları üretkenlik karşıtı iş davranışları iş ortamlarındaki güvenlik iklimini olumsuz yönde etkileyen davranışlar olarak karşımıza çıkmaktadır. Yapılan bu çalışmada, “Makine ve Ekipman İmalatı” sektöründeki çalışanların üretkenlik karşıtı iş davranışlarının iş kazalarına olan etkisinde güvenlik ikliminin düzenleyici rolünün tespiti amaçlanmıştır. Bu amaçla belirlenen iş koluna ait özel sektörde çalışan 394 kişiden anket formu yöntemiyle veriler toplanmıştır. Elde edilen verilerle IBM SPSS 26.0 ve AMOS 24 Programı kullanılarak analizler gerçekleştirilmiştir. Analizler sonrasında düzenleyici etkinin durumsal olarak nasıl değiştiği hakkında ayrıntılı fikir sahibi olabilmek için eğim analizi (slope) gerçekleştirilmiştir. Sonuç olarak elde edilen bulgulara göre iş kazalarına, üretkenlik karşıtı iş davranışlarının olumlu yönde ve anlamlı, güvenlik ikliminin olumsuz yönde ve anlamlı etkilerinin olduğu tespit edilmiştir. Bu sonuç, güvenlik ikliminin düşük olması durumunda, üretkenlik karşıtı iş davranışlarının iş kazalarına olan etkisinin daha da arttığını ve üretkenlik karşıtı iş davranışları- iş kazaları arasındaki ilişkinin, güvenlik iklimi tarafından düzenlendiğini göstermektedir. Yol analizine dâhil edilen tahmin değişkenlerinin iş kazaları üzerindeki değişimin yaklaşık %15’ini açıkladığı sonucuna ulaşılmıştır. Elde edilen sonuçlar, araştırmanın yürütüldüğü sektörde iş kazaları konusunda üretkenlik karşıtı iş davranışlarının ve güvenlik ikliminin etkisi açısından önemli ipuçları sağlayabilecektir.

**Anahtar kelimeler:** Güvenlik iklimi; iş güvenliği; iş kazası; üretkenlik karşıtı iş davranışları

## The regulatory role of the safety climate in the effect of counterproductive work behaviors on work accidents; example of machinery and equipment manufacturing industry

### Abstract

The safety climate is seen as the determining effect that shapes the behavior and attitudes of employees towards occupational accidents in a positive or negative way. The counterproductive work behaviors exhibited by the employees appear as behaviors that negatively affect the safety climate in the workplace. In this study, it is aimed to determine the regulatory role of the safety climate in the effect of the counterproductive work behaviors of the employees in the “Machinery and Equipment Manufacturing” sector on

\* Sorumlu yazar / Corresponding author.

E-mail: [fahrioluk@karatekin.edu.tr](mailto:fahrioluk@karatekin.edu.tr) (F. Oluk).

<https://doi.org/10.51753/flsrt.1123316> Yazar katkıları / Author contributions

Geliş tarihi / Received 30 Mayıs 2022 / 30 May 2022; Kabul tarihi / Accepted 29 Eylül 2022/ 29 September 2022

Çevrimiçi yayın / Available online 27 Aralık 2022 / 27 December 2022

2718-062X © 2022 This is an open access article published by Dergipark under the [CC BY](https://creativecommons.org/licenses/by/4.0/) license.

occupational accidents. For this purpose, data were collected from 394 people working in the private sector belonging to the determined business line, using the survey form method. Analyzes were carried out with the obtained data using IBM SPSS 26.0 and AMOS 24 Program. After the analyses, slope analysis was carried out in order to have a detailed idea about how the regulatory effect changed situationally. As a result, according to the findings, it has been determined that counterproductive work behaviors have positive and significant effects on occupational accidents, and the safety climate has negative and significant effects. This result shows that if the safety climate is low, the effect of counterproductive work behaviors on occupational accidents increases and the relationship between counterproductive work behaviors and occupational accidents is regulated by the safety climate. It was concluded that the estimation variables included in the road analysis explained approximately 15% of the change in occupational accidents. The results obtained will provide important clues in terms of the effect of counterproductive work behaviors and safety climate on occupational accidents in the sector where the research is conducted.

**Keywords:** Counterproductive work behaviors; occupational accident; occupational safety; safety climate

## 1. Giriş / Introduction

Son yıllarda teknolojiye meydana gelen hızlı değişimler ve gelişimler endüstri alanında büyük bir mekanik çalışma ortamını oluştursa da halen kas gücüne dayanan nitelikli çalışanlara ihtiyaç duyulmaktadır (Akkaya, 2019). Sektörlerin tüketicilerin ihtiyaçlarına karşılık verebilmesi, kendilerini geliştirebilmesi ve büyümesinde nitelikli sayıda çalışan gücü büyük rol oynamaktadır. Bu nedenle işverenler, tecrübeli çalışanlarını kaybetmek istemeyecekleri için çalışanlarını kötü yönde etkileyebilecek konular üzerinde durulması zorunlu hale gelmektedir (Polat, 2020). Yöneticiler tarafından çalışanlara yönelik düzenlemeler bazen ters tepki vermekte ve çalışanlar tarafından üretkenlik karşıtı iş davranışları olarak tanımlanan istenmeyen olaylar meydana gelebilmekte ve çalışanlar hem çalışma arkadaşlarına hem de işverenlere yönelik zarar verme niyetiyle kasıtlı eylemlerde bulunabilmektedirler (Spector ve Fox, 2005).

Üretkenlik karşıtı iş davranışlarının tanımlanmasına yönelik literatürde birçok farklı tanım yer almasına karşın, Robinson ve Benett (1995) tarafından yapılan en geniş ve kapsamlı tanıma göre; üretkenlik karşıtı iş davranışları, işyerinde çalışanlar tarafından gösterilen sapkın davranışların yönetim tarafından çalışma ortamını düzenleyen önemli normları ihlal eden hem işverene, hem diğer çalışanlara, hem de çalışma ortamına ciddi zararlar veren bilinçli davranışlar olarak tanımlanmıştır. Yapılan çalışmalarda üretkenlik karşıtı iş davranışları şu şekilde sıralanmıştır (Glinska-Newes ve Lis, 2016);

- Çalışma ortamı içerisinde diğer çalışma arkadaşlarına yönelik taciz, tehdit, görmezden gelme gibi hem fiziksel hem psikolojik olarak zarar veren davranışlar,
- Çalışanların görevlerini kasıtlı olarak yerine getirmemesi ve görevlerini ihmal etmeleri,
- Çalışma ortamına kasıtlı olarak zarar verme,
- Hem işyerine hem de çalışma arkadaşlarına ait önemli ürünlerin çalınması,
- İşten kaçınma, gerekçesiz izin kullanma, işe kasıtlı olarak geç gitme ve erken ayrılma, uzun süreli molalar verme gibi davranışlar üretkenlik karşıtı iş davranışları olarak değerlendirilmektedir.

Çalışma ortamında görülen üretkenlik dışı iş davranışlarının kasıtlı olarak hem çalışma ortamına hem de diğer çalışanlara zarar vermesi güvensiz davranışların temelini oluşturmaktadır. Hem üretkenlik karşıtı iş davranışları hem de iş

kazalarının nedenleri arasında gösterilen güvensiz davranışlar çalışanları ve işyerini olumsuz bir şekilde etkilemektedir (Tong ve ark., 2022). İş kazalarının nedenlerinin araştırılmasına yönelik yapılan çalışmalarda; kazaların %10'unun güvensiz durumlardan, %88'inin güvensiz davranışlardan ve %2'sinin ise önlenemeyen kazalardan meydana geldiği gözlemlenmiştir (Seber, 2012; Yagimli ve Ergin, 2017).

Çalışma ortamında güvensiz davranışlardan dolayı meydana gelen iş kazalarında birçok çalışan yaralanmakta ve hatta hayatlarını kaybetmektedirler. Çalışma alanlarında meydana gelen ölümlü iş kazaları sebebiyle yaşanan işçi kayıpları hem işveren için hem de devletler için büyük bir endişe kaynağı olmaktadır. Düşük oranlarda dahi olsa çalışanların hayatını kaybetmesi sosyal ve ekonomik yönden olumsuz bir durum olarak görülmektedir (Zermane ve ark., 2020). Meydana gelen iş kazalarının hem sosyal etkileri hem de insan acıları hesaplanamaz olsa da, ekonomik etkileri, sosyal ve kurumsal kayıpları da dahil olmak üzere toplumun her safhası için oldukça önemli bir sorundur (Melchior ve Zanini, 2019). Bu sebeple çalışma ortamında meydana gelebilecek iş kazalarının önlenmesi için güvensiz davranış olarak nitelendirilebilecek olayların tespit edilmesi ve önlenmesi büyük önem arz etmektedir (Yagimli ve Ergin, 2017). İş kazalarına neden olan güvensiz davranışlarda en önemli etkenin insan faktörünün, yani çalışanların olduğu görülmektedir. İş kazalarının kaynağını oluşturan ve en önemli etken olan çalışan faktörü irdelenmeli ve güvenlik iklimi düzeyleri değerlendirilmelidir (Gokcan, 2022).

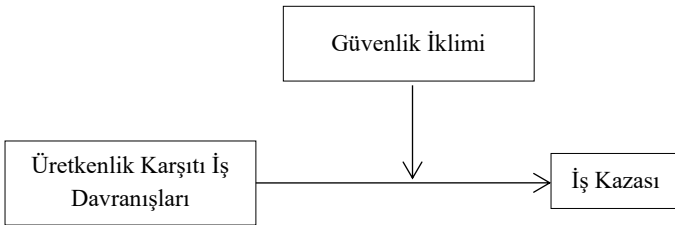
Meydana gelen iş kazalarında çalışanların büyük rol oynaması nedeniyle güvenlik iklimi iş kazalarının önlenmesinde anahtar faktörlerden birisidir (Kim ve ark., 2019). Güvenlik iklimi üzerine yapılan birçok çalışmada; güvenlik ikliminin çalışanların davranışlarını etkilemesi yoluyla daha sağlıklı ve güvenli bir çalışma ortamının oluşturulmasında büyük rol oynadığı gösterilmektedir (Bronkhorst ve ark., 2018). Güvenlik iklimi, çalışanların liderlik, iletişim ve iş organizasyonu gibi güvenlik durumuna ilişkin risk algıları olarak tanımlanmaktadır (Doyen et al., 2020). Güvenlik iklimini ölçmeye yönelik yapılan çalışmaların temelinde çalışanların güvensiz davranışlarının tespit edilmesi, iş kazalarının ve yaralanmaların önüne geçilmesine yönelik sektöre özgü önlem yöntemlerinin geliştirilmesi bulunmaktadır (Probst ve ark., 2019). İş hayatındaki öncelikli hedef, sağlık ve güvenliği korumak ve bu durumun devamlılığını sağlamaktır. Bu nedenle planlanan sistemli ve bütünsel çalışmaların tamamı iş sağlığı ve güvenliği olarak tanımlanabilir. İş sağlığı ve güvenliği iş yerlerinde pozitif güvenlik iklimi oluşuma katkı sağlayan önemli bir roldür (Celik, 2014). İş güvenliği için yürütülen faaliyetlerinin genel

amaçlarından bir tanesi; iş kazası ve meslek hastalıklarının önlemek ve oluşturacağı olumsuz sonuçlarından çalışanları ve işletmeyi koruyarak maddi ve manevi zararları ortadan kaldırarak güvenli çalışma ortamı oluşturmaktır (Kurt, 2013).

Bu çalışmada, makine ve ekipman imalatı sektöründeki çalışanların üretkenlik karşıtı iş davranışlarının iş kazalarına olan etkisinde güvenlik ikliminin düzenleyici rolünün tespiti amaçlanmıştır. Elde edilen sonuçların çalışma hayatına ve örgütsel davranış literatürüne katkı sunması beklenmektedir.

## 2. Gereç ve yöntemler / Materials and methods

Bu çalışmada makine ve ekipman imalatı sektörü çalışanlarının sergiledikleri üretkenlik karşıtı iş davranışlarının iş kazalarına olan etkisi incelenerek, çalışanların güvenlik iklimi algılarının bu etki üzerinde düzenleyici rolü olup olmadığı araştırılmıştır. Araştırmaya yol gösterici olması ve hipotezin oluşturulması açısından Şekil 1'deki model kurulmuştur. Bu model, üretkenlik karşıtı iş davranışları, güvenlik iklimi ve iş kazası arasındaki ilişkileri incelemeyi amaçlayan bir modeldir.



Şekil 1 / Figure 1. Araştırmanın modeli / Model of the research.

Bu çalışma için toplanan verilerin sunulan modele uygunluğu, AMOS 24 Programı kullanılarak Doğrulayıcı Faktör Analizi (DFA) ile test edilmiştir. İki boyut ve toplam 15 maddeden oluşan güvenlik iklimi ölçeğinin birinci düzey çok faktörlü yapısı için yapılan inceleme neticesinde verilerin normal dağılım göstermesi nedeniyle Maximum Likelihood hesaplama yöntemi kullanılmıştır.

### 2.1. Hipotez / Hypothesis

Bu çalışmanın amacına ve söz konusu modele uygun olarak oluşturulan hipotez aşağıdaki gibidir:

**H<sub>1</sub>:** Üretkenlik karşıtı iş davranışlarının iş kazalarına olan etkisinde güvenlik ikliminin düzenleyici rolü vardır. Güvenlik ikliminin düşük olması durumunda üretkenlik karşıtı iş davranışlarının iş kazalarına olan etkisi yüksek olacaktır.

### 2.2. Araştırmanın evren ve örnekleme / The universe and sample of the research

Bu çalışmanın örneklemini makine ve ekipman imalatı yapan özel sektör çalışanları oluşturmaktadır. 2020 SGK verilerine göre "Makine ve Ekipman İmalatı" yapan özel sektör işyerlerindeki çalışan sayısı 183,302 olarak tespit edilmiştir. Bu verilere istinaden örneklem büyüklüğünün evreni temsil etmesi açısından %95 güvenlikle Cohen, Manion ve Morrison (2017)'a göre belirlenen iş kolundan 423 çalışan üzerinde belirlenen ölçekler uygulanmış ve yapılan değerlendirmeler sonucunda 29 ankette eksik bölümlerin olduğu tespit edilmiş ve analizlere dâhil edilmemiştir. 394 çalışanın eksiksiz olarak doldurmuş olduğu anket formları analize tabi tutulmuştur.

### 2.3. Veri toplama araçları / Data collection tools

Katılımcılardan veri toplamak amacıyla iki farklı ölçekten ve demografik bilgilerin yer aldığı anket formundan faydalanılmıştır. Çalışanların güvenlik iklimi algısının belirlenmesi amacıyla Choudhry ve ark. (2009) tarafından geliştirilip, Turen ve ark. (2014) tarafından güvenilirlik ve geçerlilik testlerinin gerçekleştirilerek Türkçe'ye uyarlanması yapılmış olan "Güvenlik İklimi" ölçeği kullanılmıştır. Toplam 14 maddeden oluşan bu ölçekte, iş arkadaşları ve güvenlik eğitimleri ile yönetimin bakış açısı ve kurallar olmak üzere iki farklı boyut yer almaktadır. Çalışanların üretkenlik karşıtı iş davranışlarını ölçmek amacıyla Spector ve ark. (2006) tarafından geliştirilen ve Ocel (2010) tarafından güvenilirlik ve geçerlilik testlerinin gerçekleştirilerek Türkçe'ye uyarlanması yapılan "Üretim Karşıtı İş Davranışları Ölçeği" kullanılmıştır. Bu ölçek toplam 32 madde ve sabotaj, kötüye kullanma, geri çekilme ile çalma olmak üzere dört boyuttan oluşmaktadır.

### 3. Bulgular ve tartışma / Results and discussion

Bu çalışma için kullanmış olduğumuz ölçekler daha önce geliştirilmiş ve Türkçe'ye uyarlanmış olması nedeniyle toplanan verilerin sunulan modele uygunluğu, IBM SPSS 26.0 ve AMOS 24 Programı kullanılarak analiz edilmiştir. Gerçekleştirilen analizler sonucunda örnekleme ait demografik bulgular Tablo 1'de özetlenmiştir.

Tablo 1 / Table 1

Katılımcıların demografik özellikleri / Demographic characteristics of participants.

		Frekans	%
Yaş	18-30	126	32,0
	31-40	141	35,8
	41-50	97	24,6
	51 ve üstü	30	7,6
	Toplam	394	100,0
Cinsiyet	Erkek	394	100,0
	Kadın	0	0,0
Eğitim	Okuryazar değil	3	0,8
	İlköğretim	161	40,9
	Lise	168	42,6
	Üniversite	62	15,7
	Toplam	394	100,0
Tecrübe	1-10	223	56,6
	11-20	100	25,4
	21-30	48	12,2
	31 ve üstü	23	5,8
	Toplam	394	100,0
Kaza Geçirme	Evet	92	23,4
	Hayır	302	76,6
	Toplam	394	100,0

Tablo 1'e göre araştırmaya katılan çalışanların yaş dağılımları incelendiğinde çalışanların 126'sının (%32) 18-30 yaş, 141'inin (%35,8) 31-40 yaş, 97'sinin (%24,6) 41-50 yaş ve 30'unun (%7,6) ise 51 ve üzeri yaş aralığına sahip olduğu tespit edilmiştir. Çalışmaya katılanların cinsiyet grubu incelendiğinde belirlenen sektör nedeniyle 394'ü (%100) erkelerden oluştuğu tespit edilmiştir. Çalışmaya katılanların eğitim durumları incelendiğinde çalışanların 3'ünün (%0,8) okur yazar olmadığı, 161'inin (%40,9) ilköğretim, 168'inin (%42,6) lise mezunu ve 62'sinin (%15,7) üniversite mezunu olduğu saptanmıştır. Çalışan bireylerin tecrübe durumları incelendiğinde ise

223'ünün (%56,6) 1-10 yıl, 100'ünün (%25,4) 11-20 yıl, 48'inin (%12,2) 21-30 yıl ve 23'ünün (%5,8) 31 yıl ve üzeri tecrübeye sahip olduğu tespit edilmiştir. Çalışmaya katılanların 92'sinin (%23,4) iş kazası geçirdiği, 302'sinin (%76,6) iş kazası geçirmediği tespit edilmiştir.

### 3.1. DFA bulguları / CFA results

Yapılan DFA sonucunda istenilen uyum iyiliği değerleri elde edilememiştir. Bu nedenle düzeltme indekslerinin incelenmesi neticesinde gerekli modifikasyonlar yapılmış ve anlamsız faktör yüküne sahip olduğu tespit edilen *guv1* maddesi modelden çıkarılarak analiz tekrarlanmıştır. Tekrarlanan analiz neticesinde elde edilen uyum indeksleri ölçüm modelinin doğrulandığına işaret etmiştir. DFA neticesinde elde edilen uyum iyiliği değerleri ( $X^2 [60, N=394]=180,095$ ;  $p < ,01$ ;  $X^2/sd=3,002$ ; CFI= ,95; RMSEA= ,07; SRMR= ,05) önerilen iki faktörlü modelin veri ile uyumlu ve kabul edilebilir olduğunu göstermektedir. Bu sonuçlar güvenlik iklimi ölçeğinin öngörülen kuramsal yapısının (iki faktörlü model) doğrulandığını göstermiştir. DFA sonucunda ulaşılan uyum iyiliği değerleri ile kabul edilebilir asgari uygunluk değerleri (Gurbuz, 2021) ise Tablo 2'de gösterilmiştir.

**Tablo 2 / Table 2**

DFA değerleri tablosu / Table of CFA values.

İndeksler	Kabul edilebilir değerler	GİÖ
$X^2 / sd$	$3 \leq X^2 / sd \leq 5$	3,0
Sayı CFI	$,90 \leq CFI \leq ,95$	,95
SRMR	$,05 < SRMR < ,08$	,05
RMSEA	$,05 \leq RMSEA \leq ,08$	,07

GİÖ: Güvenlik İklimi Ölçeği

**Tablo 3 / Table 3**

YEM analizine ilişkin parametre tahmin değerleri (N=394) / Parameter estimation values for SEM analysis (N=394).

Madde	Path	Faktör	$\beta_0$	$\beta_1$	S.E.	C.R.	P
guv10	<---	GUVEN1	,897	1,000			
guv9	<---	GUVEN1	,835	,925	,041	22,739	<0,001
guv8	<---	GUVEN1	,859	,933	,039	24,084	<0,001
guv7	<---	GUVEN1	,821	,903	,041	22,005	<0,001
guv6	<---	GUVEN1	,753	,894	,047	18,829	<0,001
guv5	<---	GUVEN1	,783	,798	,025	31,370	<0,001
guv4	<---	GUVEN1	,652	,616	,041	15,003	<0,001
guv3	<---	GUVEN1	,674	,692	,044	15,764	<0,001
guv2	<---	GUVEN1	,691	,639	,039	16,378	<0,001
guv14	<---	GUVEN2	,717	1,000			
guv13	<---	GUVEN2	,776	1,086	,079	13,751	<0,001
guv12	<---	GUVEN2	,771	1,041	,076	13,680	<0,001
guv11	<---	GUVEN2	,764	1,124	,083	13,579	<0,001

$\beta_0$ =Standart yol katsayıları  $\beta_1$ = Standart olmayan yol katsayıları.

Tablo 3'teki bulgular incelendiğinde gerçekleştirilen DFA neticesinde GUVEN1 ve GUVEN2 altında yer alan tüm maddelere ait yol katsayıları istatistiksel olarak anlamlı bulunmuştur. Standartlaştırılmış yol katsayılarına bakıldığında GUVEN1 üzerinde en fazla etkiye sahip olan maddenin guv10 olduğu ( $\beta_0=0,897$ ), GUVEN2 üzerinde en fazla etkiye sahip olan maddenin ise guv13 olduğu ( $\beta_0=0,776$ ) görülmektedir.

Toplam 32 madde ve dört alt faktörden oluşan üretkenlik karşıtı iş davranışları ölçeğinin birinci düzey çok faktörlü yapısı doğrulayıcı faktör analizi (DFA) yöntemi ile test edilmiştir. Verilerin normal dağılım göstermesi nedeniyle Maximum Likelihood hesaplama yöntemi kullanılmıştır. Yapılan DFA

sonucunda yazında kabul edilen uyum iyiliği değerlerine ulaşamamıştır. Bunun üzerinden düzeltme indekslerinin incelenmesi neticesinde gerekli modifikasyonlar yapılmış ve analiz tekrarlanmıştır. Tekrarlanan analiz neticesinde elde edilen uyum indeksleri ölçüm modelinin doğrulandığına işaret etmiştir. DFA neticesinde elde edilen uyum iyiliği değerleri ( $X^2 [454, N=394]=1585,917$ ;  $p < ,01$ ;  $X^2/sd=3,493$ ; CFI= ,91; RMSEA= ,08; SRMR= ,04) önerilen dört faktörlü modelin veri ile uyumlu ve kabul edilebilir olduğunu göstermektedir. Bu sonuçlar üretkenlik karşıtı iş davranışları ölçeğinin öngörülen kuramsal yapısının (dört faktörlü model) doğrulandığını göstermiştir. DFA sonucunda ulaşılan uyum iyiliği değerleri ile kabul edilebilir asgari uygunluk değerleri (Gurbuz, 2021) ise Tablo 4'de gösterilmiştir.

**Tablo 4 / Table 4**

DFA değerleri tablosu / Table of CFA values.

İndeksler	Kabul edilebilir değerler	ÜKİDÖ
$X^2 / sd$	$3 \leq X^2 / sd \leq 5$	3,4
CFI	$,90 \leq CFI \leq ,95$	,91
SRMR	$,05 < SRMR < ,08$	,04
RMSEA	$,05 \leq RMSEA \leq ,08$	,08

ÜKİDÖ: Üretkenlik Karşıtı İş Davranışları Ölçeği

**Tablo 5 / Table 5**

YEM analizine ilişkin parametre tahmin değerleri (N=394) / Parameter estimation values for SEM analysis (N=394).

Madde	Path	Faktör	$\beta_0$	$\beta_1$	S.E.	C.R.	P
ukid32	<---	F1	0,857	1,000			
ukid31	<---	F1	0,905	1,048	0,041	25,479	<0,001
ukid30	<---	F1	0,899	1,059	0,042	25,125	<0,001
ukid29	<---	F1	0,841	0,967	0,044	22,121	<0,001
ukid28	<---	F1	0,887	1,042	0,043	24,484	<0,001
ukid27	<---	F1	0,865	0,960	0,041	23,327	<0,001
ukid25	<---	F1	0,825	0,837	0,039	21,378	<0,001
ukid24	<---	F1	0,803	0,838	0,041	20,423	<0,001
ukid23	<---	F1	0,854	0,683	0,030	22,746	<0,001
ukid21	<---	F1	0,835	0,979	0,045	21,854	<0,001
ukid20	<---	F1	0,885	1,029	0,015	67,055	<0,001
ukid19	<---	F1	0,912	1,056	0,041	25,894	<0,001
ukid18	<---	F1	0,838	1,005	0,046	21,975	<0,001
ukid17	<---	F1	0,873	0,999	0,042	23,696	<0,001
ukid16	<---	F1	0,879	1,035	0,043	24,013	<0,001
ukid26	<---	F2	0,639	1,000			
ukid14	<---	F2	0,668	0,897	0,081	11,058	<0,001
ukid13	<---	F2	0,619	0,994	0,096	10,405	<0,001
ukid12	<---	F2	0,650	0,957	0,088	10,822	<0,001
ukid11	<---	F2	0,724	1,022	0,087	11,774	<0,001
ukid10	<---	F2	0,708	1,043	0,090	11,578	<0,001
ukid8	<---	F2	0,691	1,103	0,097	11,354	<0,001
ukid5	<---	F2	0,658	0,947	0,087	10,925	<0,001
ukid4	<---	F3	0,611	1,000			
ukid6	<---	F3	0,739	1,324	0,120	11,069	<0,001
ukid7	<---	F3	0,613	1,117	0,115	9,715	<0,001
ukid9	<---	F3	0,678	1,075	0,103	10,456	<0,001
ukid15	<---	F3	0,650	1,065	0,105	10,154	<0,001
ukid22	<---	F3	0,748	1,382	0,124	11,153	<0,001
ukid3	<---	F4	0,572	1,000			
ukid2	<---	F4	0,813	1,341	0,178	7,52	<0,001
ukid1	<---	F4	0,601	0,978	0,119	8,245	<0,001

$\beta_0$ =Standart yol katsayıları  $\beta_1$ = Standart olmayan yol katsayıları.

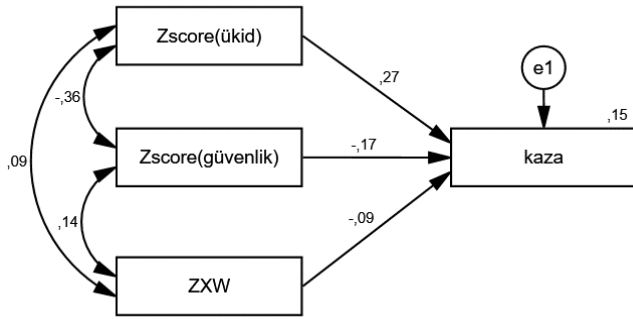
Tablo 5'teki bulgular incelendiğinde gerçekleştirilen DFA neticesinde F1,F2,F3 ve F4 altında yer alan tüm maddelere ait yol katsayıları istatistiksel olarak anlamlı bulunmuştur. Standartlaştırılmış yol katsayılarına bakıldığında F1 üzerinde en

fazla etkiye sahip olan maddenin ukıd19 ( $\beta_0=0,912$ ), F2 üzerinde ukıd11 ( $\beta_0=0,724$ ), F3 üzerinde ukıd6 ( $\beta_0=0,739$ ), F4 üzerinde ise ukıd2 olduğu ( $\beta_0=0,813$ ) görülmektedir.

### 3.2. Düzenleyici etki bulguları / Regulatory effect findings

Düzenleyici değişken, tahmin değişkeni ile sonuç değişkeni arasındaki ilişkinin yönünü ve şiddetini etkileyen bir değişkendir. Düzenleyici değişken iki değişken arasındaki ilişkinin hangi durumlarda arttığını, azaldığını veya yön değiştirdiğini (olumludan olumsuzu dönmeye) anlamamıza yardımcı olan bir değişkendir (Gurbuz, 2021).

Çalışanların üretkenlik karşıtı iş davranışlarının, iş kazalarına etkisinde güvenlik ikliminin düzenleyici rolünü test etmek amacıyla AMOS 24 Programı kullanılarak gerekli analizler gerçekleştirilmiştir. Gerçekleştirilen analizler sonucunda elde edilen yol analizi sonuçları Şekil 2’de verilmiştir.



Şekil 2 / Figure 2. Düzenleyici model çizimi / Editorial model drawing.

Yapılan düzenleyici etki analizi neticesinde elde edilen veriler Tablo 6’da gösterilmiştir. Gerçekleştirilen yol analizinde Maximum Likelihood yöntemi kullanılarak gerekli incelemeler yapılmıştır. Analiz gerçekleştirilmeden önce düzenleyici değişken ve tahmin değişkenine ilişkin değerler standardize edilmiştir. Kurulan model üzerinden gerçekleştirilen analiz sonuçlarına göre yol analizinde kullanılan tahmin değişkenleri, iş kazaları ile ilgili değişimin yaklaşık %15’ini ( $R^2=.146$ ) açıklamaktadır. İş kazalarına, üretkenlik karşıtı iş davranışlarının olumlu yönde ve anlamlı ( $\beta= .27, p<.001$ ), güvenlik ikliminin olumsuz yönde ve anlamlı düzeyde ( $\beta= -.17, p<.001$ ) etkilerinin olduğu tespit edilmiştir. Üretkenlik karşıtı iş davranışları ve güvenlik iklimi değişkenlerinin, iş kazaları üzerindeki etkileşimsel etkisinin (düzenleyici etki) anlamlı olduğu saptanmıştır ( $\beta= -.09, p<.05$ ).

Tablo 6 / Table 6

Düzenleyici etkiyi gösteren yol analizi sonuçları (N=394) / Path analysis results showing regulatory effect (N=394).

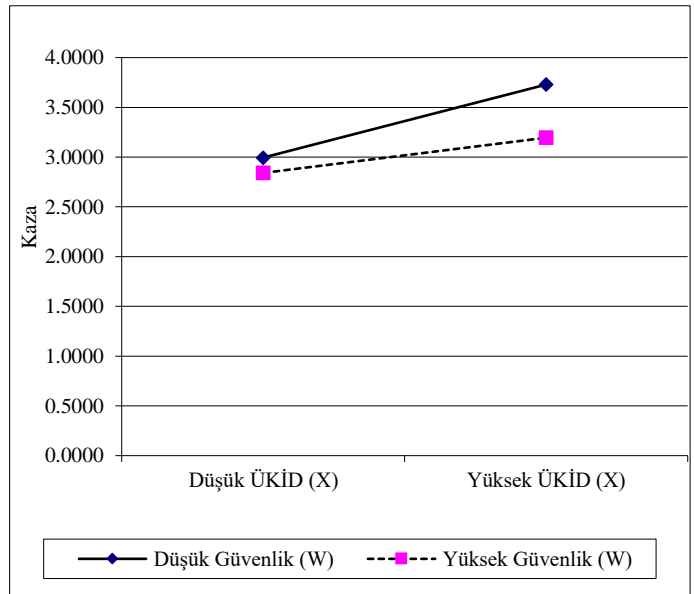
Değişkenler	$\beta$	S.H	t	p
Üretkenlik karşıtı iş davranışları(X)	,272***	,053	5,38	<0,001
Güvenlik iklimi(W)	-,171***	,053	-3,35	<0,001
X,W	-,095*	,054	-1,99	<0,046

Not:  $R^2=.146$ ; \*\*\* $p<.001$ , \* $p<.05$ , S,H,: Standart Hata, Standardize edilmiş beta katsayıları ( $\beta$ ) raporlanmıştır.

Bu işlemten sonra düzenleyici etkinin durumsal olarak nasıl değiştiği hakkında daha ayrıntılı fikir sahibi olabilmek için değişkenin yüksek ve düşük olduğu durumları ortaya koyan eğim analizi (slope) yapılması gerekmektedir. Başka bir

anlatımla güvenlik ikliminin farklı durumlarında (yüksek-düşük) üretkenlik karşıtı iş davranışlarının, iş kazası üzerindeki etkilerinin anlamlı olup olmadığına dair eğim analizi yapılması gerekmektedir.

Gerçekleştirilen eğim analizi sonucunda düzenleyici değişkene ait etkiler Şekil 3’te grafiksel olarak verilmiştir. Düzenleyici etkinin ayrıntıları incelendiğinde güvenlik ikliminin düşük ( $\beta=.36, p<.001$ ) olduğu durumlarda üretkenlik karşıtı iş davranışlarının iş kazasına olan etkisinin arttığı gözlenmiştir. Buna karşın güvenlik ikliminin yüksek ( $\beta=.17, p<.05$ ) olduğu durumlarda üretkenlik karşıtı iş davranışlarının, iş kazasına olan etkisinin daha az arttığı tespit edilmiştir. Bu bulgular doğrultusunda  $H_1$  hipotezi desteklenmiştir. Sonuç olarak, güvenlik ikliminin düşük olması durumunda, üretkenlik karşıtı iş davranışlarının iş kazalarına olan etkisinin daha da arttığı ve bu durum üretkenlik karşıtı iş davranışları-ış kazaları arasındaki ilişkinin, güvenlik iklimi tarafından düzenlendiği anlamına gelmektedir.



Şekil 3 / Figure 3. Güvenlik ikliminin düzenleyici etkisinin grafiksel gösterimi / Graphical representation of the regulatory impact of the security climate.

Ulusal ve uluslararası literatürde üretkenlik karşıtı iş davranışlarının iş kazalarına olan etkiyi inceleyen çok az sayıda çalışma bulunmaktadır. Bunun yanı sıra üretkenlik karşıtı iş davranışlarının iş kazalarına olan etkisinde güvenlik ikliminin düzenleyici rolü ile alakalı yapılan bir çalışma mevcut değildir. Bu sebeple gerçekleştirilen bu çalışmanın üretkenlik karşıtı iş davranışları ile iş kazaları arasındaki ilişkinin incelemesi ve bu ilişkide düzenleyici rol olarak güvenlik ikliminin etkisini açıklaması nedeniyle literatüre katkı sağlaması beklenmektedir.

### 4. Sonuçlar ve öneriler / Conclusions and recommendations

Araştırmada elde edilen sonuçlara göre iş kazalarına, üretkenlik karşıtı iş davranışlarının olumlu yönde ve anlamlı, güvenlik ikliminin olumsuz yönde ve anlamlı düzeyde etkilerinin olduğu tespit edilmiştir.

Üretkenlik karşıtı iş davranışları ve güvenlik iklimi değişkenlerinin, iş kazaları üzerindeki etkileşimsel etkisinin (düzenleyici etki) anlamlı olduğu saptanmıştır. Güvenlik ikliminin düşük olduğu durumlarda üretkenlik karşıtı iş davranışlarının iş kazasına olan etkisinin arttığı gözlenmiştir.

Buna karşın güvenlik ikliminin yüksek olduğu durumlarda üretkenlik karşıtı iş davranışlarının, iş kazasına olan etkisinin daha az arttığı tespit edilmiştir.

Güvenlik ikliminin düşük olması durumunda, üretkenlik karşıtı iş davranışlarının iş kazalarına olan etkisini daha da artırdığı ve üretkenlik karşıtı iş davranışları-ış kazaları arasındaki ilişkinin, güvenlik iklimi tarafından düzenlendiği kanaatine varılmıştır. İleride yapılacak çalışmalar için, ülkemiz açısından görünür ve görünmez birçok ekonomik zarara sebep olan, üretkenlik karşıtı iş davranışlarının iş kazalarına etkisinde bireylerin kişilik özellikleri, örgütsel özdeşleme, örgütsel adalet ve yönetim davranışları gibi değişkenlerin düzenleyici rolünün araştırılması önerilebilir. Farklı örneklerde üretkenlik karşıtı iş davranışlarının çalışan performansı, işten duyduğu tatmin, örgüte olan bağlılık gibi olumlu örgütsel ve bireysel durumlar

## Kaynaklar / References

- Akkaya, B. (2019). İlkokullardaki öğretmenlerin üretkenlik karşıtı iş davranışının örgütsel vatandaşlık ve örgütsel adalet ile ilişkisi. (Yayınlanmamış Doktora Tezi). Ankara Üniversitesi, Eğitim Yönetimi ve Politikası Anabilim Dalı, Ankara.
- Bronkhorst, B., Tummers, L., & Steijn, B. (2018). Improving safety climate and behavior through a multifaceted intervention: Results from a field experiment. *Safety science*, 103, 293-304.
- Choudhry, R. M., Fang, D., & Lingard, H. (2009). Measuring safety climate of a construction company. *Journal of construction Engineering and Management*, 135(9), 890-899.
- Cohen, L., Manion, L., & Morrison, K. (2017). Action research. In *Research methods in education* (pp. 440-456). Routledge.
- Celik, E. (2014). Güvenlik kültürünün güvenlik performansına etkisi: İş tatmininin aracılık rolü. *Gazi Üniversitesi Sosyal Bilimler Enstitüsü, Doktora Tezi*, Ankara.
- Doyen, B., Vlerick, P., Soenens, G., Vermassen, F., & Van Herzele, I. (2020). Team perception of the radiation safety climate in the hybrid angiography suite: A cross-sectional study. *International Journal of Surgery*, 77, 48-56s.
- Głinska-Newes, A., & Lis, A. (2016). Paradoks Współwystępowania Organizacyjnych Głinska-Newes Zachowań Obywatelskich I Kontraprodukcyjnych. *Research Papers of the Wrocław University of Economics/Prace Naukowe Uniwersytetu Ekonomicznego we Wrocławiu*, 422, 265-275.
- Gokcan, A., (2021). Gümüşhane ili altın madeni çalışanlarının iş sağlığı ve güvenliği algısının değerlendirilmesi. *Gümüşhane Üniversitesi, Yüksek Lisans Tezi, Fen Bilimleri Enstitüsü, Gümüşhane*.
- Gurbuz, S. (2021). *Amos ile Yapısal Eşitlik Modellemesi*. Ankara: Seçkin Yayıncılık. 1-199.
- Kim, N. K., Rahim, N. F. A., Iranmanesh, M., & Foroughi, B. (2019). The role of the safety climate in the successful implementation of safety management systems. *Safety science*, 118, 48-56.
- Kurt, R. (2013). *Herkes İçin İş Sağlığı ve Güvenliği Rehberi* (Birinci Baskı). Ankara: Seçkin Yayıncılık. 1-1143.
- Melchior, C., & Zanini, R. R. (2019). Mortality per work accident: A literature mapping. *Safety Science*, 114, 72-78.
- Ocel, H. (2010). Üretim karşıtı iş davranışları ölçeği: Geçerlik ve güvenilirlik çalışması. *Türk Psikoloji Yazıları*, 13(26), 18-26.
- Polat, M. (2020). Psikolojik sözleşme ihlallerinin üretkenlik karşıtı iş davranışlarına etkisi: Bir alan araştırması. *Ağrı İbrahim Çeçen Üniversitesi Sosyal Bilimler Enstitüsü Dergisi*, 6(1), 377-408.
- Probst, T. M., Goldenhar, L. M., Byrd, J. L., & Betit, E. (2019). The Safety Climate Assessment Tool (S-CAT): A rubric-based approach to measuring construction safety climate. *Journal of safety research*, 69, 43-51.
- Robinson, S. L., & Bennett, R. J. (1995). A typology of deviant workplace behaviors: A multidimensional scaling study. *Academy of management journal*, 38(2), 555-572.
- Seber, V. (2012). İşçi sağlığı ve güvenliğinde risk analizleri nasıl yapılır?. *Elektrik Mühendisliği*, 445, 30-34.
- SGK, (2020). Sosyal Güvenlik Kurumu İstatistik Yıllıkları, [http://www.sgk.gov.tr/wps/portal/sgk/tr/kurumsal/istatistik/sgk\\_istatistik\\_ik\\_yilliklari](http://www.sgk.gov.tr/wps/portal/sgk/tr/kurumsal/istatistik/sgk_istatistik_ik_yilliklari). Last accessed on March 03, 2022.
- Spector, P. E., & Fox, S. (2005). *Counterproductive work behavior: Investigation of actors and targets*. Washington, DC: APA Books.
- Spector, P. E., Fox, S., Penney, L. M., Bruursema, K., Goh, A., & Kessler, S. (2006). The dimensionality of counterproductivity: Are all counterproductive behaviors created equal?. *Journal of vocational behavior*, 68(3), 446-460.
- Tong, R., Wang, X., Wang, L., & Hu, X. (2022). A dual perspective on work stress and its effect on unsafe behaviors: The mediating role of fatigue and the moderating role of safety climate. *Process Safety and Environmental Protection*. 165, 929-940.
- Turen, U., Gokmen, Y., Tokmak, I., & Bekmezci, M. (2014). Güvenlik iklimi ölçeğinin geçerlilik ve güvenilirlik çalışması. *Süleyman Demirel Üniversitesi İktisadi ve İdari Bilimler Fakültesi Dergisi*, 19(4), 171-190.
- Yağimli, M. & Ergin, H. (2017). Türkiye’de İş Kazalarının Üssel Düzeltme Metodu ile Tahmin Edilmesi. *Marmara Fen Bilimleri Dergisi*, 29(4), 118-123.
- Zermane, A., Tohir, M. Z. M., Baharudin, M. R., & Yusoff, H. M. (2020). Analysis of the Contributing Factors for Fatal Accidents due to Falls from Heights in Malaysia and the USA. *Safety Engineering Interest Group*, 28, 15-36.

**Cite as / Atf şekli:** Oluk, F., Gokcan, A., & Demir, G. (2022). Üretkenlik karşıtı iş davranışlarının iş kazalarına olan etkisinde güvenlik ikliminin düzenleyici rolü; makine ve ekipman imalatı sektörü örneği. *Front Life Sci RT*, 3(3), 128-133.



## Research article

# Improving the adventitious rooting ability of hard-to-root olive (*Olea europaea* L.) cultivar cuttings through inhibiting strigolactone biosynthesis

Aslihan Ozbilen<sup>\*1</sup> , Fatih Sezer<sup>2</sup> , Kemal Melih Taskin<sup>2</sup> 

<sup>1</sup> Canakkale Onsekiz Mart University, Faculty of Science, Department of Biology, 17100, Canakkale, Türkiye

<sup>2</sup> Canakkale Onsekiz Mart University, Faculty of Science, Department of Molecular Biology and Genetics, 17100, Canakkale, Türkiye

## Abstract

Strigolactones (SLs) are synthesized in roots and control plant development. As phytohormones, SLs regulate plant architecture, including roots. Recently, the inhibiting effects of SLs on adventitious rooting have been identified. Olive (*Olea europaea* L.) is consumed for oil and table in Mediterranean countries and is an economically important crop. Turkey is one of the countries with the highest olive production. Olive has mostly propagated asexually via cuttings, however, the rooting capacities of some agriculturally important olive cultivars are very low. Indole Butyric Acid (IBA) is commonly used to promote the rooting of olive cuttings, however, it can be inadequate. Ayvalık is an easy-to-root cultivar and one of the most common cultivars grown for oil production and Domat is a hard-to-root cultivar in which IBA is insufficient for inducing rooting. In our study, the effects of synthetic SLs *rac*-GR24 and SLs biosynthesis inhibitor TIS108 on the rooting ability of olive cuttings were investigated. As a result, the adventitious rooting ability was increased when a hard-to-root cultivar was treated with TIS108, indicating a promising future for olive-cutting rooting. Therefore, our study will provide potentially new tools for propagation strategies using SLs in fruit trees.

**Keywords:** Cutting rooting; GR24; olive; strigolactones; TIS108

## 1. Introduction

Strigolactones (SLs) are carotenoid-derived plant metabolites and known to be germination stimulants for parasitic plant seeds for a long time (Cook et al., 1966). Then, they are found to be involved in the mutual interaction with arbuscular mycorrhizal fungi (Akiyama et al., 2005) and involved in the inhibition of lateral bud growth (Gomez-Roldan et al., 2008; Umehara et al., 2008). As endogenous phytohormones, SLs control plant architecture. Up to date, lots of studies have been carried out about SLs also affect root growth, primary root length, lateral root formation, root-hair elongation, adventitious rooting, root tip anatomy, stem elongation, leaf expansion in *Arabidopsis thaliana*, maize, petunia, rice, *Medicago truncatula*, *Vitis vinifera*, and *Solanum lycopersicum*. (Stirnberg

et al., 2002; Snowden et al., 2005; Kapulnik et al., 2011; Ruyter-Spira et al., 2011; Arite et al., 2012; Guan et al., 2012; Kohlen et al., 2012; Rasmussen et al., 2013; de Saint Germain et al., 2013; De Cuyper et al., 2015; Santoro et al., 2020; Xu et al., 2021).

Olive (*Olea europaea* L.), one of the oldest cultivated trees in the Mediterranean Region (Rugini, 1986; Zohary et al., 2012) is commercially important since olive oil and table olive are consumed quite a lot in the Mediterranean diet. Therefore, olive production is one of the important agricultural sectors that have the potential for high income. Olive can be propagated by cuttings, grafting, or in vitro techniques, however, propagation via cuttings is the most widely used method in many countries (Fabbri et al., 2004).

Olive has generally propagated asexually via cuttings in a

\* Corresponding author.

E-mail address: [aozbilen@comu.edu.tr](mailto:aozbilen@comu.edu.tr) (A. Ozbilen).

<https://doi.org/10.51753/flsrt.1186955> Author contributions

Received 10 October 2022; Accepted 05 December 2022

Available online 30 December 2022

2718-062X © 2022 This is an open access article published by Dergipark under the [CC BY](https://creativecommons.org/licenses/by/4.0/) license.

humid environment since the production of seeds is slow. However, the rooting capacities of some agriculturally important olive cultivars are very limited and can only be propagated by inoculation (Fabbri et al., 2004; Cetintas Gerakakis and Ozkaya, 2005). The exterior and interior factors that affect rooting capacities such as time of planting, size of cuttings, and properties of rooting media were reported (Cetintas Gerakakis and Ozkaya, 2005). Ayvalik is one of the most common cultivars grown in Turkey for oil production and is an easy-to-root cultivar (ER). The Olive Ayvalik cultivar is cultivated for its high oil quality (Isfendiyaroglu et al., 2009) and comprises 19% of the olive trees in Turkey (Kiralan and Bayrak, 2013).

Many studies revealed that auxins have the best effect on adventitious rooting (Fabbri et al., 2004). The olive cuttings are usually treated with Indole Butyric Acid (IBA) to promote rooting and the concentrations of plant growth regulator treated also affect the rooting abilities (Serrano et al., 2002). However, for a hard-to-root cultivar (HR) Domat, which bears large fruits, IBA is insufficient for inducing rooting (Cetintas Gerakakis and Ozkaya, 2005; Turkoglu and Durmus, 2005).

Recent studies on SLs are mostly carried out on model organisms, such as *Arabidopsis* or rice. However, little is known about the effects of SLs on fruit trees. Olive is an economically important crop in Mediterranean countries, and therefore, we investigated the effects of *rac*-GR24 as an SL analog and TIS108 as an SL inhibitor (Ito et al., 2013) on olive ER and HR cuttings. Finding a solution for rooting problems of HR cultivars is so important since grafting techniques are quite expensive. As a result, this study shows that TIS108 usage for HR olive cultivars provides new tools for cutting propagation strategies of fruit trees.

## 2. Materials and methods

Olive is mostly propagated via cuttings (Fabbri et al., 2004). For this reason, we aimed to determine the effects of *rac*-GR24 and TIS108 applications on the rooting ability of cuttings. We used the ER and the HR cuttings (Cetintas Gerakakis and Ozkaya, 2005).

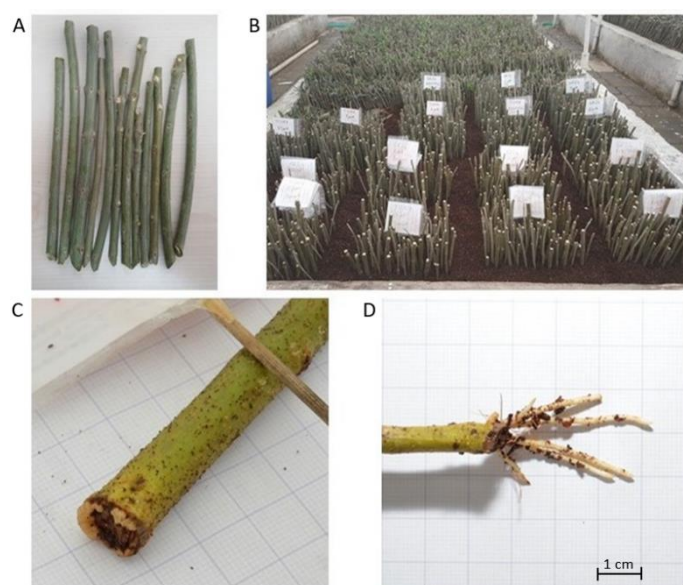


**Fig. 1.** A) Olive Cuttings prepared from olive trees, 25-30 cm each. B) Cuttings treated with *rac*-GR24 and TIS108 and planted in growing blocks. C) Callus formation on stem cuttings. D) Root formation on stem cuttings.

For each cultivar, 700 cuttings were tested (Fig. 1A). We treated cuttings with 1, 5, and 10  $\mu$ M *rac*-GR24 or TIS108 (Strigolab, Turin, Italy), and non-treated control groups were also included. Thus, for each treatment group, we had 100 cuttings for each cultivar.

For the applications, the basal pieces of both two olive cultivar cuttings were dipped into the plant growth regulator solutions (1, 5, and 10  $\mu$ M) one by one for 5 seconds and then planted into growing blocks that have a high water-holding capability (Fig. 1B). The cuttings were held in greenhouse conditions (25°C, 90-95% humidity) in the Edremit Directorate of Olive Production Station (Edremit, Balikesir). Ten weeks later of the treatment, the cuttings were evaluated in terms of the formation of both callus and roots since the callus formation from the wounded parts is the first stage of adventitious rooting of cuttings (Fig. 1C-D).

## 3. Results

We investigated the callus formation and rooting ability of ER Ayvalik and HR Domat cuttings in the presence of either *rac*-GR24 or TIS108.

At the end of the 10 weeks, 46% of explants belonging to the ER control group produced callus (Fig. 2). In the *rac*-GR24 treatment groups, callus production varied from 30 to 36%, while TIS108 induced callus in 36 to 57% of the explants for the ER. In all application groups for *rac*-GR24 in the ER, the callus formation rates are lower than the control group while the 5  $\mu$ M TIS108 group in which the callus formation was increased. However, only 9% of the explants belonging to the control group of HR-produced callus (Fig. 2). In the *rac*-GR24 treatment groups, callus production varied from 4 to 12%, while TIS108 induced callus 2 to 16% of the explants for the HR. For *rac*-GR24 applications, only the 10  $\mu$ M applied group showed a slight increase in callus formation compared to the control and for TIS108 applications both 5 and 10  $\mu$ M applied groups showed an increase in callus formation and this increase is compatible with the dose increase. According to these data, the best results for ER group were achieved with 5  $\mu$ M TIS108 application (57%) and for HR cultivar with 10  $\mu$ M TIS108 application (16%).

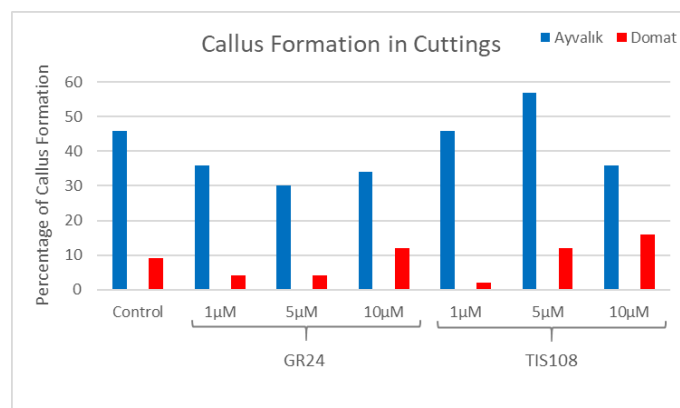


**Fig. 2.** Callus formation percentages of ER and HR olive cultivars

Afterwards, the cuttings which have roots were counted. At the end of the 10 weeks, the rooting rate was 1% in the control group of the ER (Fig 3). In the *rac*-GR24 treatment groups, rooting rates varied from 0 to 2%, while TIS108 induced rooting of 4 to 8% of the explants for the ER. For *rac*-GR24 applications, only the 10  $\mu$ M *rac*-GR24 applied group did not

show any roots. For HR, the rooting rate was 1% in the control group (Fig. 3). In the *rac*-GR24 treatment groups, rooting rates varied from 1 to 4%, while TIS108 induced rooting of 0 to 3% of the explants for the HR. For TIS108 applications, while 1  $\mu$ M application did not show any roots, 5 and 10  $\mu$ M applied groups showed increased rooting compared to the control group. According to these results, TIS108 is promising for inducing callus production and rooting of cuttings for both ER and HR olive cultivars.

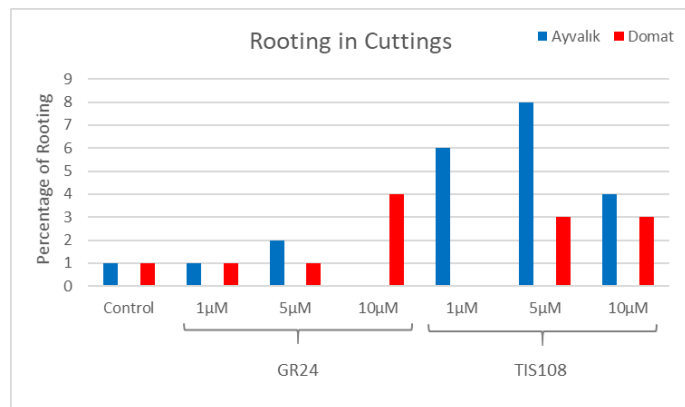


Fig. 3. Rooting percentages of ER and HR olive cultivars.

#### 4. Discussion

The rooting abilities of some economically important olive cultivars are very limited. Therefore, we determined the effects of *rac*-GR24 and TIS108 on cuttings of HR and ER olive cultivars. SLs have been shown to suppress adventitious rooting in plants such as tomato, *A. thaliana*, and pea (Kohlen et al., 2012; Rasmussen et al., 2013). Similarly, in this study *rac*-GR24 suppressed both callus formation and adventitious rooting in cuttings of ER. For HR, 1 and 5  $\mu$ M *rac*-GR24 applications could suppress callus formation and root formation. It is unclear whether this suppressive property of SL is direct or indirect (Kohlen et al., 2012). This feature may arise because of the shortage of the transport of auxin hormone, which promotes adventitious rooting, to the lower parts of the plant. (Crawford et al., 2010; Shinohara et al., 2013). Besides, in *A. thaliana* and

#### References

- Akiyama, K., Matsuzaki, K. I., & Hayashi, H. (2005). Plant sesquiterpenes induce hyphal branching in arbuscular mycorrhizal fungi. *Nature*, 435(7043), 824-827.
- Arite, T., Kameoka, H., & Kyojuka, J. (2012). Strigolactone positively controls crown root elongation in rice. *Journal of Plant Growth Regulation*, 31(2), 165-172.
- Cook, C. E., Whichard, L. P., Turner, B., Wall, M. E., & Egley, G. H. (1966). Germination of witchweed (*Striga lutea* Lour.): isolation and properties of a potent stimulant. *Science*, 154(3753), 1189-1190.
- Crawford, S., Shinohara, N., Sieberer, T., Williamson, L., George, G., Hepworth, J., ... & Leyser, O. (2010). Strigolactones enhance competition between shoot branches by dampening auxin transport. *Development*, 137(17), 2905-2913.
- Cetintas Gerakakis, A., & Ozkaya, M. T. (2005). Effects of cutting size, rooting media and planting time on rooting of Domat and Ayvalik Olive (*Olea europaea* L.) cultivars in shaded polyethylene tunnel spt. *Journal of Agricultural Sciences*, 11(03), 334-338.
- De Cuyper, C., Fromentin, J., Yocco, R. E., De Keyser, A., Guillotin, B., Kunert, K., ... & Goormachtig, S. (2015). From lateral root density to nodule number, the strigolactone analogue GR24 shapes the root architecture of *Medicago truncatula*. *Journal of Experimental Botany*, 66(1), 137-146.
- de Saint Germain, A., Ligerot, Y., Dun, E. A., Pillot, J. P., Ross, J. J., Beveridge, C. A., & Rameau, C. (2013). Strigolactones stimulate internode elongation independently of gibberellins. *Plant Physiology*, 163(2), 1012-1025.
- Fabbri, A. G., Bartolini, G., Lambardi, M., & Kailis, S. (2004). *Olive propagation manual*. (pp. 1-164). Landlinks Press.
- Gomez-Roldan, V., Fermas, S., Brewer, P. B., Puech-Pagès, V., Dun, E. A., Pillot, J. P., ... & Rochange, S. F. (2008). Strigolactone inhibition of shoot branching. *Nature*, 455(7210), 189-194.
- Guan, J. C., Koch, K. E., Suzuki, M., Wu, S., Latshaw, S., Petrucci, T., ... & McCarty, D. R. (2012). Diverse roles of strigolactone signaling in maize architecture and the uncoupling of a branching-specific subnetwork. *Plant Physiology*, 160(3), 1303-1317.
- Ito, S., Umehara, M., Hanada, A., Yamaguchi, S., & Asami, T. (2013). Effects of strigolactone-biosynthesis inhibitor TIS108 on Arabidopsis. *Plant Signaling & Behavior*, 8(5), e24193.
- Isfendiyaroglu, M., Ozeker, E., & Baser, S. (2009). Rooting of "Ayvalik" olive cuttings in different media. *Spanish Journal of Agricultural Research*, 7(1), 165-172.
- Kapulnik, Y., Delaux, P. M., Resnick, N., Mayzlish-Gati, E., Wininger, S., Bhattacharya, C., ... & Koltai, H. (2011). Strigolactones affect lateral

pea, it was stated that the decrease in cell division or differentiation in the tissue expected to form adventitious roots, indicates that SL restricts organogenesis (Rasmussen et al., 2013).

For ER, 10  $\mu$ M *rac*-GR24 application suppressed rooting completely while the same dose increased rooting for HR. For TIS108 applications all groups showed an increase in adventitious rooting for ER and HR except the 1  $\mu$ M TIS108 application group for HR. Increased adventitious rooting was also observed in petunia, tomato, *A. thaliana*, and pea SL mutants (Kohlen et al., 2012; Rasmussen et al., 2013). According to these results, a more detailed analysis might be required to explain the effects of TIS108 for adventitious rooting in HR.

In conclusion, finding a solution to the rooting problem in hard-to-root olive cultivars will replace the very expensive grafting technique and pave the way for the development of less costly and easier methods. Enlightening the usage areas of SLs in woody plants will provide new opportunities in breeding, propagation, or productivity programs. Besides, in this study, the SLs inhibitor TIS108 increased the callus production and rooting ability of cuttings for HR cultivar, which is promising for quitting the expensive inoculation technique.

**Acknowledgments:** This study is based on a Ph.D. thesis entitled "Characterization of the Genes Involved in Strigolactone Biosynthesis in Olive (*Olea europaea* L.)" from Canakkale Onsekiz Mart University, supported by The Scientific and Technological Research Council of Turkey (TUBITAK) with a Project Number 2150543 and COST Action (FA1206). We thank TUBITAK for their support and the doctoral scholarship (2211-A program). We also thank the Edremit Directorate of Olive Production Station (Edremit, Balıkesir) for providing the biological material.

**Conflict of interest:** The authors declare that they have no conflict of interests.

**Informed consent:** The authors declare that this manuscript did not involve human or animal participants and informed consent was not collected.

- root formation and root-hair elongation in Arabidopsis. *Planta*, 233(1), 209-216.
- Kiralan, M., & Bayrak, A. (2013). Oxidative and antiradical stabilities of two important virgin olive oils from Ayvalik and Memecik olive cultivars in Turkey. *International Journal of Food Properties*, 16(3), 649-657.
- Kohlen, W., Charnikhova, T., Lammers, M., Pollina, T., Tóth, P., Haider, I., ... & López-Ráez, J. A. (2012). The tomato *CAROTENOID CLEAVAGE DIOXYGENASE8 (SICCD8)* regulates rhizosphere signaling, plant architecture and affects reproductive development through strigolactone biosynthesis. *New Phytologist*, 196(2), 535-547.
- Rasmussen, A., Depuydt, S., Goormachtig, S., & Geelen, D. (2013). Strigolactones fine-tune the root system. *Planta*, 238(4), 615-626.
- Rugini, E. (1986). *Olive (Olea europaea L.)*. *Biotechnology in Agriculture and Forestry*. (pp. 1-267). Springer, Heidelberg.
- Ruyter-Spira, C., Kohlen, W., Charnikhova, T., van Zeijl, A., van Bezouwen, L., de Ruijter, N., ... & Bouwmeester, H. (2011). Physiological effects of the synthetic strigolactone analog GR24 on root system architecture in Arabidopsis: another belowground role for strigolactones?. *Plant Physiology*, 155(2), 721-734.
- Santoro, V., Schiavon, M., Gresta, F., Ertani, A., Cardinale, F., Sturrock, C. J., ... & Schubert, A. (2020). Strigolactones control root system architecture and tip anatomy in *Solanum lycopersicum* L. plants under P starvation. *Plants*, 9(5), 612.
- Serrano, J. M., Serrano, M. C., & Amaral, E. (2002). Effect of different hormone treatments on rooting of *Olea europaea* cv. *Galega vulgar* cuttings. *Acta Horticulturae*, 586, 875-877.
- Shinohara, N., Taylor, C., & Leyser, O. (2013). Strigolactone can promote or inhibit shoot branching by triggering rapid depletion of the auxin efflux protein PIN1 from the plasma membrane. *PLoS Biology*, 11(1), e1001474.
- Snowden, K. C., Simkin, A. J., Janssen, B. J., Templeton, K. R., Loucas, H. M., Simons, J. L., ... & Klee, H. J. (2005). The Decreased apical dominance1/*Petunia hybrida* *CAROTENOID CLEAVAGE DIOXYGENASE8* gene affects branch production and plays a role in leaf senescence, root growth, and flower development. *The Plant Cell*, 17(3), 746-759.
- Stirnberg, P., van De Sande, K., & Leyser, H. O. (2002). MAX1 and MAX2 control shoot lateral branching in Arabidopsis. *Development*, 129, 1131-1141.
- Turkoglu, N., & Durmus, M. (2005). A study on root formation of four olive varieties by application of hormone. *Asian Journal of Plant Sciences*, 4(5), 455-457.
- Umehara, M., Hanada, A., Yoshida, S., Akiyama, K., Arite, T., Takeda-Kamiya, N., ... & Yamaguchi, S. (2008). Inhibition of shoot branching by new terpenoid plant hormones. *Nature*, 455(7210), 195-200.
- Xu, Y., Wang, J., Wang, R., Wang, L., Zhang, C., Xu, W., ... & Jiu, S. (2021). The role of strigolactones in the regulation of root system architecture in grapevine (*Vitis vinifera* L.) in response to root-restriction cultivation. *International Journal of Molecular Sciences*, 22(16), 8799.
- Zohary, D., Hopf, M., & Weiss, E. (2012). *Domestication of Plants in the Old World: The origin and spread of domesticated plants in Southwest Asia, Europe, and the Mediterranean Basin*. (pp. 1-237). Oxford University Press, United States.

**Cite as:** Ozbilen, A., Sezer, F., & Taskin, K. M. (2022). Improving the adventitious rooting ability of hard-to-root olive (*Olea europaea* L.) cultivar cuttings through inhibiting strigolactone biosynthesis. *Front Life Sci RT*, 3(3), 134-137.